Detection of Stiffness and Mass Changes Separately Using Output-only Vibration Data

by

Ngoan Tien Do

A thesis submitted in partial fulfillment of the requirements for the degree of

Master of Science

in

Structural Engineering

Department of Civil and Environmental Engineering

University of Alberta

Abstract

Structural Health Monitoring (SHM) is a rapidly developing field, which is expected to play an important role in management of infrastructure systems by providing critical information about the structural changes or damage in the structure under monitoring. Among the different components of SHM, data analysis methods and damage detection algorithms are widely considered among the most critical components. For real life applications, the effects of operational and environmental factors on the damage detection process should be appropriately considered since these effects can mask structural damage. In this study, a new vibration based damage detection method for detection of changes in stiffness (e.g. due to damage) and mass (e.g. due to operational effects) is introduced. For this purpose, an improved method using the Autoregressive Moving Average model with eXogenous inputs (ARMAX) in conjunction with a sensor clustering technique is developed. In order to separate the changes in stiffness and mass, two different damage features (DFs) are developed based on the relative difference of ARMAX coefficients: Mass DFs (MDFs), which aim to eliminate operational effects, and Stiffness DFs (SDFs), which detect structural damage. Numerical and experimental case studies are employed for verification of the methodology. First, a numerical study of a 4-DOF spring mass system and the IASC-ASCE (International Association of Structural Control; American Society of Civil Engineers) numerical benchmark problem are presented. Then, a small-scale four-storey steel structure is developed and tested in the laboratory to study the proposed approach with experimental data. Similar to the results of the numerical studies, the methodology is successful in not just determining the location and severity of the damage, but also distinguishing exactly changes in mass and stiffness in the experimental structure. The limitations of the methodology in its current form and recommendations for future work are also discussed at the end of the thesis.

Acknowledgements

First of all, I would like to express my greatest respect and gratitude to my supervisor, Dr. Mustafa Gul, who has always been patient and supportive during my graduate studies at the University of Alberta. He has introduced me to a new area of civil engineering that has been more exciting than anything I have studied before. My research would have never been completed if I did not have such great support and mentorship. Also, many thanks to Dr. Samer Adeeb for providing me with a basic background in pipeline structures; I will never forget his great instructions and friendliness.

I am grateful to the committee members of my MSc defense, Dr. J.J. Roger Cheng and Dr. Samer Adeeb for their time and constructive feedback.

I would like to say thank you to all members in our research group including Saeideh Fallah Nafari, Aimee De Laurentiis, Lihua Zhang, Haiyang Zhang, Branislav Kostic, Qipei Mei, and Nicholas Kwan-Wong for his help during the laboratory experiments, and Jianfeng Gu, who have all accompanied me in my journey and have given me a lot of good advice.

Most importantly, thank you to my fiancé, Thanh-Thuy, and my family for constantly caring about me during my study. I would like to send them all my love for such invaluable encouragement and sympathy they have given me.

Table of Contents

List of Figures

List of Tables

List of Nomenclature

$\boldsymbol{M}$	Mass Matrix
$\boldsymbol{C}$	Damping Matrix
$\boldsymbol{K}$	Stiffness Matrix
$x_i(t)$	Displacement of the i^{th} DOF at time t
$\dot{x}_i(t)$	Velocity of the i^{th} DOF at time t
$\ddot{x}_i(t)$	Acceleration of the i^{th} DOF at time t
$y_i(t)$	Replacement of $\ddot{x}_i(t+\Delta t)-\ddot{x}_i(t)$
$M_{baseline}$	Built Mass related matrix of the baseline case
M_{damage}	Built Mass related matrix of the damaged case
SDF_{ij}	Stiffness DF for the sensor j in the i^{th} sensor cluster
MDF_{ij}	Mass DF for the sensor j in the i^{th} sensor cluster

CHAPTER 1: INTRODUCTION

1.1 Introduction to Structural Health Monitoring

Complex and costly problems related to civil infrastructure systems have become a major burden on the government agencies and infrastructure owners. A majority of civil infrastructure systems are now facing various problems due to deteriorations caused by operational and environmental loads, natural disasters, and other situations. As structures approach the end of their design life, improvement of their safety and increase of their performance is critical. A number of factors, including improper maintenance and inspection, can result in major failures.

Among the aging and deteriorating civil infrastructure systems, bridges are one of the most critical. For example, in the 2013 *Report Card for America's Infrastructure* published by the U.S Federal Highway Administration (FHWA), the average age of 607,308 bridges surveyed is 42 years. 11% of those bridges were classified as "structurally deficient" and 24.9% were found to be "functionally obsolete". In Canada specifically, the total investment backlog for bridges is estimated to be $121 billion (Canada Statistic). Recent incidents, including the collapse of the I-35W Mississippi River Bridge in the US, the partial collapse of a pier of the CPR Bonnybrook Bridge in Alberta, Canada due to scouring from a flood, and the collapse of the De la Concorde Overpass in Quebec, Canada, also demonstrate the significance of the problem.

Due to safety and economical concerns, Structural Health Monitoring (SHM) is becoming an important component in the management of civil infrastructure systems by assessing the condition of structures well before critical damage can amass. To complement visual inspections, which are time-consuming and less reliable in detecting damage and problems, an automated SHM system benefits authorities by providing a proactive decision making tool for improved reliability and reduced life-cycle costs.

The last few decades witnessed a rapid development in the field of SHM due to dramatic technological progress, which has allowed engineers to acquire desired data in a much easier way. In spite of benefits from technological development, it is widely

acknowledged that challenges in the analysis of the acquired data still remain. Therefore, the most important purpose of the SHM system is that anomalies can be detected regardless of operational or loading conditions (Bernal et al., 2004; Fan et al., 2011; J. P. Lynch et al., 2006). In the existing literature, widely available technologies, especially from computer science and electrical engineering, result in a wide range of possible SHM techniques (Dharap et al., 2006; Hearn et al., 1991; Im et al., 2013; Moaveni et al., 2013; A. K. Pandey et al., 1991). Moreover, a number of SHM systems have been installed on all kinds of civil infrastructures in real-world scenarios (Carpinteri et al., 2006; Chae et al., 2012; Dharap et al., 2006; Ko et al., 2005; Koo et al., 2013; Kurata et al., 2011; VanZwol et al., 2008; Wong, 2004).

1.2 Introduction to Damage Detection Techniques and Time Series Analysis

Generally, there is a misconception that SHM and damage detection are different names for the same concept when in fact damage detection is just one important component of a SHM system as a whole. SHM possesses a much broader scope that includes the hardware of the monitoring system, long-term monitoring of the structure, analysis of the data, and provision of information for decision making. On the other hand, damage detection is one of the most important components of SHM that employs various techniques to identify the presence, location, and severity of damage, which must be known before any maintenance actions can be taken.

According to Anders Rytter (1993), the sophistication of damage detection techniques can be evaluated based on four levels of detail that the techniques can determine: (1) identification of the existence of damage; (2) localization of the damage; (3) determination of damage's severity; and (4) estimation of remaining time that the structure can properly operate. Among various damage detection techniques available in the literature, the first three levels have attracted great attention and identification of the existence of damage is necessary since further investigation can be conducted only once damage has been detected.

Damage detection methods can be categorized as either local or global. Local methods aim to detect damage in a relatively small area on the structure; an example of this is the use of ultrasonic waves (Attarian et al., 2014; Giurgiutiu, 2005; Kessler et al., 2002).

These methods require a relatively dense sensor network and depend largely on boundary conditions and discontinuities on the structure's surface. Therefore, one drawback of these methods is that it is almost impractical to predict the locations of damage where an array of sensors must be mounted. Due to the fact that the method presented in this thesis does not relate to local methods, these methods will not be discussed further in this thesis.

Global methods (Overbey, 2007, Magalhães, 2012), however, track the global behaviour of the whole structure in either the time or the frequency domain. The general idea of this method is that any changes in local stiffness, mass, or damping can influence the global properties of the structures, e.g. natural frequencies, mode shapes, and damping parameter. Thus, these parameters can be tracked and used as damage features based on vibration data recorded from sensors installed at locations on the structure. From this information, the inverse problem must be solved; that is, the dynamic response is used to calculate the dynamic parameters of the structure. The global techniques that employ the dynamic properties mentioned above are known as parametric methods.

Over the last few decades, time series analysis has been greatly adopted in the field of SHM. A time series is a sequence of data in the time domain recorded at uniform time intervals. Time series analysis refers to statistically modelling a time-dependent sequence that is observed in the time domain. The good feature of time series analysis based methods is that they do not try to define modal parameters or other structural parameters as damage features. Therefore, it can be treated as a non-parametric method. In the field of SHM, there are some commonly used time series models, such as the Auto-Regressive (AR) model, the Moving Average (MA) models, and the Box-Jenkins (B-J) model. There are a number of technical papers where time series analysis has been employed, demonstrating the fact that this method is quite promising (Gul et al., 2009b; Monroig et al., 2006; Nair et al., 2006; Hoon Sohn & Farrar, 2001; Trendafilova et al., 2008). More details of recent time series based damage detection techniques and more references are discussed in the Literature Review section.

As mentioned above, time series analysis has been widely used in the damage detection process although there are still some issues that need to be addressed, such as the optimizing of the model's orders, choosing the appropriate types of time series, damage

feature extraction, and so on in order to improve the SHM system's effectiveness as a whole. In this thesis, the time series model is utilized so that only acceleration data is employed and two damage sensitive features are built to detect damage in stiffness and eliminate operational effects, e.g. changes in mass based on the models' coefficients.

1.3 Objectives and Scope

As mentioned above, in this thesis the time series model is utilized to develop a new technique that can detect changes in mass and stiffness separately by creating two damage features – the Mass Damage Feature and Stiffness Damage Feature – using output-only vibration data. To the best of the author's knowledge, this is the first time changes in mass are investigated quantitatively in conjunction with changes in the stiffness using output-only vibration data. Overall, the thesis has two main parts. In Part I – Theoretical Development and Numerical Case Studies-- an improved method based on Autoregressive Moving Average model with eXogenous inputs (ARMAX) is presented. Two numerical applications are presented to validate the effectiveness of the proposed technique. In Part II – Experimental Validation-- after discussing theory and numerical case studies, a laboratory-scale shear-type structure along with the development of the SHM framework is presented. Different damage scenarios are examined in order to demonstrate the capabilities of the proposed technique.

1.4 Organization of the thesis

The thesis is organized as follows:

Chapter 2 presents a review of damage detection methods available in the literature. First, some parametric methods are reviewed and then the benefits and drawbacks of the use of modal frequencies and mode shapes as damage features are examined. Secondly and more importantly, a review of the history and recent achievements of damage detection techniques based on time series models is conducted.

Chapter 3 provides a brief introduction of time series models and the underlying methodology of the proposed method for damage detection based on the use of time series analysis. The mathematical definitions of two Damage Features (DFs) are discussed.

Chapter 4 contains two numerical case studies to verify the methodology presented. Ambient vibration from different damage cases are recorded and used as inputs. The choice of sensor clusters and the results of two different damage features for mass and stiffness are introduced.

Chapter 5 presents the experimental verification of the proposed methodology. The finite element modeling, design and construction of the structure is presented in this chapter. Finally, the development of the SHM system, including the data acquisition system, sensors placement, and software, is detailed.

Chapter 6 contains various damage scenarios and the results of the DFs from each damage case. The effectiveness of the methodology in detecting, locating, and quantifying the damage caused by stiffness and mass changes separately is demonstrated.

Chapter 7 completes the thesis with the summary and conclusions. Relevant issues and possible plans for improvement are also mentioned.

CHAPTER 2:LITERATURE REVIEW OF DAMAGE DETECTION TECHIQUES

In this chapter, a literature review of important and recent publications in SHM is presented starting with an overview of some classical methods in damage detection.

SHM is a multi-disciplinary subject involving many different components, such as experimental testing, sensors, data acquisition systems, data transfer and storage, signal processing, and damage detection methods. Thanks to the benefits from the rapid development of advanced technologies in the areas of computer science and electrical engineering, it is now more convenient and cheaper to acquire large amounts of data. However, despite abundant data, the proper way to detect damage is still a big challenge. The main objective of this thesis is to develop methods for damage detection based on time series analysis. In this chapter, a detailed literature review about existing methods for damage detection is presented. For the completeness of the review, an introduction to the widely used vibration based damage detection methods in general is included in the first section, and a specific review about the history and latest accomplishment in methods based on time series analysis is presented in the second section.

2.1 Literature Review of Parametric Methodologies

During the early development of SHM, changes in basic modal properties such as natural frequencies, modal damping, and mode shape vectors were the most commonly used parameters as damage features. The reason is that these characteristics depend directly on the physical properties of structures such as stiffness, mass, and damping. In the following paragraph, a literature review on modal frequencies based damage detection and subsequently the limitations of this method are presented.

Hearn et al. (1991) conducted two experimental studies for stiffness damage detection based on the changes of natural frequencies and modal damping coefficients. The tests used a welded steel frame and wire ropes, whose damage were created by fatigue loading and saw-cuts respectively. From a perturbation of the equation of motion, natural frequency changes can be derived and locations and severity of stiffness reduction can be

found. Ju et al. (1988) presented a pre- and post-measure of natural frequencies of an experimental cantilever beam with damage within the mid length of the beam. Based on the theory of "fracture hinge" the authors could identify the position of the damage although there were some significant errors about the damage's intensity. More information about the frequency change based damage detection can be found in a 1997 technical review by Salawu, where the author discussed the advantages and disadvantages of using natural frequencies as a damage sensitive feature. Overall, frequency based methods can be found as one of the earliest methodologies in SHM due to its simplicity. However, researchers have found many problems arising from this method, one of which is the insensitivity of natural frequencies to structural damage. As can be seen in the above studies, most authors had failed in evaluating the damage's intensity and its location when only relying on changes of natural frequencies as an indicator (Doebling et al., 1998). For these reasons, researchers have been looking for new methodologies while continuing to employ natural frequencies in conjunction with other parameters to construct new damage features (J.-T. Kim et al., 2003; Maity et al., 2005; Zhong et al., 2008).

While natural frequencies cannot provide any spatial information, mode shapes can and are thus better solutions for damage. The introduction of Modal Assurance Criterion (MAC) (Allemang et al., 1982) has been very useful since it is one of the common tools to compare the identified mode shapes. West (1984) may be the first researcher that employed mode shapes to detect location of damage without any requirement of defining finite element models. The author used MAC to determine the correlation between the mode shapes of the Space Shuttle Orbiter body flap at the undamaged stage and the damaged stages created by acoustic loading. Before calculating correlation levels, the mode shapes are partitioned by different techniques, and the MAC between different partitioned mode shapes is used to localize the damage. Ahmadian et al. (2000) proposed a damage localization technique using mode shapes information. Given that the substructures' mode of vibration will not be affected by damage except for the substructure where the damage happened and also that participation factors of the higher substructure mode shapes in the deflections are only non-zero when local damage occurs, two indicators for damaged positions are formulated. Siebel et al. (2012) presented

numerical and experimental studies of a wind turbine where Operational Modal Analysis (OMA) was conducted to define mode shapes based on strain gages and accelerometers. Two algorithms have been proposed to investigate damage, namely Modal Strain Energy and Gapped Smoothing Technique. First, mode shapes are defined from strain and acceleration data and then the two proposed methods are applied using OMA data to evaluate different mode shapes extracted from various damaged scenarios in which damage is to be revealed. Mode shape based damage detection can be categorized in the same category of basic modal parameters. However, methods that use only natural frequencies cannot reveal the partial information, which is a weak point when compared with methods employing mode shape information. Nevertheless, there are some drawbacks of using basic modal shapes for damage detection. One of the disadvantages is that high mode shapes, which are sensitive to minor damage, are not easy to excite by ambient vibration. Also, computed mode shapes are vulnerable under environmental effects, and thus fault detections can be made.

Zhang and Johnson (2013) proposed a system identification technique for shear-type structures. In their method, a system is divided into simple substructures and equations of motion which were built for each substructure were used for story stiffness and damping estimation by solving the optimization problem. The authors applied Least-square method to identify source of errors. A numerical five-story shear structure was introduced to demonstrate the effectiveness of their method. Another system identification of shear-bending models was introduced by Kuwabara et al. (2013) by determining the limit value a proposed identification function which is constructed from the equation of motion. Subsequently, damage detection was conducted by combining the proposed technique with ARX model. Ikeda et al. (2014) introduced a smart system identification method by using horizontal floor accelerations. Combinations of ARX model, Taylor series and Transfer function. In their application, the author observed that the numerical shear-bending system can reasonably simulate the vibration records and the natural frequencies and stiffness can be estimated appropriately. Minami et al. (2012), also conducted a relatively similar method for system identification and damage detection using time series models.

In parametric methods, finite element models and numerical formulations are widely employed in conjunction with measured vibration data in various damage techniques. This kind of method is categorized into a distinct branch that is called the model updating method. Basically, the method aims to intensively modify the finite element model or mathematical models so as to capture the baseline and damaged structures based on the comparison between the simulated and measured vibration data where the difference has to be as small as possible. Once those models can capture the behaviour of the structure, the inverse problem can be solved to define the damage. Box et al. (1994) conducted a survey on the state of the art of model updating in the field of structural dynamics. They defined model updating as a process of correcting the finite element models to improve the correlation between the measured vibration data and those from the FE models. Based on different algorithms in changing constraints, mesh size, optimization, etc., different techniques were introduced and various condensation methods were available for building the damage sensitive features. One example is the comparison among the stiffness matrices of the FE model to locate and quantify the extent of damage.

Ching et al. (2006) introduced a combination of both the Bayesian model updating and Gibbs sampler techniques for the framework of damage detection. Based on the Bayesian technique, the structural parameters are estimated and updated. The Gibbs sampler made the technique more robust as it can reduce the dimensions of high-dimensional parameter space resulting in a more practical methodology. However, this method requires a sufficient amount of monitored locations for best results. Shiradhonkar et al. (2011) presented a method to detect and locate damage in a beam of a finite element moment resistant frame. Given that there is a lack of response at some degrees of freedom (DOFs), the responses at those DOFs were estimated by interpolating the measured locations. Then the modal parameters, which are the damage features, are calculated using frequency domain decomposition and empirical transfer functions. Similar to all finite element modal updating, this method requires much time, effort, and engineering expertise to update the FE model. Also, the FE model is modified based on measured vibration data that is greatly affected by operational and environmental factors. Therefore, uncertainties remain and conclusions may not be accurate since the actual behaviour of the structure is not explained thoroughly.

Link et al. (2012) demonstrated their methodology about the FE model updating method for the purpose of damage detection conducted on the Gaertnerplatz Bridge in Germany. A FE model of the bridge was first created and then updated based on the monitored vibration data to represent the healthy state. The monitored data, which was gathered over a period of three years, was used to identify the chosen parameters of the FE model using a simplified interval updating technique. After considering temperature effects and variations due to noise, they concluded that there was no structural degradation. Again, the greatest challenge is that the updating process of the FE model requires much effort, as well as intensive knowledge and experience in finite element analysis. In general, it is worth saying that FE models or other physical based models give researchers useful information about the state of structures. However, damage detection methods based on those models require great efforts and intensive expertise in finite element analysis in order to closely reveal and diagnose any symptoms occurring in the real structure.

In addition to the parametric methods mentioned above, a variety of methods are available in the literature, such as the Principal Component Analysis based damage detection (De Boe et al., 2003; Kullaa, 2003; Mujica et al., 2014; Hoon Sohn et al., 2000), Frequency domain analysis, e.g. the Wavelet Analysis (Kim et al., 2004; Reda Taha, 2010), Frequency Response Functions (Lee et al., 2002; A. Pandey et al., 1994; Park et al., 2003; Sampaio et al., 1999), Singular Value Decomposition, and Complex Mode Indicator Function (CMIF) (Catbas et al., 2006; Liu et al., 2014; Shih et al., 1988).

Non-parametric methods in general or statistical pattern recognition techniques such as Artificial Neural Networks (Hoon Sohn et al., 2002; Zhao et al., 1998) and Time Series Modelling (Gul et al., 2009a, 2011a; Nair et al., 2007; Nair et al., 2006; Hoon Sohn, Farrar et al., 2001) have specifically gained great momentum in the field of SHM due to their ability to deal with massive data. This capability improves the reliability since the variations in the recorded data are also taken in to account. Among the different statistical pattern recognition techniques, the time series analysis is chosen to be the basis of this thesis. Therefore, an exclusive literature review on time series models will be presented in the following section.

2.2 Literature Review of Time Series Based Damage Detection Methods

Time series analyses are used to analyze a sequence of time-dependant data sets in order to understand their statistical characteristics. Originally, time series models were employed in economics for stock price tracking and prediction, in population modelling, and in electrical engineering. In the SHM field specifically, time series modelling was first introduced by Andersen (1997) in the system identification of civil structures. As mentioned previously, researchers have found it very advantageous in using time series models for damage detection (De Roeck et al., 2002; Nair et al., 2006; Hoon Sohn & Farrar, 2001). In the next paragraph, a literature review of damage detection methods based on the use of various time series models is presented.

Hoon Sohn, Farrar et al. (2001) first presented a damage detection method by combining autoregressive (AR) and autoregressive models with exogenous inputs (ARX). The strain data measured from three sensors on a surface-effect patrol boat were used to fit the time series models. Ratios of standard deviation of the residual errors before and after damage were chosen to be the first damage feature. In addition, the Mahalanobis distance of AR coefficients was calculated as the second damage feature. The results from the two damage features showed a good indication of damage. However, information about damage location and severity were not revealed clearly. Bodeux et al. (2000) introduced the application of Auto-Regressive with Moving Average Vector (ARMAV) models in structure dynamics for system identification and damage detection. In their method, the Prediction Error Method was used to define the model's parameters by assuming zero mean white noise excitation. From their successful application on a Steel-Quake benchmark structure, they proved that the modal parameters are well identified. Also, the damage was investigated based on the evaluation of model parameter uncertainties. However, the authors admitted the limitation that the locations of damage were not properly identified. A modified approach based on ARX models was proposed for the damage detection process (Y Lei et al., 2003) where the authors considered the effects of excitation variation and the ARX models' orders. Similar to other related papers, the residual errors of the unknown cases and undamaged cases were compared to construct the damage feature. The numerical ASCE benchmark structure was employed in their

application where medium and severe damage were detected and localized successfully. On the other hand, the authors reported that the minor damage was being studied to improve the effectiveness of the modified technique. Monroig et al. (2006) presented a method where second order ARX models were built based on the equation of motion and decentralized method for local damage detection. The results from a numerical application similar to the ASCE benchmark problem showed that damage could be detected and localized, although some false-positive and false-negative results need to be addressed. Gul and Catbas (2011) introduced a new sensor clustering technique along with time series modelling for the damage detection process. They grouped acceleration data into different clusters in which each cluster is represented by the Auto-Regressive model with eXogenous input (ARX) models. Locations and severity of damage in the applications of the 4-DOF system and experimental and numerical vibration data from a steel grid structure was revealed based on the changes of fit ratios for the ARX models.

In the above paragraph, we can see that different time series models were adopted for the damage detection process. In those papers, coefficients of time series models were used as damage sensitive features and damage could be found by simply tracking the changes of those coefficients before and after damage. Therefore, in order to improve the effectiveness of the damage detection process, combinations of time series models and other statistical pattern recognitions have been utilized and proposed for damage detection in SHM.

Gul and Catbas (2009) proposed their statistical pattern recognition technique using a combination of Random Decrement technique and Auto Regressive (AR) models and Mahalanobis distance. The ambient vibration data was first reconstructed by using Random Decrement. Then, AR models were used to fit all processed data in the baseline and unknown cases. Subsequently, the Mahalanobis distance was calculated for all feature vectors for outlier detection to evaluate structural state of the structure. The results from the two experimental case studies were successful in detecting changes in stiffness and boundary conditions, although some issues such as threshold determination should be addressed before applying this method to automated SHM systems. Nair et al. (2006) utilized the first three auto-regressive components in the Auto-Regressive Moving Average (ARMA) models that are employed to fit the vibration signals as the damage

sensitive feature. In order to confirm confidently that damage exists in the structure, a statistical summarization, i.e. a t-test, was used. Also, two different indices were introduced for damage localization. Numerical and experimental vibration data from the ASCE benchmark structure were used to validate the method. The researchers confirmed that the minor and major damage were detected and located exactly.

A combination of Auto Regressive (AR) Models and an Artificial Neural Network (ANN) were introduced in a study conducted by Lautour and Omenzetter (2010). Acceleration data from healthy and damaged states are fitted into the AR models. Subsequently, AR coefficients are used as the inputs of ANN to train and classify damage and estimate the remaining stiffness of the structure. Results from a 3-storey bookshelf structure and Phase II ASCE benchmark structure demonstrated a good evaluation of damage. However, the drawback of this methodology is that supervised data should be available in order to train the ANNs to classify damage. Xing and Mita (2012) divided a monitored structure into more simple substructures. The authors applied ARMAX models based on the equation of motion, and concluded that the natural frequencies can be estimated at different states of the structure. A 5-storey building was employed to validate their methodology both numerically and experimentally. After comparing the natural frequencies of the substructures before and after damage, the researchers revealed the locations of damage exactly. The drawback of this method is that an excitation source should be available. Figueiredo et al. (2011) evaluated the effectiveness of using different AR model's orders for damage detection. In their study, four techniques – Akaike information criterion, partial autocorrelation function, root mean squared error, and singular value decomposition – were used to optimize the number of AR coefficients. A three-story base-excited frame structure was used to validate the estimated model's orders, and the experiment showed that the techniques can propose a lower bound of the orders, although these techniques gave relatively different results. Most importantly, the comparative case studies showed the importance of choosing the proper order to optimize the model's effectiveness.

Noman et al. (2012) presented a method of damage detection using data from a long-term monitoring of the Portage Creek Bridge in Victoria, British Columbia, Canada. AR models were used to fit acceleration and strain data and the first three model coefficients

were chosen to be the damage features. These damage features were plotted into an X-bars chart to discern damage. It was observed that there was no serious damage during the monitored period except for a slight degradation toward the end of the period. Mosavi et al. (2012) presented a damage detection technique on a two-span steel girder. Acceleration data from all sensors are fitted into the Multivariate vector autoregressive models. Then, the Mahalanobis distance is calculated as the damage feature to compare the difference between the model's coefficients at the healthy and damaged cases. In addition, Fisher criterion was employed to evaluate the variance of the damage features where a damage decision is made based on the sensor location with the highest variation in the damage feature. Results from the steel girder test are promising. However, some issues that need to be addressed include the high density of the sensors' layout requirements and the effects of loading conditions. Huang et al.(2013) introduced a damage detection method based on the use of Vector Auto Regressive (VAR) Model. Data from baseline and unknown cases were divided into smaller sections in order to build the VAR coefficient matrix whose diagonal components were extracted to construct Mahalanobis Distance, which is in turn used to build Deflection Coefficients (DC) and an operating characteristic curve as two damage features. Application of a 6-DOF numerical system and a transmission tower model showed that the method can identify and detect damage. However, the severity of damage was not defined very well.

Yao and Pakzad (2014) compared the effectiveness of two damage features, e.g. the Mahalanobis distance of AR coefficients and the Cosh distance of AR model spectra. A 10-DOF bridge model was created with several damage scenarios to check the effectiveness of the two damage features. This comparison showed that both DFs are sensitive to both local damage and noise levels, indicating that the interaction among structure, environment, and excitation results in the changes in the DFs. Therefore, these scientists concluded that those DFs are effective in structures under stable operating conditions. Roy et al. (2015) employed the ARX model to predict the acceleration signal of one DOF using acceleration data from the other DOFs from which four different damage sensitive features (DSFs) are extracted based on the ARX's coefficients, Kolmogorov–Smirnov (KS) test statistical distance, and the model residual error. Results from three different applications including numerical and experimental structures showed

that the DSFs could localize the stiffness damage positions and the intensity of damage can be defined; however, in some cases with multiple damage positions, one of the DSFs seems unable to clearly define the amount of stiffness reduction.

Lakshmi and Rao (2014) applied Principle Component Analysis to recorded acceleration data to reduce the dimensions of raw data. The processed data was in turn fitted into combined AR-ARX models where the variances of prediction errors were compared to define the current state of the monitored structure. A numerical study of a simply supported beam and experimental benchmark structure were used to demonstrate the method's effectiveness. This experiment demonstrated that the method can detect and locate damage but the severity of damage should be further examined. In addition, time series models were utilized in conjunction with other techniques e.g. finite element model based methods.

Bao et al. (2013) proposed a combined technique to develop a damage detection method for a finite element subsea pipeline system. The acceleration data was first partitioned and normalized to eliminate effects of loading conditions. Next, auto-correlation functions and partial-correction functions were computed for the input of ARMA models and their orders respectively. Mahalanobis Distance was finally built for the constructed ARMA coefficients for the Damage Indicator. The numerical results showed that the method can detect and locate damage effectively even with noise effects.

Time series model's orders are also an important aspect. Various models have been employed with the models' orders being chosen based mostly on experience or optimization methods. In the literature, many studies focus on defining the optimized model's orders. Figueiredo et al. (2011) evaluated the effectiveness of using different AR model's orders for damage detection. In their study, four techniques – Akaike information criterion, partial autocorrelation function, root mean squared error, and singular value decomposition – were used to optimize the number of AR coefficients. A three-story base-excited frame structure was used to validate the estimated model's orders, and the experiment revealed that the techniques can propose a lower bound of the orders, although these techniques gave relatively different results. Most importantly, the

comparative case studies showed the importance of choosing the proper order to optimize the model's effectiveness.

As can be seen from the above review, SHM researchers have paid a lot of attention to damage detection process and time series models in particular. However, for real-life applications, a number of issues still need to be resolved since the complexity of civil infrastructure systems remains a challenge for scientists. One significant problem is that effects of operational and environmental factors may be overwhelming compared to physical damage in the monitored structure, and therefore, a wrong conclusion about damage detection may easily be made. In order to address the operational effects, the next section introduces the literature review of these effects on structures' dynamic response due to mass changes such as traffic crossing.

2.3 Literature Review of Operational Effects on SHM and Identification of Mass and Stiffness Changes

One operational effect that is difficult to measure precisely is mass loading e.g. traffic crossing. In this section, a literature review of the influence of mass on modal parameters and damage detection process as well as of the efforts to separate mass changes in SHM is conducted.

Kim et al. (1999) may be among the first researchers who mentioned effects of mass on the modal frequencies of monitored structures. In their research, different operational vibrations caused by vehicle crossing were recorded at three bridges. The data was then divided into two groups based on the type of vehicles crossing the bridges, i.e. heavy vehicles (trucks, buses) and light vehicles (passenger cars). The results calculated from two data sets showed that the modal frequencies of moderate and long-span bridges hardly changed. However, up to a 5.4% difference in natural frequencies of a short span bridge is observed when vibration data caused by heavy vehicles was used in comparison to the other data set.

De Roeck et al. (2002) investigated the effects of different traffic loading on the identified modal frequencies mode shapes of a bridge model. By modelling various types of vehicles and road roughness, the authors observed that the natural frequencies reduced

when heavier moving vehicles are employed compared to the empty structure. Also, the road surface configuration affects the vehicle-structure interaction significantly. The mass effects from a vehicle are partially eliminated due to the vehicle's suspension system. However, these observations need to be studied more thoroughly since the effects of multiple traffic crossing were not considered and more effort is needed to develop a complete vehicle model. Zhang et al. (2002) found that the damping ratios of the monitored cable-stayed bridge increased significantly when the deck's vibration reached a certain level that is in turn affected greatly by the traffic loading. However, mode shapes and natural frequencies changed insignificantly during 24-hour monitoring. Hoon Sohn (2007) conducted research on the effects of environmental and operational factors on the damage detection process and provided a review of those effects. In addition, Sohn reviewed different normalization methods, e.g. Auto-associate neural network, Regression analysis, Singular value decomposition to eliminate those effects from the true damage of monitored structures. Mei et al. (2015) adopted the substructure damage identification technique and ARMAX model to identify damage of each smaller structure. The method employed acceleration data to fit into the ARMAX model where the first AR coefficients were used to identify damage by comparing the coefficient between the healthy and damaged cases. However, this method is only able to identify and quantify stiffness changes.

Figueiredo and Park (2011) employed different machine learning algorithms, e.g. the auto-associative neural network, factor analysis, Mahalanobis square distance, and singular value decomposition. Damage was simulated by replacing different columns and operational effects are simulated by adding mass at the base of the structure. Acceleration data recorded from a 3-storey frame structure in laboratory was fitted into AR models. Afterwards, AR coefficients are used as the inputs of the machine learning methods. Overall, Mahalanobis square distance seemed to be the best method, although all machine learning methods work effectively in defining damage regardless of the operational effects. However, all methods required all scenarios of operational effects for training the data, which is a drawback since it is almost impossible to capture all sources of operational variability. Zhan et al. (2014) improved their previous studies in the effort of separating mass and stiffness changes in shear type structures. Using Finite element

method based Finite Impulse Response (FFIR) (Hong, Kim, & Lee, 2010), these scientists reconstructed displacement and velocity from acceleration data. The mass normalized stiffness coefficients from which relative change in stiffness and mass are evaluated are developed by the least square method. However, the method still showed some drawbacks, one of which is that many approximate equations are made in order to build four unknown parameters for damage detection. Therefore, the method can only detect damage greater than 20% reduction in mass and stiffness with some errors. Also, multiple damage scenarios should be studied for more confident results.

Bighamian and Mirdamadi (2013) applied the method named extracted system digital pulse response (EDPR) for separately detected damage in mass and stiffness. By using this method, each instrumented point becomes equivalent to a SDOF system where percentage of mass and stiffness before and after damage can be estimated. Their numerical applications were quite promising since mass and stiffness damage were revealed effectively. The disadvantage of this method is that source of vibration have to be available which are almost impossible in real life applications. Also, prediction of potential damage locations is not very feasible for more complicated structures.

Overall, most technical papers in structural health monitoring have been focused on stiffness reduction and efforts of environmental elimination (Ying et al., 2012; Xing & Mita, 2012). However, operational effects such as mass from external sources could have negative impact on the damage detection process since together with environmental factors, operational effects can mask the structural state of monitored structures and wrong decisions in SHM may be made due to these influences. Therefore, there is no doubt to say that mass change as an operational effect should be studied exclusively and it is worth saying that the idea in thesis in separately detecting mass and stiffness changes in terms of locations and severity is one of the first researches ever conducted in the literature.

In this research, an improved method is derived from the equation of motion. The method proposed by Mei and Gül (2014) was further developed and improved to obtain Stiffness DFs and Mass DFs separately. After a sequence of mathematical transformations and loop calculations, information about mass and stiffness of the structure is related to the

Auto Regressive Moving Average model with eXogenous inputs (ARMAX) models. Therefore, two Damage Features, which are Stiffness DFs and Mass DFs, are constructed in order to detect, locate and quantify the damage in stiffness and mass separately. The contribution of this methodology is that changes in mass and stiffness would be assessed simultaneously and independently. This is very useful in applications where operational effects such as mass changes due to traffic loading in bridges can make the damage detection process more complicated.

CHAPTER 3:METHODOLOGY

3.1 Background to Time Series Models

Time series modelling is the statistical time-dependent modelling of a sequence of observed data points. A brief description about the ARMAX model, the specific model used in this paper, is given in Eq.3.1. More discussions about the time series models theory can be found in the literature (Lu & Gao, 2005; Omenzetter & Brownjohn, 2006; Hoon Sohn et al., 2001).

$$\begin{aligned} y(t) + a_1 y(t - \Delta t) + \cdots + a_{n_a} y(t - n_a \Delta t) = b_1 u(t - \Delta t) + \cdots + b_{n_b} u(t - n_b \Delta t) \\ + e(t) + d_1 e(t - \Delta t) + \cdots + d_{n_c} e(t - n_c \Delta t) \end{aligned} \tag{3.1}$$

Where $y(t)$ is the output, $u(t)$ is the input of the model, $e(t)$ is the error term, and a_i, b_i, d_i are the parameters of the model, and the model orders are given in the terms of n_a, n_b, n_d. A general form of the above equation can be written as Eq.3.2:

$$A(q)y(t) = B(q)u(t) + D(q)e(t) \tag{3.2}$$

The terms $A(q)$, $B(q)$ and $D(q)$ are polynomials in delay operators q^j as shown in Eq.(3.3):

$$\begin{aligned} A(q) &= 1 + a_1 q^{-1} + \cdots + a_{n_a} q^{-n_a} \\ B(q) &= b_1 q^{-1} + b_2 q^{-2} \cdots + b_{n_b} q^{-n_b} \\ D(q) &= 1 + d_1 q^{-1} + d_2 q^{-2} \cdots + d_{n_c} q^{-n_c} \end{aligned} \tag{3.3}$$

From the Eq.3.3, it is straightforward to understand the meaning of the delay operator. For example, a data set $x(t)$ at time t multiplied by q^j is equal to $x(t-j\Delta t)$. From the general form of time series models, different time series models are created by changing the order of $A(q)$, $B(q)$, and $D(q)$. AR (Auto Regressive) process, for instance, is created with the order n_a, whereas n_b, n_d are set to be zero. An MA (Moving Average) process is created by setting n_a, n_b to be both zeros and a non-zero value of n_c. The ARMAX model is produced when exogenous inputs $u(t)$ are considered as shown in Eq.3.2. For easy

understanding, these time series models are demonstrated in the following figures. A block diagram of ARMAX model is shown in Figure 3.1:

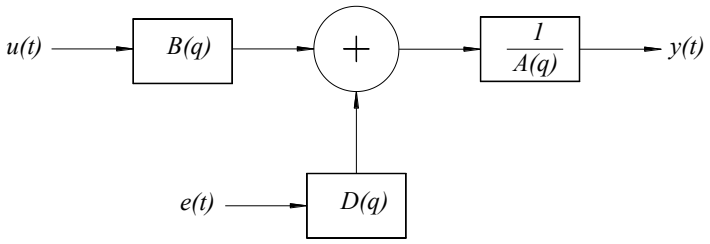

Figure 3.1. A block diagram of the ARMAX model (adapted from Ljung 1999)

3.2 ARMAX Models for Different Sensor Clusters

First, the equation of motion, which is the governing equation for the dynamic response of structures, is described herein. The vibration of one degree of freedom of a structure is strongly dependent on time, the prior state of the structure, and external inputs. Therefore, it is believed that vibration data can be considered as a time series sequence, and statistical characteristics of the time series should be extracted to track the behaviour of the structure. It is, therefore, worth noting that the time series model (the ARMAX model in this thesis) would be the best fit to describe the structure's dynamic profile. Eq. 3.4 below shows the general equation of motion as N degrees of freedom system.

$$\boldsymbol{M}\ddot{\boldsymbol{x}}(t)+\boldsymbol{C}\dot{\boldsymbol{x}}(t)+\boldsymbol{K}\boldsymbol{x}(t)=\boldsymbol{f}(t) \tag{3.4}$$

Where, *M, C*, and *K* are the N by N mass, damping, and stiffness matrices of the system, respectively. The vectors $\ddot{x}(t), \dot{x}(t), \text{and } x(t)$ are acceleration, velocity, and displacement at time instant *t*. The external forcing vector on the system is denoted by *f(t)*.

We can write Eq. 3.4 in matrix form with the order N×N degree of freedom, as shown in Eq. 3.5.

$$\begin{bmatrix} m_{11} & \cdots & m_{1N} \\ \vdots & \ddots & \vdots \\ m_{N1} & \cdots & m_{NN} \end{bmatrix}\begin{Bmatrix} \ddot{x}_1 \\ \vdots \\ \ddot{x}_N \end{Bmatrix}+\begin{bmatrix} c_{11} & \cdots & c_{1N} \\ \vdots & \ddots & \vdots \\ c_{N1} & \cdots & c_{NN} \end{bmatrix}\begin{Bmatrix} \dot{x}_1 \\ \vdots \\ \dot{x}_N \end{Bmatrix}+\begin{bmatrix} k_{11} & \cdots & k_{1N} \\ \vdots & \ddots & \vdots \\ k_{N1} & \cdots & k_{NN} \end{bmatrix}\begin{Bmatrix} x_1 \\ \vdots \\ x_N \end{Bmatrix}=\begin{Bmatrix} f_1 \\ \vdots \\ f_N \end{Bmatrix} \tag{3.5}$$

In order to derive the correlation between the ARMAX model and the equation of motion, the i^{th} row in Eq. 3.5 is chosen for analyzing and shown in Eq.3.6. Rearranging Eq.3.6 results in Eq.3.7:

$$\begin{aligned}\left(m_{i1}\ddot{x}_1(t)+\cdots+m_{iN}\ddot{x}_N(t)\right)+\left(c_{i1}\dot{x}_1(t)+\cdots+c_{iN}\dot{x}_N(t)\right)\\ +\left(k_{i1}x_1(t)+\cdots+k_{iN}x_N(t)\right)=f_i(t)\end{aligned} \tag{3.6}$$

$$\begin{aligned}\ddot{x}_i=\frac{f_i}{m_{ii}}-\frac{m_{i1}\ddot{x}_1+\cdots+m_{i,i-1}\ddot{x}_{i-1}+m_{i,i+1}\ddot{x}_{i+1}\cdots+m_{iN}\ddot{x}_N}{m_{ii}}\\ -\frac{c_{i1}\dot{x}_1+c_{i2}\dot{x}_2+\cdots+c_{iN}\dot{x}_N}{m_{ii}}-\frac{k_{i1}x_1+k_{i2}x_2+\cdots+k_{iN}x_N}{m_{ii}}\end{aligned} \tag{3.7}$$

By assuming the mass distribution at the center of each degree of freedom (lumped mass), we can determine that the acceleration on the right side of Eq.3.7 are zeros due to zero values of any off-diagonal entries of the mass matrix. For simplicity, it is proposed that damping terms in the above equation could be neglected due to their small contribution to the equation's balance. The remaining parts are shown in Eq. 3.8 from which derivative is taken twice, resulting in Eq. 3.9:

$$\ddot{x}_i=\frac{f_i}{m_{ii}}-\frac{k_{i1}x_1+k_{i2}x_2+\cdots+k_{iN}x_N}{m_{ii}} \tag{3.8}$$

$$\ddot{\ddot{x}}_i=\frac{\ddot{f}_i}{m_{ii}}-\frac{k_{i1}\ddot{x}_1+k_{i2}\ddot{x}_2\cdots+k_{iN}\ddot{x}_N}{m_{ii}} \tag{3.9}$$

The purpose of calculating the second derivative in Eq. 3.9 is that acceleration would be the only information required in this study. By applying the forward difference method (Levy & Lessman, 1961) shown in Eq. 3.10., we see that the left side of Eq. 3.9 is transformed by using this method to create a new transformation shown in Eq.3.11:

$$\dddot{x}_i = \frac{\ddot{x}_i(t+\Delta t) - \ddot{x}_i(t)}{\Delta t}$$
$$\dddot{x}_i = \frac{\frac{\ddot{x}_i(t+2\Delta t) - \ddot{x}_i(t+\Delta t)}{\Delta t} - \frac{\ddot{x}_i(t+\Delta t) - \ddot{x}_i(t)}{\Delta t}}{\Delta t} \tag{3.10}$$

$$\frac{\frac{\ddot{x}_i(t+2\Delta t) - \ddot{x}_i(t+\Delta t)}{\Delta t} - \frac{\ddot{x}_i(t+\Delta t) - \ddot{x}_i(t)}{\Delta t}}{\Delta t} = \frac{\ddot{f}_i}{m_{ii}} - \frac{k_{i1}\ddot{x}_1(t) + k_{i2}\ddot{x}_2(t) + \cdots + k_{iN}\ddot{x}_N(t)}{m_{ii}} \tag{3.11}$$

As can be seen from Eq. 3.11, the acceleration $\ddot{x}_i(t)$ appears in both sides of the equation, possibility resulting in a trivial solution. Therefore, new sequence $y_i(t)$ is defined to represent the left components in Eq.3.11. The final transformation of the equation of motion is shown in Eq. 3.12:

$$\frac{y_i(t+\Delta t) - y_i(t)}{\Delta t^2} = \frac{\ddot{f}_i}{m_{ii}} - \frac{k_{i1}\ddot{x}_1(t) + k_{i2}\ddot{x}_2(t) + \cdots + k_{iN}\ddot{x}_N(t)}{m_{ii}} \tag{3.12}$$

By comparison, the ARMAX model (Eq. 3.2) can be used to represent Eq. 3.12, where $y_i(t)$ and $\ddot{x}_i(t)$ are considered as output and input terms. In the ARMAX model, the error terms can represent the damping parts and the excitation force in the equation of motion and noise as well. Apparently, the orders n_a and n_b for the ARMAX model can be chosen as 1 and 1 by simply comparing the corresponding output, input terms, and Eq. 3.12. The order of 3 is assigned for n_c based on the investigation of testing different orders whereby the order of 3 is sufficient to account for the influence just mentioned above. Finally, the ARMAX model for the i^{th} row of the equation of motion of a multi DOF system can be expressed as in Eq. 3.13:

$$y_i(t+\Delta t) + a^i y_i(t) = b_1^i \ddot{x}_1(t) + b_2^i \ddot{x}_2(t) + \cdots + b_N^i \ddot{x}_N(t) + e(t) + d_1 e(t-\Delta t) + d_2 e(t-\Delta t) \tag{3.13}$$

Again, the ARMAX model in Eq. 3.13 represents the i^{th} equation of motion of N degree of freedom system. Due to the sparse property of the stiffness and mass matrix, it can be

assumed that the signal of a DOF can affect only its adjacent DOFs. Thus, the ARMAX model can be constructed in a simpler way where only neighbor DOFs or a sensor cluster is employed in each model, and the output sensor in an ARMAX model is the reference channel of this sensor cluster. Details about sensor clustering technique is decribed in the next section. It is noted that the above mathematic transformation was conducted previously (Mei, Gul [2014]) and it is introduced here for a logical understanding. The following sections discuss the extension of this methodology for developing separate detections of mass and stiffness damage features, a state of assessment not accomplished before.

3.3 Sensor Clustering

Based on the ARMAX model built for the equation of motion of a DOF in a system shown in Eq. 3.13, vibration at one sensor is chosen to fit the part at the left side of the equation, which is called the reference channel. Vibration data at the other sensors or DOF are chosen to fit the right part of the equation. Due to the nature of the shear-type structure, vibration at one DOF is affected only by adjacent DOFs. Therefore, for an *N*-DOF system, there are N ARMAX models with output as the reference channel and inputs only come from adjacent channels, meaning that an ARMAX model only employs a cluster of sensors instead of all sensors. Therefore, it helps to significantly reduce the complexity of the equation of motion. Details of the sensor clustering technique can be found from a study conducted by Gul & Catbas (2011).

A 3-DOF system is given to describe the technique schematically. The first sensor cluster used to build the ARMAX model includes the first and second channels where the first channel is chosen as the reference channel. As shown in Figure 3.2, the second channel is chosen as the reference channel of the second sensor cluster and all channels are employed in this sensor cluster since dynamic response of the second channel is affected by all channels connected to it. Lastly, the third sensor cluster uses the third sensor as the reference channel and second channel as it is adjacent to the third DOF.

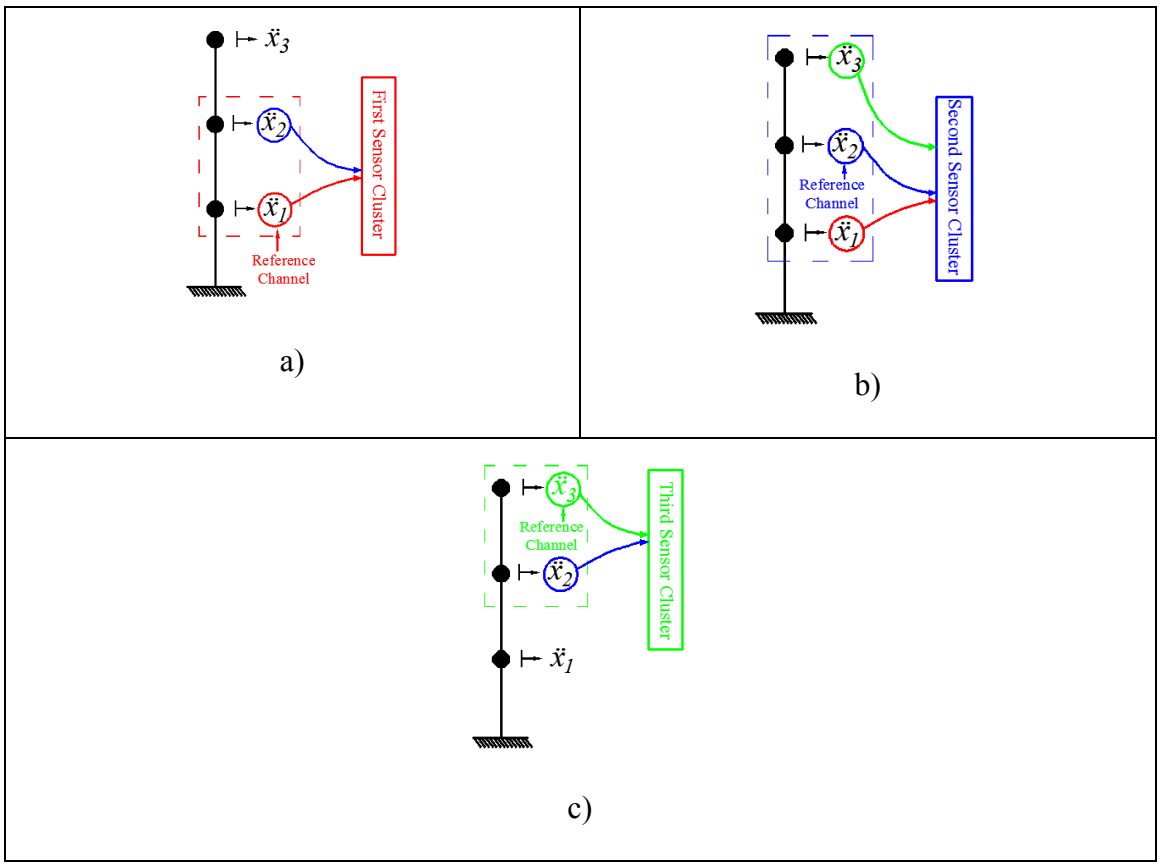

Figure 3.2. ARMAX Models for different clusters: (a) the 1st sensor cluster; (b) the 2nd sensor cluster; (3) the 3rd sensor cluster.

3.4 Building Damage Features

3.4.1 Mass Damage Features (MDFs)

By comparison, we can see the *B(q)* terms of ARMAX models can represent the terms $\frac{k_{ij}}{m_{ii}}$ in the equation of motions of different sensor clusters:

$$b^{i}_{j,baseline} = \begin{bmatrix} b^{1}_{1} & b^{1}_{2} & \dots & b^{1}_{n} \\ b^{2}_{1} & b^{2}_{2} & \dots & b^{2}_{n} \\ \vdots & \vdots & \dots & \vdots \\ b^{n}_{1} & b^{n}_{2} & \dots & b^{n}_{n} \end{bmatrix} \cong \begin{bmatrix} \frac{k_{11}}{m_{11}} & \frac{k_{12}}{m_{11}} & \dots & \frac{k_{14}}{m_{11}} \\ \frac{k_{21}}{m_{22}} & \frac{k_{22}}{m_{22}} & \dots & \frac{k_{24}}{m_{22}} \\ \vdots & \vdots & \vdots & \vdots \\ \frac{k_{n1}}{m_{nn}} & \frac{k_{n2}}{m_{nn}} & \dots & \frac{k_{nn}}{m_{nn}} \end{bmatrix} \tag{3.14}$$

From Eq. 3.14, we can create two matrices relating to either mass or the stiffness matrix of the system. The first mass-related matrix is induced by calculating the ratio b^{i}_{j}/b^{i}_{i} with b_i being the *B* terms of the i^{th} sensor cluster, whereas the stiffness-related matrix is defined by defining the *B* terms at the baseline and unknown case plus some modification which is presented next. With this calculation, we can define the mass-related matrix and stiffness-related matrix of the system in the baseline case and unknown case by employing only *B(q)* coefficients of the two cases that we call b^{i}_{j} and d^{i}_{j} .

Mass-related matrix of the baseline case is as follows:

$$\begin{bmatrix} \frac{b^{1}_{1}}{b^{1}_{1}} & \frac{b^{1}_{2}}{b^{1}_{1}} & \dots & \frac{b^{1}_{n}}{b^{1}_{1}} \\ \frac{b^{2}_{1}}{b^{2}_{2}} & \frac{b^{2}_{2}}{b^{2}_{2}} & \dots & \frac{b^{2}_{n}}{b^{2}_{2}} \\ \vdots & \vdots & \dots & \vdots \\ \frac{b^{n}_{1}}{b^{n}_{n}} & \frac{b^{n}_{2}}{b^{n}_{n}} & \dots & \frac{b^{n}_{n}}{b^{n}_{n}} \end{bmatrix} \cong M_{baseline} = \begin{bmatrix} \frac{m_{11}}{m_{11}} & \frac{m_{22}}{m_{11}} & \dots & \frac{m_{nn}}{m_{11}} \\ \frac{m_{11}}{m_{22}} & \frac{m_{22}}{m_{22}} & \dots & \frac{m_{nn}}{m_{22}} \\ \vdots & \vdots & \vdots & \vdots \\ \frac{m_{11}}{m_{nn}} & \frac{m_{22}}{m_{nn}} & \dots & \frac{m_{nn}}{m_{nn}} \end{bmatrix} \tag{3.15}$$

Similarly, we can define the mass-related matrix for the unknown case based on the B-terms:

$$\begin{bmatrix} \frac{d_1^1}{d_1^1} & \frac{d_2^1}{d_1^1} & \cdots & \frac{d_n^1}{d_1^1} \\ \frac{d_1^2}{d_2^2} & \frac{d_2^2}{d_2^2} & \cdots & \frac{d_n^2}{d_2^2} \\ \vdots & \vdots & \cdots & \vdots \\ \frac{d_1^n}{d_n^n} & \frac{d_2^n}{d_n^n} & \cdots & \frac{d_n^n}{d_n^n} \end{bmatrix} \cong M_{damage} = \begin{bmatrix} \frac{m_{11}^{'}}{m_{11}^{'}} & \frac{m_{22}^{'}}{m_{11}^{'}} & \cdots & \frac{m_{nn}^{'}}{m_{11}^{'}} \\ \frac{m_{11}^{'}}{m_{22}^{'}} & \frac{m_{22}^{'}}{m_{22}^{'}} & \cdots & \frac{m_{nn}^{'}}{m_{22}^{'}} \\ \vdots & \vdots & \vdots & \vdots \\ \frac{m_{11}^{'}}{m_{nn}^{'}} & \frac{m_{22}^{'}}{m_{nn}^{'}} & \cdots & \frac{m_{nn}^{'}}{m_{nn}^{'}} \end{bmatrix} \tag{3.16}$$

Where, d^i_j and m' are the $B(q)$ coefficients and lumped mass components of the unknown case. From Eq. 3.15 and Eq. 3.16, we take the relative change of the ratio m_{ii}/m_{jj} between the baseline and unknown case as shown in the following equation:

$$\Delta_{ji}(\%) = \frac{m_{ii}^{'} / m'_{jj} - m_{ii} / m_{jj}}{m_{ii} / m_{jj}} \% \tag{3.17}$$

The next step is to determine damage in the mass by following the loop calculation. For instance, the m_{11} and m'_{11} in the first column of Eq. 3.15 and Eq. 3.16 is the numerator, whereas the other lumped mass components are the denominators in those mentioned columns, meaning a decrement in m_{11} will result in a decrease in Δ. In contrast, an increment in Δ results from a decrease in the other mass components since they are the denominators. By assuming damage does not happen in the way that all the mass components change at the same time, which is usually not the case in the normal conditions of most structures. In addition, the change in mass should either increase or decrease (ways of detecting multiple decreases and increases in mass is being studied in the current work), we can know how much the mass component m_{11} reduced by taking the maximum reduction of Δ_{j1} of the first column of the matrix Δ_{ij}. Therefore, the new mass-related matrix is created by changing component $m^{'}_{11}$ in the denominator of the first row in Eq. 3.16 to m_{11} as shown below:

$$\begin{bmatrix} \frac{m'_{11}}{m_{11}} & \frac{m'_{22}}{m_{11}} & \cdots & \frac{m'_{nn}}{m_{11}} \\ \frac{m'_{11}}{m'_{22}} & \frac{m'_{22}}{m'_{22}} & \cdots & \frac{m'_{nn}}{m'_{22}} \\ \vdots & \vdots & \vdots & \vdots \\ \frac{m'_{11}}{m'_{nn}} & \frac{m'_{22}}{m'_{nn}} & \cdots & \frac{m'_{nn}}{m'_{nn}} \end{bmatrix} \tag{3.18}$$

Similarly, following the same procedure, we can change all m'_{11} appearing in the denominators in Eq. 3.16 into m_{ii}. At the end of the loop we can create the mass-related matrix of the unknown case where the only difference from the baseline mass-related matrix is the component m'_{ii} in the nominator. Finally, the mass-related matrix of the unknown case can be defined as follows:

$$M_{damaged} = \begin{bmatrix} \frac{m'_{11}}{m_{11}} & \frac{m'_{22}}{m_{11}} & \cdots & \frac{m'_{nn}}{m_{11}} \\ \frac{m'_{11}}{m_{22}} & \frac{m'_{22}}{m_{22}} & \cdots & \frac{m'_{nn}}{m_{22}} \\ \vdots & \vdots & \vdots & \vdots \\ \frac{m'_{11}}{m_{nn}} & \frac{m'_{22}}{m_{nn}} & \cdots & \frac{m'_{nn}}{m_{nn}} \end{bmatrix} \tag{3.19}$$

From the mass-related matrix of the baseline case and the inferred mass matrix in Eq. 3.19, we now can estimate the percentage of mass reduced by taking the relative difference between the two mass-related matrices from Eq. 3.15 and Eq. 3.19:

$$MDFs = \frac{M_{i,j}^{damaged} - M_{i,j}^{baseline}}{M_{i,j}^{baseline}} \times 100\% \tag{3.20}$$

3.4.2 Stiffness Damage Features (SDFs)

As mentioned previously, the *B(q)* terms of the ARMAX models are equivalent to $\frac{k_{ij}}{m_{ii}}$, the stiffness and mass components of the structure. By determining the *B(q)* coefficients of the baseline and unknown case, two matrices associated with the baseline and unknown cases, one of which is shown in Eq. 3.14, and the other matrix of the unknown case are shown as follows.

$$\begin{bmatrix} d_1^1 & d_2^1 & \dots & d_n^1 \\ d_1^2 & d_2^2 & \dots & d_n^2 \\ \vdots & \vdots & \dots & \vdots \\ d_1^n & d_2^n & \dots & d_n^n \end{bmatrix} \cong \begin{bmatrix} \frac{k'_{11}}{m'_{11}} & \frac{k'_{12}}{m'_{11}} & \dots & \frac{k'_{14}}{m'_{11}} \\ \frac{k'_{21}}{m'_{22}} & \frac{k'_{22}}{m'_{22}} & \dots & \frac{k'_{24}}{m'_{22}} \\ \vdots & \vdots & \vdots & \vdots \\ \frac{k'_{n1}}{m'_{nn}} & \frac{k'_{n2}}{m'_{nn}} & \dots & \frac{k'_{nn}}{m'_{nn}} \end{bmatrix} \tag{3.21}$$

Since changes in mass components have been evaluated, it is straightforward to get stiffness changes by simply changing the m'_{ij} in Eq. 3.21 into m_{ij} to produce a new matrix as shown in Eq. 3.22, where the stiffness terms are the only difference between baseline and unknown case.

$$b^i_{\text{j,damaged}} \cong \begin{bmatrix} \frac{k'_{11}}{m_{11}} & \frac{k'_{12}}{m_{11}} & \dots & \frac{k'_{14}}{m_{11}} \\ \frac{k'_{21}}{m_{22}} & \frac{k'_{22}}{m_{22}} & \dots & \frac{k'_{24}}{m_{22}} \\ \vdots & \vdots & \vdots & \vdots \\ \frac{k'_{n1}}{m_{nn}} & \frac{k'_{n2}}{m_{nn}} & \dots & \frac{k'_{nn}}{m_{nn}} \end{bmatrix} \tag{3.22}$$

The Stiffness Damage Feature is presented in Eq. 3.23

$$SDFs = \frac{d^{i}_{j,\text{damaged}} - b^{i}_{j,baseline}}{b^{i}_{j,baseline}} \times 100\% \tag{3.23}$$

i : sensor clusters; j: adjacent sensors

In the next chapter, two applications based on the proposed methodology will be presented to confirm theoretically their effectiveness before a lab-scale experimental study is discussed in Chapter 5 and Chapter 6.

CHAPTER 4:NUMERICAL CASE STUDIES

In this section, two numerical applications, i.e., 4-DOF mass spring system and Phase I IASC-ASCE Benchmark problem, are introduced respectively. The first application was first presented in the 7th International Conference on Structural Health Monitoring of Intelligent Infrastructure (SHMII-7, Italy 2015) and the second application was accepted and orally presented in the 10th International Workshop on Structural Health Monitoring 2015 (IWSHM 10th , Stanford University, USA)

4.1 Case Study I: 4-DOF Mass Spring System

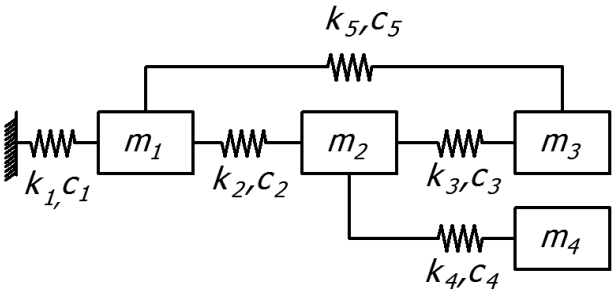

Figure 4.1. Numerical model used for the case study

In order to be consistent and show improvement in the methodology, the same numerical 4-DOF system employed in previous studies (Q. Mei & Gül, 2014) is used in this thesis. The structural properties of this structure are described as follows: m_1 = 3500 kg, $m_2 = m_3$ = 2500 kg, m_4 = 2000 kg, k_1= 2×10^7 N/m and k_2= k_3= k_4= k_5= 7×10^7 N/m. The classic Rayleigh damping matrix is utilized to define the damping matrix (Eq. 4.1) of the system, assuming a 3% damping ratio for the first two modes.

$$C = a_0 M + a_1 K \tag{4.1}$$

Based on the properties of the system, it is straightforward to express its Stiffness and Mass matrices, as shown in Eq. 4.2 and Eq. 4.3:

$$K = \begin{bmatrix} k_1 + k_2 + k_5 & -k_2 & -k_5 & 0 \\ -k_2 & k_2 + k_3 + k_4 & -k_3 & -k_4 \\ -k_5 & -k_3 & k_3 + k_5 & 0 \\ 0 & -k_4 & 0 & k_4 \end{bmatrix} = \begin{bmatrix} 160 & -70 & -70 & 0 \\ -70 & 210 & -70 & -70 \\ -70 & -70 & 140 & 0 \\ 0 & -70 & 0 & 70 \end{bmatrix} \left(MN/m \right) \quad (4.2)$$

$$M = \begin{bmatrix} m_1 & 0 & 0 & 0 \\ 0 & m_2 & 0 & 0 \\ 0 & 0 & m_3 & 0 \\ 0 & 0 & 0 & m_4 \end{bmatrix} = \begin{bmatrix} 3500 & 0 & 0 & 0 \\ 0 & 2500 & 0 & 0 \\ 0 & 0 & 2500 & 0 \\ 0 & 0 & 0 & 2500 \end{bmatrix} (kG) \quad (4.3)$$

The excitation sources are set to act at all DOFs simultaneously with a 1000 Hz sampling frequency to record acceleration response since this sampling frequency is much higher than the fourth natural frequency of the system, which is 53.47 Hz. In addition, 10% artificial Gaussian white noise was added to the response signals to make the vibration data more realistic and account for environmental variations. For each damage scenario, 10 trials are tested and the results are represented by their mean values and standard deviation.

According to the sensor clustering technique, there are four sensor clusters used to build 4 ARMAX models representing the 4 DOFs of the system. The first sensor cluster has the first DOF as the reference channel and uses the adjacent first, second, and third DOF channels. Similarly, the second cluster has the second DOF as the reference channel and uses all DOF channels. In the third sensor cluster, the 3rd DOF is the reference channel and this cluster also employs the first DOF as adjacent ones. Lastly, the fourth sensor cluster has the fourth DOF as the reference channel and uses the second DOF channel. By creating ARMAX models for these sensor clusters in the baseline and damaged case, the location and severity of damage can be revealed. In the next sub-sections, six damage cases are introduced with the severity increased from minor to serious damage in either stiffness or mass, or both.

4.1.1 Baseline Case

It is noted that 10% noise was added in all simulated vibration data in order to closely represent realistic data. Therefore, in this case, a hundred trials were run in order to see the effects of 10% noise on the computed damage features and define the threshold from which higher values of damage features can be defined as damage. The results of Stiffness Damage Features (SDFs) and Mass Damage Features (MDFs) are shown in the following tables.

Table 4.1: SDFs in Percent for BC

	Ref Channel	1st	2nd	3rd	4th
SDFs	1st	0.58 (0.17)	-1.64 (0.7)	2.11 (0.45)	N/A
	2nd	-0.86 (0.59)	-0.07 (0.16)	0.79 (0.48)	-0.68 (0.42)
	3rd	1.55 (0.41)	0.39 (0.68)	0.7 (0.16)	N/A
	4th	N/A	1.01 (0.63)	N/A	0.7 (0.15)

From Table 4.1, the average of SDFs is shown in each entry with the standard deviation in the parenthesis. Each entry in the SDFs represents the change in the corresponding entry of the structure's stiffness matrix. As can be seen, although there was nothing changed in the structure, 2.11% was found in the SDF_{12} due to the noise effect. Therefore, it can be concluded that 2.11% would be the sensitivity of the methodology for this specific problem and any damage with DFs lower than this value would not be found by using the proposed method. The results, Mass Damage Features (MDFs), appear in Table 4.2.

Table 4.2: MDFs in Percent for BC

	Ref Channel	1st	2nd	3rd	4th
MDFs	1st	0 (0)	-0.78 (1.02)	0.56 (0.61)	N/A
	2nd	0.8 (1.03)	0 (0)	0.4 (0.89)	-1.68 (0.89)
	3rd	-0.55 (0.61)	-0.39 (0.88)	0 (0)	N/A
	4th	N/A	1.71 (0.92)	N/A	0 (0)

It is observed in Table 4.2 that the maximum of MDFs was found to be 1.71%. Therefore, the threshold is chosen as 2.1% for MDFs, which means that any values greater than this threshold in MDFs would be defined as damage.

After trying different trials, it is decided that 10 trials are sufficient for statistical analysis since the results of SDFs and MDFs changed very slightly when increasing the number of trials higher than 10. Therefore, from this point onwards, 10 trials will be chosen for each damage case.

4.1.2 Damage Pattern 1: $k_2' = 0.8 \times k_2$

A 20% stiffness reduction at stiffness k_2 between the 1st and the 2nd DOF is simulated and the *B-term* coefficients were constructed before and after damage in order to build the Stiffness Damage Features (SDFs) and Mass Damage Features (MDFs) shown in Table 4.3. For each entry in the Table, the average and standard deviation (in the parenthesis) in percentage of 10 trials are constructed. In Table 1, the SDF_{12} and SDF_{21} are -20.80% and -20.87%, respectively, which are close to -20%, the amount of actual damage at k_2. It is clear that 20% reduction at k_2 causes an overall reduction of 9.45% (SDF_{11}) and 6.90% (SDF_{22}) in the stiffness associated with the first DOF and the second DOF, respectively. The above results revealed almost exactly the actual damage in the structure since it is apparent that the 20% reduction in k_2 is accounted for by the 8.75% and 6.67% stiffness reduction in K_{11} and $K_{22,}$ respectively. The MDFs shown in Table 4.3 are almost zero since there no mass damage occurred in the system. It is also noted that there are some entries in the SDFs and MDFs with relatively high standard deviation of 1.17% due to the 10% noise added into the data.

Table 4.3: DFs in Percent for Damage Pattern 1 (20% reduction in k_2)

	Ref Channel	1st	2nd	3rd	4th
SDFs	1st	-9.45 (0.22)	-20.80 (0.55)	-1.37 (0.62)	N/A
	2nd	-20.87 (0.49)	-6.90 (0.16)	-0.58 (0.40)	0.88 (0.38)
	3rd	-0.44 (0.42)	0.03 (0.65)	0.11 (0.18)	N/A
	4th	N/A	-0.77(0.55)	N/A	0.07 (0.07)
	Ref Channel	1st	2nd	3rd	4th
MDFs	1st	0 (0)	0.09 (1.16)	-0.93 (0.82)	N/A
	2nd	-0.08 (1.17)	0 (0)	-0.61 (0.84)	1.66 (0.88)
	3rd	0.95 (0.84)	0.62 (0.85)	0 (0)	N/A
	4th	N/A	-1.63 (0.85)	N/A	0 (0)

It is noted again in the MDFs matrix that each column in that matrix represents the mass changes of a DOF. Therefore, the MDF matrix can be further simplified by taking the average of each column to have only one number that can track changes in mass of the that DOF. This way, we can have a new matrix that contains distinct information about damage in stiffness and mass of the structure with the mass information being placed in the last row of the matrix as shown in Table 4.4.

Table 4.4: DFs in Percent for Damage Pattern 1 (20% reduction in k_2)

	Ref Channel	1st	2nd	3rd	4th
SDFs	1st	-9.45 (0.22)	-20.8 (0.55)	-1.37 (0.62)	N/A
	2nd	-20.87 (0.49)	-6.9 (0.16)	-0.58 (0.4)	0.88 (0.38)
	3rd	-0.44 (0.42)	0.03 (0.65)	0.11 (0.18)	N/A
	4th	N/A	-0.77 (0.55)	N/A	0.07 (0.07)
MDFs		0.43 (1)	-0.31 (0.96)	-0.77 (0.83)	1.66 (0.88)

4.1.3 Damage Pattern 2: $k_2'=0.8\times k_2, k_4'=0.9\times k_4$

A more serious damage scenario was created where 10% reduction in k_4 occurs along with the damage in k_2. As observed from Figure 4.1, k_2 is related to DOF 1 and 2, whereas k_4 is related to DOF 2 and 4. Therefore, it is expected that the SDFs between DOF 1&2 and 2&4 will change to reflect damage in k_2 and k_4. As can be seen in Table

4.5, SDF_{11}, SDF_{12}, SDF_{21} are almost the same as they were in Table 4.5, which indicates 20% damage at k_2. In addition, change in k_4 has also affected other components of the SDFs matrix, one of which is the diagonal SDF_{22}, e.g. -10.54%, which shows exactly the damage at the K_{22} component of the [K] matrix since the change in $K_{22} = (0.2k_2+0.1\ k_4+ k_3)/ (k_2+ k_4+ k_3) = 10\%$ (Q. Mei & Gül, 2014) . A relative equal amount of -10% is also found at SDF_{24}, SDF_{42}, and SDF_{44} in Table 4.5 owing to the 10% change in k_4, the only component of the stiffness entries K_{24}, K_{42}, and K_{44}. No significant changes are found in MDFs since there no damage happened in the mass of the structure.

Table 4.5: DFs in Percent for Damage Pattern 2 (20% reduction in k_2 + 10% reduction in k_4)

	Ref Channel	1st	2nd	3rd	4th
SDFs	1st	-8.95 (0.15)	-19.45 (0.63)	-0.29 (0.25)	N/A
	2nd	-20.14 (0.44)	-10.54 (0.13)	-0.16 (0.15)	-10.28 (0.32)
	3rd	0.32 (0.42)	0.4 (0.44)	0.33 (0.08)	N/A
	4th	N/A	-8.85 (0.36)	N/A	-9.27 (0.14)
MDFs		-0.11 (0.69)	1.01 (0.67)	-0.58 (0.44)	-1.57 (0.47)

4.1.4 Damage Pattern 3: $m_4' = 0.8 \times m_4$

The third damage case was created in order to show the methodology could also discover damage in mass separately. Instead of a stiffness reduction, 20% reduction in mass at the fourth DOF was simulated. In this way, a significant change at the fourth column of the MDFs is expected to show since each column entry in the MDFs represents a DOF.

Table 4.6: DFs for Damage Pattern 3 (20% reduction in m_4)

	Ref Channel	1st	2nd	3rd	4th
SDFs	1st	-0.57 (0.28)	-1.82 (0.55)	-1.06 (0.51)	N/A
	2nd	-1.09 (0.56)	0.17 (0.16)	0.35 (0.45)	0.09 (0.34)
	3rd	-0.76 (0.29)	-0.19 (0.61)	0.48 (0.26)	N/A
	4th	N/A	0.09 (0.34)	N/A	1.55 (0.78)
MDFs		0.53 (0.81)	-0.42 (0.6)	0.12 (0.71)	-18.76 (0.64)

SDFs in Table 4.6 show insignificant changes meaning that there is no damage in or of the structure's stiffness. However, the fourth column entry of the MDFs revealed a value

of -18.76%, which is close to the amount of mass changed in the fourth DOF (20%). This result demonstrates a good example of the advantage of the method in distinguishing mass and stiffness changes.

4.1.5 Damage Pattern 4: $k_2' = 0.8 \times k_2$, and $m_2' = 0.8 \times m_2$

It is worth mentioning that the previous study (Q. Mei & Gül, 2014) seems unable to indicate damage when there are complicated changes in mass and stiffness happening simultaneously since only one DFs is used to represent those changes in the structure. As can be seen in Table 4.7, the SDFs are nearly similar to the SDF matrix in Damage Pattern 1, which indicates a 20% stiffness reduction at k_2 has been observed. As explained previously, each column entry in the MDF matrix represents a mass component of the system. It is clear that an amount of -19.48% in the 2nd column of the MDF matrix indicates there was a reduction in m_2 roughly at 20%.

Table 4.7: DFs in Percent for Damage Pattern 4 (20% reduction in k_2 + 20% reduction in m_2)

	Ref Channel	1st	2nd	3rd	4th
SDFs	1st	-8.52 (0.21)	-17.19 (0.72)	-1.55 (0.47)	N/A
	2nd	-18.74 (0.39)	-6.58 (0.75)	1.33 (0.61)	0.9 (0.55)
	3rd	-0.62 (0.46)	-0.58 (0.54)	-1.15 (0.14)	N/A
	4th	N/A	0.89 (0.53)	N/A	-0.09 (0.16)
MDFs		-0.46 (0.63)	-19.48 (0.6)	0.5 (0.6)	0.02 (0.28)

Table 4.8 shows the values of the built Damage Features from the same Damage Pattern based on the methodology presented in the previous study. As we can see, readers can infer some damage from those DFs. However, it is a little confusing that an increase in DFs means mass has increased, whereas a decrease in DFs means reduction in stiffness. Thus, comprehensive inference should be conducted based on the built DFs before any conclusions can be made. For instance, DF_{21} in Table 4.8 has a value of 0.92, which tells us there is no damage related to DOF 2. However, since damage in mass also occurred in that DOF, the combination of two damages resulted in no changes in DF_{21}. Therefore, the previous study seems to be not highly effective in multiple damage scenarios and the

current methodology has made a step forward in defining different Damage Features for different properties.

Table 4.8. DFs in Percent for Damage Pattern 4 based on the previous study (Q. Mei & Gül, 2014)

Ref Channel	1st	2nd	3rd	4th
1st	-8.52 (0.21)	-17.19 (0.72)	-1.55 (0.47)	N/A
2nd	0.92 (0.63)	16.02 (0.23)	25.84 (0.58)	25.32 (0.4)
3rd	-0.62 (0.46)	-0.58 (0.54)	-1.15 (0.14)	N/A
4th	N/A	0.89 (0.53)	N/A	-0.09 (0.16)

4.1.6 Damage Pattern 5: $C_{33}'=0.8\times C_{33}$

It was assumed previously that damping factors did not significantly affect the balance of the equation of motion. Thus, this component was eliminated for simplicity. However, there is a doubt that change in damping may affect the SDFs and MDFs in indicating changes in stiffness and mass, respectively. Therefore, the purpose of this section is to show that SDFs and MDFs are not dependent on damping or there are not significant changes in those damage features if damping of the structure changes.

Table 4.9: DFs in Percent for Damage Pattern 5 (20% reduction in C_{33})

	Ref Channel	1st	2nd	3rd	4th
SDFs	1st	-0.66 (0.14)	0.97 (1.32)	-0.27 (0.49)	N/A
	2nd	0.5 (1.73)	-0.66 (0.16)	0.5 (0.31)	0.96 (0.34)
	3rd	-0.69 (0.47)	1.13 (0.53)	-0.47 (1.2)	N/A
	4th	N/A	0.91 (0.94)	N/A	0.23 (0.13)
MDFs		-0.23 (0.72)	0.03 (0.95)	-0.1 (0.7)	0.6 (1.39)

Obviously, there are no significant changes in the SDFs and MDFs, which means that no changes in mass and stiffness occur in the structure, and damage in damping did not affect the indicators of stiffness and mass. It is noted that the damping change detection is beyond the scope of this study.

4.1.7 Damage Pattern 6: $k_2'=0.8\times k_2$, $C_{33}'=0.8\times C_{33}$ and $m_4'=0.8\times m_4$

In this Damage Pattern, multiple damage scenarios happen simultaneously in mass, stiffness, and damping of the structure. First, SDFs of this case shown in Table 4.10 are closely the same as those shown in Table 4.3, which means a 20% stiffness reduction in k_2 has been revealed. In addition, Table 4.10 contains values of MDFs that are considerably similar to those shown in Table 4.6 in DP3, that is, - 20% mass reduction at DOF 4. Therefore, the damage features have successfully detected multiple damages, including mass and stiffness changes, and they do not depend on the damping change, which confirms the methodology's hypothesis.

Table 4.10: SDFs in Percent for Damage Pattern 6 (20% reduction in k_2, m_4 and C_{33})

	Ref Channel	1st	2nd	3rd	4th
SDFs	1st	-7.84 (0.14)	-18.7 (0.4)	0.12 (0.26)	N/A
	2nd	-18.89 (0.46)	-6.91 (0.12)	-1.96 (0.37)	-0.06 (0.32)
	3rd	-1.79 (0.45)	-1.49 (0.46)	-1.04 (0.16)	N/A
	4th	N/A	-0.06 (0.32)	N/A	0.78 (0.71)
MDFs		-1.07 (0.47)	-0.1 (0.35)	1.24 (0.54)	-18.1 (0.51)

4.1.8 Damage Pattern 7: Blind Test

The author have purposely created the above damage cases to see how effective the method is in detecting damage in mass and stiffness. However, this strategy is quite subjective since the damage is known even before the calculation of DFs. Therefore, in this case, the damage is created randomly using a generator that can create damage in mass and stiffness with no perception from the researchers. A random damage generator was added in the Matlab code that can randomly generate a simultaneous reduction in the mass and stiffness of the structure up to 100%. From Table 4.11, it is obvious that K_{34}, K_{43}, K_{44} is -62.9%, -62.71, -63.32%, respectively. Those entries are related directly to the stiffness k_4, which is between the DOF 2 and DOF 4. Also, -20.93% was found at K_{22} that continues to confirm the damage at k_4 since this stiffness is one component contributing to the K_{22}. Therefore, it can be concluded that the stiffness k_2 between the DOF 2 and 4 has suffered from a damage at relatively 60%. In addition, the MDFs showed that the mass component m_1 has reduced by 16% and the other mass remained unchanged after

damage. By checking the true damage in the system, it is determined that the damage generator has made a 60% reduction at k_4. Therefore, it can be confirmed that the SDFs and MDFs have successfully evaluated the damage in the system.

Table 4.11: SDFs in Percent for Damage Pattern 7 (Blind Test)

	Ref Channel	1st	2nd	3rd	4th
SDFs	1st	-0.69 (0.52)	-0.33 (0.7)	-0.34 (0.17)	N/A
	2nd	1.09 (0.45)	-20.93 (0.11)	-0.22 (0.39)	-62.9 (0.16)
	3rd	-0.34 (0.17)	2.48 (0.34)	0.36 (0.17)	N/A
	4th	N/A	-62.71 (0.22)	N/A	-63.32 (0.04)
MDFs		-16.48 (0.52)	0.61 (0.68)	-1.32 (0.24)	-0.52 (0.6)

4.2 Case study II: Application to the IASC-ASCE Benchmark Problem

Rapid development in Structural Health Monitoring requires a unique application that researchers can utilize to validate their methodologies and various methods can be easily compared based on results from one application. There are some typical structures, one of which is the IASC-ASCE Benchmark problem developed by a joint research group. The International Association of Structural Control (IASC) and the Dynamics Committee of the American Society of Civil Engineers (ASCE) collaborated to form a task group in 1999 to create a benchmark structure (Johnson et al. 2004). The group had chosen a 4-storey shear type steel building located in the Earthquake Engineering Research Laboratory at the University of British Columbia for developing a benchmark structure. The structure (Figure 4.2.a) has an area of 2.5×2.5 m with two bays in both horizontal directions.

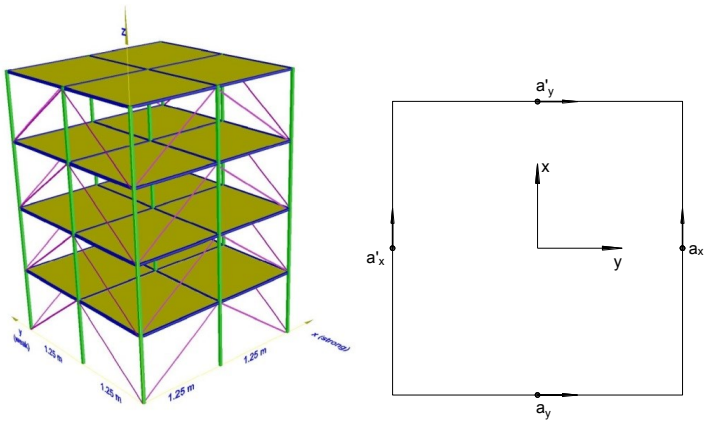

a) b)

Figure 4.2: Illustration of the ASCE Benchmark Structure (a), and Sensor instrumentations (b)

A great amount of researchers have applied their approaches to either the numerical or experimental benchmark problem. Caicedo et al. (2004) employed the Phase I simulated benchmark problem to apply their methodology based on a combined technique, e.g. natural excitation technique, eigensystem realization algorithm, and least squares methods, to calculate the modal properties and estimate the stiffness of the structures. By employing acceleration data and partial knowledge of mass information, researchers can detect the severity and locations of damage. Lynch (2005) introduced a new approach based on the use of the ARX model and transfer function, and their application to the experimental results from the Phase II IASC-ASCE benchmark problem, which was excited by a shaker, showed good results. Transfer function poles are calculated in a traditional method and the migration of transfer function poles are used as damage indicators. However, the requirement of an excitation source makes this method become quite infeasible since it is extremely hard to record the excitation forces in reality. Recently, Zhang el at. (2013) presented a method based on flexibility indices using inter-story deflection and flexibility curvature for damage detection. The advantage of this method is that there is no need to know mass information in order to identify structural flexibility. Two applications in both numerical and experimental IASC-ASCE benchmark structure are shown and damage was successfully identified. Again, one issue similar to the aforementioned method is that a vibration source is also needed. Therefore, the

proposed method can detect, quantify, and localize damage by employing output only data, in this case acceleration, which is easy to obtain in practice.

Simulated data in Phase I of the IASC-ASCE benchmark problem (the 120 DOF finite element model) has been utilized in this study as an application. For this application, a sampling frequency of 1000 Hz has been chosen since it is approximately twice as much as the 25th modal frequency of 481.44 Hz. This sampling frequency means the recorded data can effectively capture up to the 25^{th} frequency mode, which is more than the number of desired modes required in most vibration-based damage detection methods. Filtered Gaussian white noise is employed to model excitation sources and applied at the center of each floor to simulate either wind load or ambient vibrations. Note that excitations are applied to either the x or y direction in order to excite vibration in those directions since structural properties of shear type structures in one direction can only be affected by structural properties in the corresponding direction. Therefore, vibrations in two directions are recorded independently to detect damage in those directions. There are four accelerometers at each floor, with two accelerometers dedicated to each direction (Figure 4.2.b). Similar to the first case study, 10% noise has been added to all acceleration signals to account for environmental and data logger errors. In addition, the average of the two signals monitoring in the same direction is calculated and is used as the input for the model. By using the average values, errors due to noise or imperfections can be minimized. Figure 4.3 shows typical acceleration data in the x-direction at each floor in the baseline case as recorded by the two sensors attached to the x-direction of each floor.

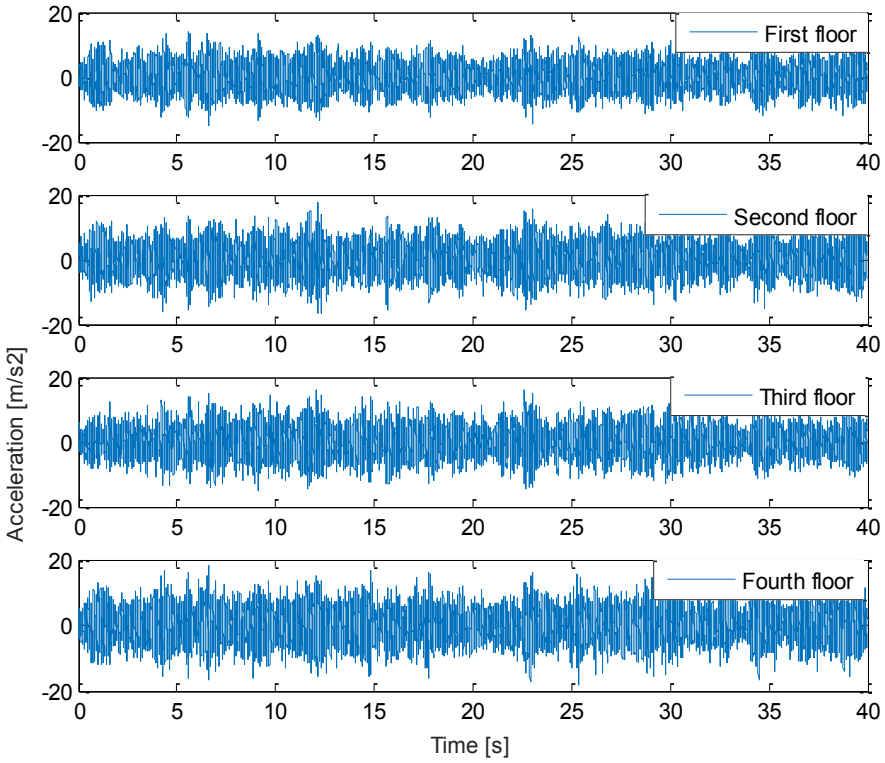

Figure 4.3: Samples of acceleration at each floor in x direction (10% noise added)

There are six damage patterns originally defined by removing different braces (Johnson et al., 2004) to create major damage, minor damage, and asymmetrical damage that mainly focus on stiffness reduction. In addition to those previously defined damage, the authors purposely simulated more damage related to mass reduction in order to demonstrate advantages of the proposed methods. In the following sub-sections, six damage cases in stiffness and two damage cases in mass are introduced accordingly. The eight damage cases are listed below:

- Damage Pattern 1 (DP1): Removal of all braces on the first floor;
- Damage Pattern 2 (DP2): Removal of all braces on the first and third floors;
- Damage Pattern 3 (DP3): Removal of one brace on the first floor;
- Damage Pattern 4 (DP4): Removal of one brace on one side of the first and third floor;
- Damage Pattern 5 (DP5): DP4 + Unscrewing of the left end of the north floor beam of the first floor on the west face of the structure;

- Damage Pattern 6 (DP6): Reduction of the stiffness of a brace to two-third of its original value;
- Damage Pattern M1 (DPM1): Reduction of mass on the fourth floor; and
- Damage Pattern M2 (DPM2): Damage Pattern M1 + Damage Pattern 1.

Note the author purposely created the last two damage patterns in addition to the original damage cases to show the effectiveness of the method in separating the mass change as an operational effect. Again, 10 trials have been generated in each damage case and the damage features are shown as the average of ten trials and the standard deviation (in the parenthesis).

4.2.1 Baseline Case

Similar to the first numerical application, a hundred trials had been tried in this baseline. The results of SDFs and MDFs are shown in Table 4.12

Table 4.12: DFs in Percent for BC

Direction	Ref Channel	1st	2nd	3rd	4th
x direction	1st	-0.01 (0.18)	-0.06 (0.58)	N/A	N/A
	2nd	0.11 (0.44)	-0.18 (0.23)	0.03 (0.41)	N/A
	3rd	N/A	0.01 (0.36)	0.1 (0.25)	-0.07 (0.38)
	4th	N/A	N/A	-0.04 (0.33)	0.08 (0.3)
	MDFs	0.17 (0.93)	-0.09 (0.77)	0.03 (0.62)	-0.02 (0.62)
y direction	1st	-0.02 (0.24)	-0.33 (0.73)	N/A	N/A
	2nd	0.06 (0.58)	-0.04 (0.29)	0.49 (0.5)	N/A
	3rd	N/A	-0.3 (0.47)	0.21 (0.3)	-0.25 (0.45)
	4th	N/A	N/A	0.14 (0.48)	-0.2 (0.32)
	MDFs	0.4 (1.1)	-0.59 (0.98)	0.6 (0.88)	-0.39 (0.86)

As can been seen from the results, the average values of SDFs and MDFs are relatively small. However, standard deviation is quite higher than the corresponding mean value, indicating the computed damage features deviate quite greatly from their mean values. The highest standard deviation of SDFs and MDFs are 0.73% and 0.98% respectively. Therefore, it is decided that these numbers would be the sensitivity of the methodology for this specific application. After trying different trials, the author decided that 10 trials would be appropriate for the application since the results did not change much when increasing the number of trials to more than 10.

4.2.2 Damage Pattern 1: All Braces of the First Floor are Broken

Removal of all braces at the first floor was chosen as a simulation of stiffness damage of this floor in both directions. This scenario features acceleration in all directions in order to detect damage in the corresponding directions. The DFs calculated are shown in Table 4.13 where each row of the SDFs represents one sensor cluster, whereas each column of the MDFs (the last row) represents the corresponding floor or DOF. SDF_{11} in both *x* and *y* directions show large changes at -24.65% and -36.7%, which are almost exactly the percentages of the actual damage that happened (-22.60% and -35.51% in *x* and *y* directions Johnson et al. [2004]) in the structure. No significant changes are found at the other SDFs entries since damage affects only the first floor.

Table 4.13: DFs in Percent for Damage Pattern 1

Direction	Ref Channel	1st	2nd	3rd	4th
x direction	1st	-24.65 (0.04)	0.17 (0.28)	N/A	N/A
	2nd	-0.05 (0.11)	-0.15 (0.04)	1.53 (0.27)	N/A
	3rd	N/A	0.07 (0.08)	-0.78 (0.07)	-1.27 (0.17)
	4th	N/A	N/A	-0.23 (0.14)	0.38 (0.17)
	MDFs	-0.22 (0.33)	-0.6 (0.32)	1.25 (0.3)	-1.04 (0.29)
y direction	1st	-36.7 (0.09)	-0.03 (0.18)	N/A	N/A
	2nd	1.68 (0.15)	0.13 (0.12)	-0.04 (0.2)	N/A
	3rd	N/A	-0.01 (0.24)	0.13 (0.09)	0.03 (0.17)
	4th	N/A	N/A	-1.03 (0.19)	-0.88 (0.14)
	MDFs	1.71 (0.27)	-0.82 (0.32)	-0.55 (0.33)	1.07 (0.31)

MDFs were also constructed and are shown in Table 4.13. As expected, the MDFs values show no remarkable changes since there are no changes in the mass of the structure. Some entries with positive false errors at slightly high values, e.g. 1.5%, appear because of the noise added to all signals to simulate more realistic data.

4.2.3 Damage Pattern 2: All Braces of the First and Third Floor are Broken

This stiffness damage involves two positions at the first and third floor of the structure. Therefore, non-zero values at the entries related to these floors would be shown in the SDFs. As observed in Table 4.14, SDF_{11} in the two directions have values at -23.8% and -37.05%, respectively. These are similar to the values in the previous damage pattern, thereby indicating the same damage at the first floor has been discovered (all braces on

this floor have been removed). In addition, SDFs between the second and third floor show us how influential the removal of all braces between these floors are. The total stiffness reduction in the x-direction at the second and third floors can be found based on the SDF_{33} and $SDF_{44,}$ e.g. -25.52% and -29.44%, respectively. On the other hand, this damage has made a reduction in stiffness between the second and the third floor of approximately 50%. Again, the other entries in the SDFs in *x* direction are not exactly zero, mostly because of the 10% noise addition. Those errors can be seen as false positives since they do not affect the entries where damage has actually happened. It is acknowledged that threshold values should be defined based on statistical analysis in order to minimize effects of such errors (Gul & Catbas, 2009). Regarding the SDFs in the *y* direction, they followed the same pattern as their x-direction counterpart. The only difference is that the severity of SDFs at damaged positions is greater since this direction is weaker than the *x* direction is.

Table 4.14: DFs in Percent for Damage Pattern 2

Direction	Ref Channel	1st	2nd	3rd	4th
x direction	1st	-23.8 (0.09)	0.81 (0.35)	N/A	N/A
	2nd	-2.7 (0.14)	-25.52 (0.09)	-49.69 (0.18)	N/A
	3rd	N/A	-49.25 (0.14)	-29.44 (0.06)	-5.01 (0.13)
	4th	N/A	N/A	0.87 (0.18)	1.08 (0.11)
	MDFs	-3.48 (0.4)	2.24 (0.42)	2.67 (0.36)	-4.84 (0.28)
y direction	1st	-37.05 (0.12)	0.84 (0.25)	N/A	N/A
	2nd	0.11 (0.19)	-37.56 (0.09)	-73.64 (0.13)	N/A
	3rd	N/A	-74.03 (0.18)	-39.3 (0.1)	-3.53 (0.21)
	4th	N/A	N/A	-1.64 (0.18)	-1.69 (0.11)
	MDFs	-0.73 (0.34)	-0.36 (0.63)	1.72 (0.67)	-1.92 (0.37)

Considering the MDFs in both directions (Table 4.14), no high values are found in MDFs, which is reasonable since there is actually no damage in the mass of the structure. Although some relatively high errors continued to exist in Table 4.14, those are not systematic errors since they only showed up in this damage pattern.

4.2.4 Damage Pattern 3: One Brace of the First Floor is Broken

One brace at the first floor in *y* direction was removed in this damage pattern. In this case, the damage is insignificant compared with the previous cases and it is expected that SDFs in x-direction would be nearly zero since damage in the *y* direction clearly does not influence the stiffness in the *x* direction. Table 4.15 shows that no large changes were found in the SDFs in the *x* direction, whereas the $SDF_{11,y}$ value of -10.66% suggests a deterioration in the stiffness at the first floor, and it is ¼ as much as it was in the Damage Pattern 1. Examining in more detail, this value is reasonable since there are four braces in at each floor in one direction and one brace should account for ¼ the total stiffness of all braces. MDFs in Table 4.15 have small values showing that there was no mass damage occurring in this damage pattern.

Table 4.15: DFs in Percent for Damage Pattern 3

Direction	Ref Channel	1st	2nd	3rd	4th
x direction	1st	0.01 (0.11)	-0.04 (0.32)	N/A	N/A
	2nd	0.07 (0.13)	-0.04 (0.08)	0.21 (0.27)	N/A
	3rd	N/A	-0.06 (0.17)	0.03 (0.11)	-0.03 (0.14)
	4th	N/A	N/A	0 (0.15)	-0.02 (0.06)
	MDFs	0.11 (0.34)	-0.19 (0.36)	0.15 (0.31)	-0.03 (0.23)
y direction	1st	-10.66 (0.1)	-0.7 (0.22)	N/A	N/A
	2nd	1.09 (0.25)	-0.22 (0.12)	-0.89 (0.28)	N/A
	3rd	N/A	0.02 (0.17)	0.06 (0.12)	0.43 (0.14)
	4th	N/A	N/A	-0.22 (0.1)	-0.85 (0.09)
	MDFs	1.8 (0.4)	-0.42 (0.39)	-0.78 (0.29)	0.65 (0.2)

4.2.5 Damage Pattern 4: One Brace for Each of the First Floor and Third Floor is Broken

It is expected that SDFs related to the first and third floor in either the x or y directions show high values since damage occurred on those floors. Also, removal of only one brace in the first and third floor results in asymmetrical effects in the structure. In fact, SDFs in the *x* direction show damage around the second and third floor, whereas damage in the first floor has been discovered in the *y* direction (Table 4.16). On the other hand, no significant changes are found in the MDFs, demonstrating that there are no changes in

mass. These results demonstrate that the method can effectively locate damage even in the case where the structure is asymmetrical.

Table 4.16: DFs in Percent for Damage Pattern 4

Direction	Ref Channel	1st	2nd	3rd	4th
x direction	1st	-0.49 (0.09)	0.44 (0.24)	N/A	N/A
	2nd	-0.74 (0.2)	-7.82 (0.07)	-15.05 (0.38)	N/A
	3rd	N/A	-13.94 (0.15)	-7.64 (0.08)	0.33 (0.13)
	4th	N/A	N/A	0.01 (0.14)	-0.07 (0.09)
	MDFs	-1.17 (0.34)	1.25 (0.45)	-0.81 (0.38)	0.32 (0.24)
y direction	1st	-10.8 (0.09)	-0.93 (0.19)	N/A	N/A
	2nd	1.24 (0.23)	-0.15 (0.08)	-0.87 (0.2)	N/A
	3rd	N/A	-0.02 (0.23)	0.05 (0.08)	0.53 (0.06)
	4th	N/A	N/A	-0.14 (0.21)	-0.78 (0.13)
	MDFs	2.19 (0.39)	-0.64 (0.35)	-0.75 (0.27)	0.66 (0.22)

4.2.6 Damage Pattern 5: Damage Pattern 4 + Unscrewing of Left End of North Floor Beam, at First Floor on West Face of Structure

This simulated case stipulates that only one end of the beam on the first floor was unscrewed when combined with Damage Pattern 4. As shown in Table 4.17, the SDFs in both directions have values almost the same as those in Table 4.16, thus indicating that Damage Pattern 4 has been successfully detected and quantified. However, the unscrewing problem was not detected because of the difference in the stiffness matrices between the baseline, and the unscrewing damage was observed to be insignificant (Johnson et al., 2004). The method is therefore still effective since unscrewed damage has not noticeably changed the overall stiffness of the model. On the other hand, the MDFs revealed approximately zero values since there was no change in mass in both directions.

Table 4.17: DFs in Percent for Damage Pattern 5

Direction	Ref Channel	1st	2nd	3rd	4th
x direction	1st	-0.55 (0.09)	0.43 (0.32)	N/A	N/A
	2nd	-0.58 (0.17)	-7.84 (0.07)	-14.71 (0.27)	N/A
	3rd	N/A	-14.04 (0.17)	-7.59 (0.09)	0.17 (0.14)
	4th	N/A	N/A	0.08 (0.21)	-0.08 (0.15)
	MDFs	-1 (0.42)	0.9 (0.42)	-0.43 (0.37)	0.09 (0.33)
y direction	1st	-10.8 (0.09)	-0.93 (0.19)	N/A	N/A
	2nd	1.24 (0.23)	-0.15 (0.08)	-0.87 (0.2)	N/A
	3rd	N/A	-0.02 (0.23)	0.05 (0.08)	0.53 (0.06)
	4th	N/A	N/A	-0.14 (0.21)	-0.78 (0.13)
	MDFs	2.19 (0.39)	-0.64 (0.35)	-0.75 (0.27)	0.66 (0.22)

4.2.7 Damage Pattern 6: Area of One Brace on One Side of the First Storey is Reduced to 2/3

This damage pattern is similar to Damage Pattern 3 where one brace at the first floor is broken. Instead, however, one brace's stiffness is reduced by 1/3 its original strength in this case. Therefore, the SDFs are expected to show similar pattern as those shown in Damage Pattern 3, but with lower magnitudes. As Table 4.18 shows, the SDFs in the x-direction have quite small values that indicate that there is no damage in this direction. In addition, -3.1% is the value at $SDFs_{11,y,}$ signalling that approximately 3% stiffness reduction has occurred in the first floor. By comparison, this value is meaningful since it is almost 1/3 as much as it was in Damage Pattern 3 (-10.66%), that is, the exact amount of stiffness reduction (the brace reduced by 1/3 its stiffness). The other SDFs entries in the y-direction are close to zero and thus indicate that no other damage has occurred. Again, in this case, no changes have been shown in the MDFs, demonstrating that the mass remained unchanged.

Table 4.18: SDFs in Percent for Damage Pattern 6

Direction	Ref Channel	1st	2nd	3rd	4th
x direction	1st	0.01 (0.09)	0 (0.35)	N/A	N/A
	2nd	-0.04 (0.16)	0.02 (0.07)	-0.1 (0.37)	N/A
	3rd	N/A	0.09 (0.19)	-0.01 (0.08)	0.06 (0.15)
	4th	N/A	N/A	-0.07 (0.14)	-0.01 (0.09)
	MDFs	-0.03 (0.44)	0.12 (0.48)	-0.16 (0.38)	0.13 (0.24)
y direction	1st	-3.1 (0.1)	-0.16 (0.3)	N/A	N/A
	2nd	-0.05 (0.22)	0.03 (0.09)	0 (0.2)	N/A
	3rd	N/A	0.21 (0.19)	0.01 (0.06)	0.14 (0.15)
	4th	N/A	N/A	0.11 (0.2)	-0.03 (0.09)
	MDFs	0.11 (0.43)	0.06 (0.35)	-0.12 (0.3)	0.03 (0.32)

4.2.8 Damage Pattern M1: Mass of the Fourth Floor is Reduced by 20%

This modelling is the first time in this case study that damage in mass has been created with 20% reduction at the fourth floor in order to validate the methodology's ability of indicating mass damage separately. It can be clearly concluded that no stiffness reduction has been found since the SDFs in both directions are unnoticeable (Table 4.19). There are, however, some changes in the MDFs easily seen in Table 4.19, where the MDF_4 values in both directions are relatively equal at -21.68% and -19.53%, respectively. Surprisingly, these values are almost the same as the mount of mass reduction (20%) in the fourth floor. Therefore, it is proved that the method is successful in separately detecting and quantifying the damage in mass and stiffness as well.

Table 4.19: DFs in Percent for Damage Pattern M1

Direction	Ref Channel	1st	2nd	3rd	4th
x direction	1st	-0.58 (0.08)	-0.09 (0.41)	N/A	N/A
	2nd	-0.7 (0.13)	-0.06 (0.1)	0.56 (0.33)	N/A
	3rd	N/A	0.9 (0.14)	-0.11 (0.09)	-1.07 (0.17)
	4th	N/A	N/A	-1.07 (0.17)	-1.17 (0.39)
	MDFs	-0.61 (0.52)	0.48 (0.47)	-0.17 (0.21)	-21.68 (0.26)
y direction	1st	-1.12 (0.06)	-0.25 (0.39)	N/A	N/A
	2nd	1.24 (0.27)	-0.27 (0.06)	-1.09 (0.3)	N/A
	3rd	N/A	-0.65 (0.18)	-0.75 (0.12)	-0.01 (0.17)
	4th	N/A	N/A	-0.01 (0.17)	-0.81 (0.36)
	MDFs	1.49 (0.57)	-0.51 (0.48)	-0.22 (0.21)	-19.53 (0.23)

4.2.9 Damage Pattern M2: Damage Pattern 1 + Damage Pattern M1

The above sections have demonstrated that the proposed approach can indicate the mass and stiffness changes based on the MDFs and SDFs values, respectively. However, those sections only showed that the method worked effectively when either mass or stiffness changed in the structure. Therefore, this section introduces a combined damage in both mass and stiffness based on the removal of all braces at the first floor (Damage Pattern 1) and 20% mass reduction at the fourth floor (Damage Pattern M1). The purpose of this section is to show the method's capability of evaluating both mass and stiffness damage in a more complicated scenario, in this case simultaneous damage. The results of stiffness damage features are demonstrated in Table 4.20. The $SDFs_{11,x}$ and $SDFs_{11,y}$ are close to the corresponding values shown in Table 4.3. This approximation indicates that damage in the stiffness was successfully discovered. Similarly, changes in mass can be found in the same Table where the fourth column entries contain almost the same values as those in Table 4.19, which means, again, mass damage has been revealed exactly.

Table 4.20: SDFs in Percent for Damage Pattern M2

Direction	Ref Channel	1st	2nd	3rd	4th
x direction	1st	-24 (0.1)	-1.07 (0.27)	N/A	N/A
	2nd	-0.84 (0.12)	0.26 (0.05)	0.69 (0.34)	N/A
	3rd	N/A	0.51 (0.18)	-0.41 (0.11)	-1.79 (0.13)
	4th	N/A	N/A	-1.79 (0.13)	-0.22 (0.15)
	MDFs	0.23 (0.34)	-0.2 (0.38)	0.09 (0.21)	-20.97 (0.11)
y direction	1st	-36.93 (0.06)	-0.07 (0.2)	N/A	N/A
	2nd	1.07 (0.22)	-1 (0.1)	-0.37 (0.27)	N/A
	3rd	N/A	-1.05 (0.3)	-0.32 (0.18)	-1.09 (0.21)
	4th	N/A	N/A	-1.09 (0.21)	-1.14 (0.39)
	MDFs	1.14 (0.37)	-0.9 (0.42)	0.34 (0.24)	-20.06 (0.28)

4.3 Discussion of Numerical Results

The results from two numerical applications were very promising. The location and severity of damage were identified correctly, although minor errors appeared in some cases due to the effects of noise and the numerical system itself. In general, there are some points of limitations that need to be discussed from the numerical case studies:

- Based on 100 trials in the baseline of each case study, the sensitivity of the methodology for the two specific applications herein vary up to 2.1%.
- According to the definition of Rytter (1993), the method has reached level 3 of damage detection, the determination of damage's severity. In addition, the methodology can localize damage in a global manner rather than a local manner. In other words, the methodology cannot locate exactly which structural components experienced damage, although the floors with damage can be identified.
- As can be seen in the methodology, stiffness and mass information before and after damage are shown as the relative differences among DOFs. As a result, the severity of damage is defined as the relative change instead of absolute change. Therefore, the proposed method may not work for absolute bracing systems where stiffness is dependent throughout the whole systems and for one DOF system as well.

CHAPTER 5:EXPERIMENTAL VALIDATION

In the previous study conducted by Mei (2014), a new technique was proposed for damage detection. However, their applications were limited in numerical studies. Therefore, in addition to developing separate SDFs and MDFs, other major contributions of this thesis are the experimental verifications of the proposed methodology and validation of the work conducted by Mei (2014).

5.1 Preliminary Design

An experimental study has been conducted in order to demonstrate the proposed method with experimental data. Since the methodology is applicable to shear-type structures in the current form (improvement of the methodology for other structures such as bridges is planned as future work), the authors aim to create a simple shear-type structure with several stories made from steel. The main objective of the experimental part is that it is designed for the goal of damage detection and operational effect elimination (mass changes). After careful consideration, a laboratory scale four-storey structure was chosen for experimental validation of this paper's method.

The experimental system is constructed from symmetric angle sections and steel plates connected together by brackets. The height of each floor is 0.4 m and the floor area is 0.4m x 0.4m (Figure 5.1). The column sections L $1\frac{1}{4} \times 1\frac{1}{4} \times \frac{3}{16}$" are chosen as the baseline case of the structure. In this structure the columns are not continuous from the base to the fourth storey. Instead, they are constructed separately at each floor in order to simulate damage easily at different floors by replacing columns with either different cross sections or material properties. The columns are fastened at each end with four 5/16" bolts. The brackets used are L$1\frac{3}{4} \times 1\ \frac{3}{4} \times \frac{3}{16}$" angles welded to the steel slabs. For the foundation, we decided that the bottom columns are connected to a steel slab from which the whole structure is clamped to the concrete floor of the lab using bolt connections. Details of the support can be found in the next sections of this chapter.

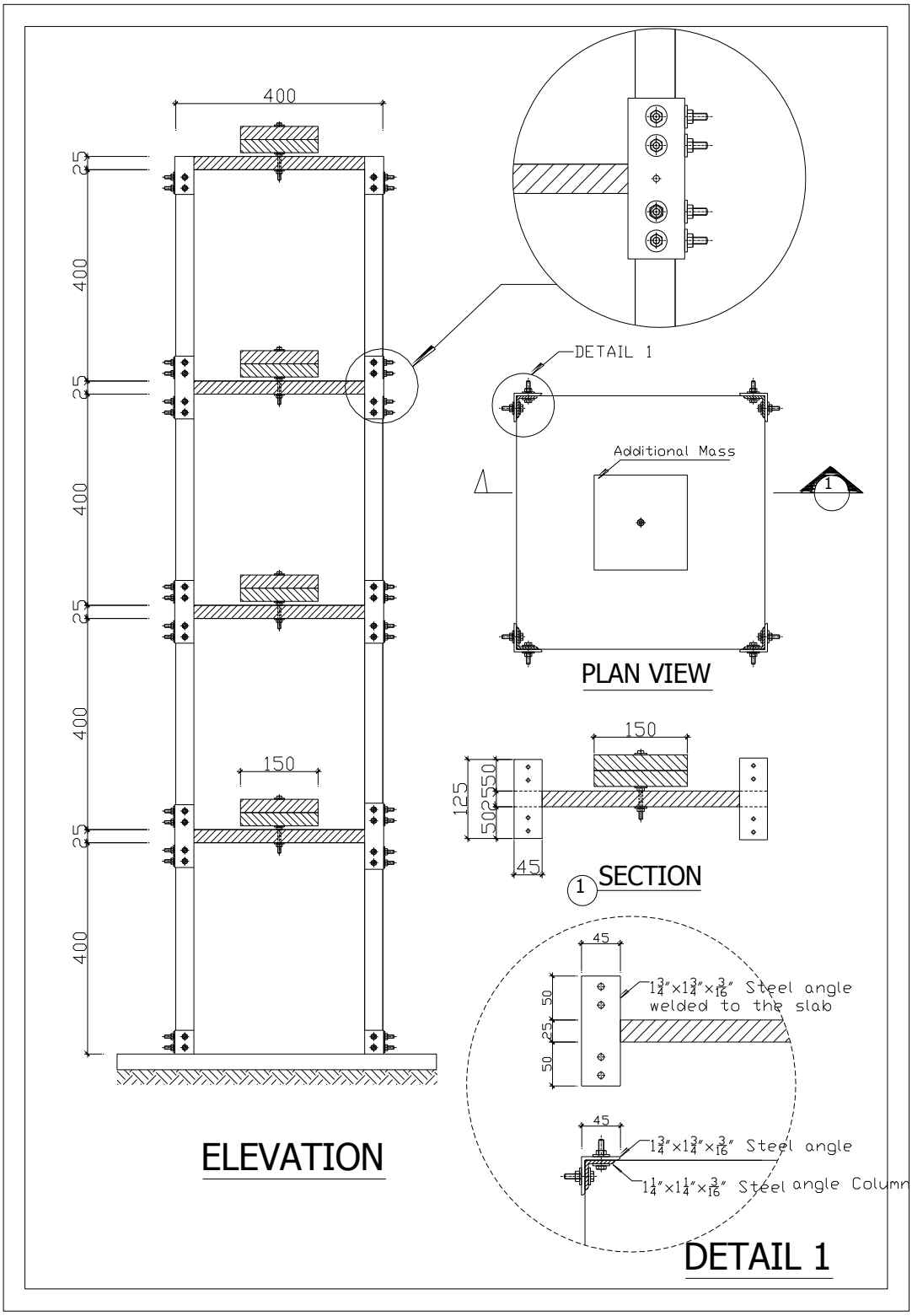

Figure 5.1. Elevation view and connection details of the structure (all dimensions in mm)

Operational effects are also simulated using a 150×150×24.5 mm lumped mass weighing 4.5 kg made from the same material used for the steel slabs. The lumped mass blocks are attached to the slabs using bolt connections. Note that the lumped mass is installed in such a way that the slabs and lumped mass act as the same body to ensure the consistent response of the whole structure. Plan view and connector details are depicted in Figure 5.1.

5.2 Finite Element Analysis

The geometric configuration of the structure was first analyzed in the finite element software SAP2000. The purpose of this step is to confirm that the structure behaves like a shear-type structure and vibration data from different damage simulation is also recorded from which the methodology can be applied. The model has the following dimensions: area elements size is adopted to be 0.05m, and frame elements have maximum dimension of 0.1m. Since the structure is symmetric in geometry, the orientation of the frame is the same in all dimensions (Figure 5.2).

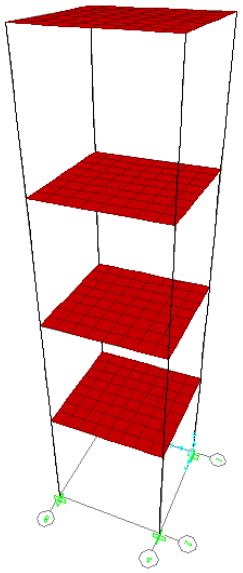

Figure 5.2. Finite element model of the structure

The structure is supported by four fixed supports with all translational and rotational DOFs restrained. Because the model is considered as symmetric, we analyzed only in-

plane vibration (X-Z plane). Lateral acceleration data was collected at four joints (channels) located at the column-slab connection joints at each floor.

The model is initially excited by two pairs of multiple impulse forces located at the two corners of the first and third floor. The reason for using multiple impulse forces is that this kind of force can be easily actuated by using impact hammers or fingertips. A sample of applied force is shown in Figure 5.3:

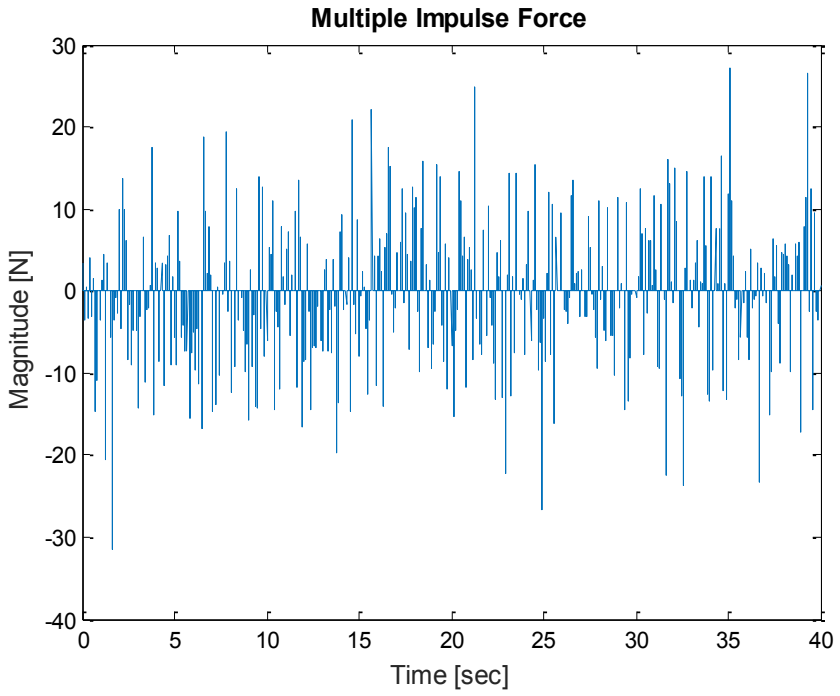

Figure 5.3. Multiple Impulse Force Sample

The first step of the finite element analysis is the modal analysis that includes the calculation of modal parameters such as natural frequencies and mode shapes, which are the basis to confirm shear-type behaviour of the structure. An Eigenvector method is used for this step and a constant damping ratio of 2% was adopted for all analysis. Again, acceleration data is recorded at the four channels mentioned above at the sampling frequency of 1000 Hz.

The first natural frequency was found to be 14.99 Hz, which is quite close to the first natural frequency in the weak direction of the Phase-I IASC-ASCE benchmark problem, which was 11.79 Hz in y direction (Johnson et al., 2004). This comparison helps confirm

the appropriate choice of this type of structure over other experimental structures in the literature.

Mode shapes are investigated in order to ensure that the rotational mode of the slab is small compared with the translational modes. It can be seen from Figure 5.4 that the first 4 mode shapes of the structure confirm its shear-type behaviour since rotational modes of the slabs are much smaller than the translational modes and are almost zero.

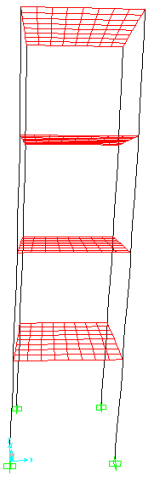

a) Mode 1 (f =12.61 Hz)

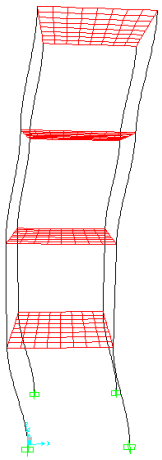

b) Mode 2 (f = 41.44 Hz)

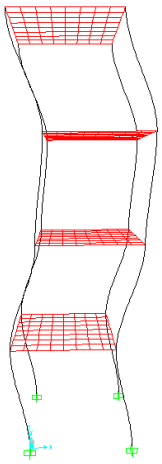

c) Mode 3 (f = 63.33 Hz)

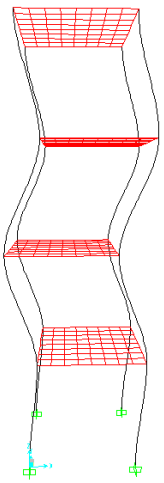

d) Mode 4 (f = f = 95.06 Hz)

Figure 5.4 . Mode shapes identified from the finite element model

After the assessment of modal parameters, acceleration at four points corresponding to the 4 DOFs of the structure mentioned previously is collected and used as the inputs of the proposed method. Different damage scenarios were applied in order to confirm two objectives: 1) the validation of the methodology using simulated data and 2) the feasibility of the chosen sections and material for damage simulation in the lab later on. Overall, the current geometric configurations showed reasonable results in both the computed Damage Feature and the ease of fabrication. Due to the thesis page limit, damage features of different simulated damage cases are not shown here.

5.3 Construction

After successfully simulating the structure using SAP2000, there is greater confidence that the structure fits experimental needs with the chosen configurations. Thanks to the cooperation of the technologists in the University's Structural Lab, the physical work to construct the experimental structure was complete in two weeks. Once the material arrived, it was cut into small species to form columns, slabs, and lumped mass, as shown in Figure 5.5.

a)

b)

c)

d)

Figure 5.5. Steel components: a) Columns; b) Slabs; c) Lumped mass; d) Brackets

Subsequently, 360 holes were drilled on all columns and brackets in order to create connections among the columns and slabs. Careful measurement is required since the holes on the species need to be aligned well so that bolts can get through. The process of drilling and tapping is shown in Figure 5.6.

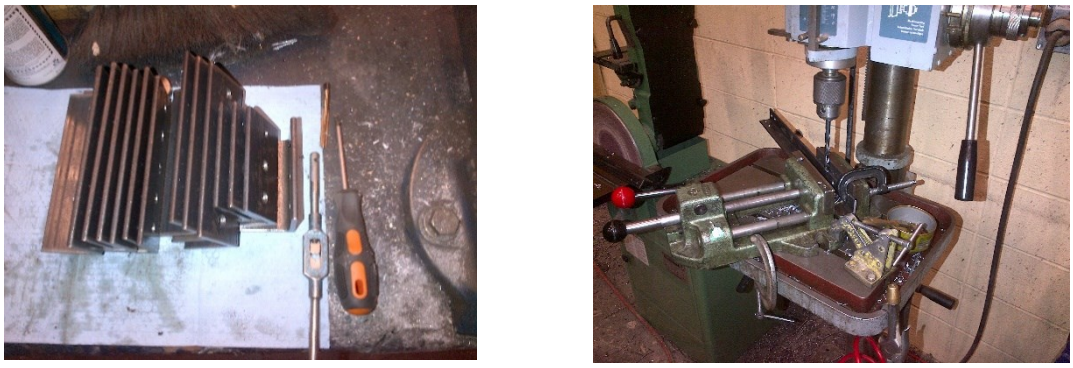

Figure 5.6. Drilling and tapping process

After all steel components are prepared, they are erected to form the final test structure. It is mentioned above that the supports are chosen to be fixed. Therefore, the whole structure is connected to a steel slab at the bottom column where an HSS beam of 1.2 m length clamps the structure to the concrete floor using bolt connections. Thus, with this connection, the fixed supports can be created with confidence. Details of the structure and end connections are shown in Figure 5.7. As can be seen, the Baseline case of the structure is chosen as follows: two lumped masses at the first floor, one lumped mass at the third and fourth floor, and no mass at the second floor.

a) b)

Figure 5.7. Elevation view of the test system: a) North-South; b) East-West direction

5.4 Development of Monitoring System

In this section, the design of a continuous monitoring system is introduced. The main purpose is to create a rugged and reliable system to acquire acceleration data at each floor.

5.4.1 Accelerometers

Integrated Electronics Piezoelectric (IEPE) uniaxial accelerometers from the PCB model 393A03 were selected as the vibration sensors. The sensor possesses a sensitivity of 1000 mV/g, a frequency range of 0.5 to 2000 Hz, a light weight of 210 grams, and a moderate size (30.2×56.1 mm). Integrated signal conditioning is a beneficial feature of this type of sensor due to the properties of piezoelectric material built inside it. The sensors have an operating temperature range from -54 to $+121^0$C. They are waterproof depending on the

cable used, an advantage for outdoor monitoring, although this feature may not be applied in the test. The sensors were mounted on the structure using a metal/concrete epoxy via mounting pads provided from PCB. The sensor placements are shown in Figure 5.8. It is worth noting that only data from four sensors mounted at the center of each floor is used for the analysis and data from the fifth sensor installed at the corner of the highest floor is used only to check whether there is vibration in the corresponding direction when the force is applied in the other direction.

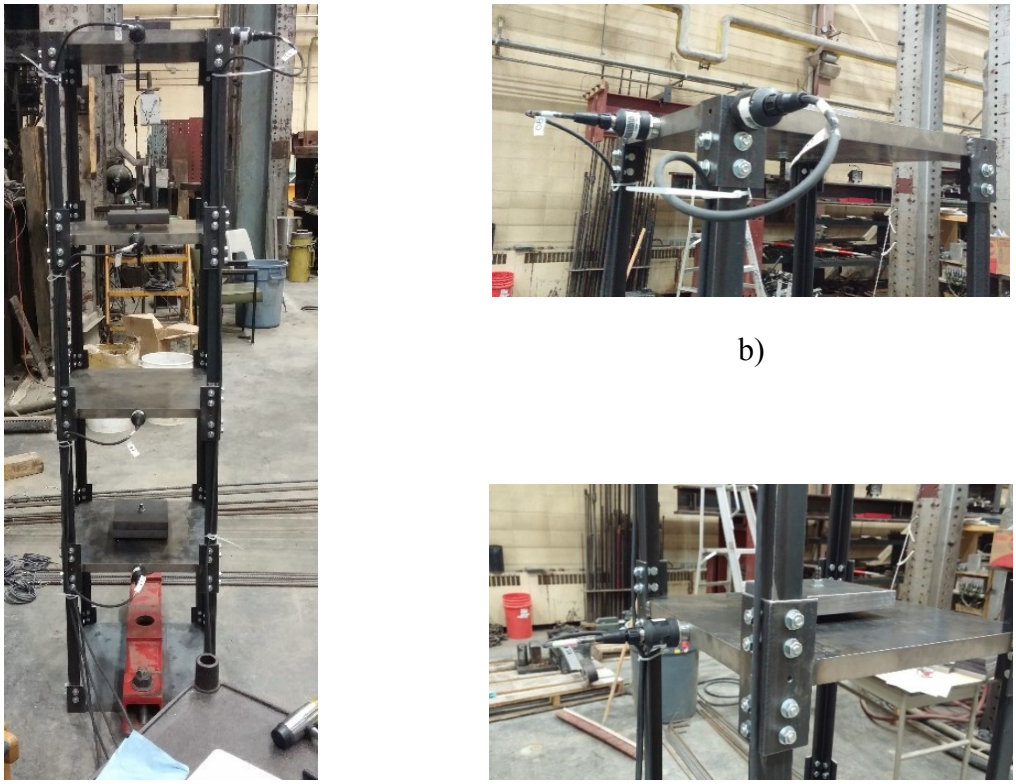

a) b) c)

Figure 5.8. Sensor layout

5.4.2 Data Acquisition

The components of the Data Acquisition system are all manufactured by National Instruments (NI). The core component of the acquisition system is the NI cRIO-9074 chassis that possesses a Field Programmable Gate Array (FPGA) chip that allows users to customize the chip with relative ease and speed. Fast and reliable performance is why FPGA-type chassis has been recently gaining momentum. The chassis has a 500 MB solid-state storage drive, eight slots for the installation of NI cRIO modules, two Ethernet ports for computer connections, and an operating temperature range from -20 to +55^{o}C. Details of the chassis can be found in Figure 5.9.

Figure 5.9. Chassis NI 9074

To acquire the analog signal from accelerometers, two National Instruments: NI-9234 (Figure 5.10) 24-bit Integrated Electronics PiezoElectric (IEPE) input modules are employed. Each module can simultaneously monitor four accelerometers with a wide range of sampling frequency that users can choose from, up to a maximum of 51.2 kHz. Software-selectable options include IEPE signal conditioning with anti-aliasing filters. One major advantage of this module is that it possesses a built-in amplifier for the accelerometer signal, which means an external amplifier is not needed. This module has an operating temperature between -40 and +70^{o}C.

Figure 5.10. NI 9234 Module (Picture adopted from NI website)

The cRIO-9074 chassis and NI modules need to be programmed before use. National Instruments provides users the LabVIEW software (Figure 5.11a) with the RealTime and FPGA add-ins in order to design flexible systems that can be customized by users. First, the cRIO Reference Project available at www.ni.com was utilized as the starting point to develop the monitoring system. Then I undertook a more intensive development in order to fulfill the specific requirements of the SHM system in the experiment.

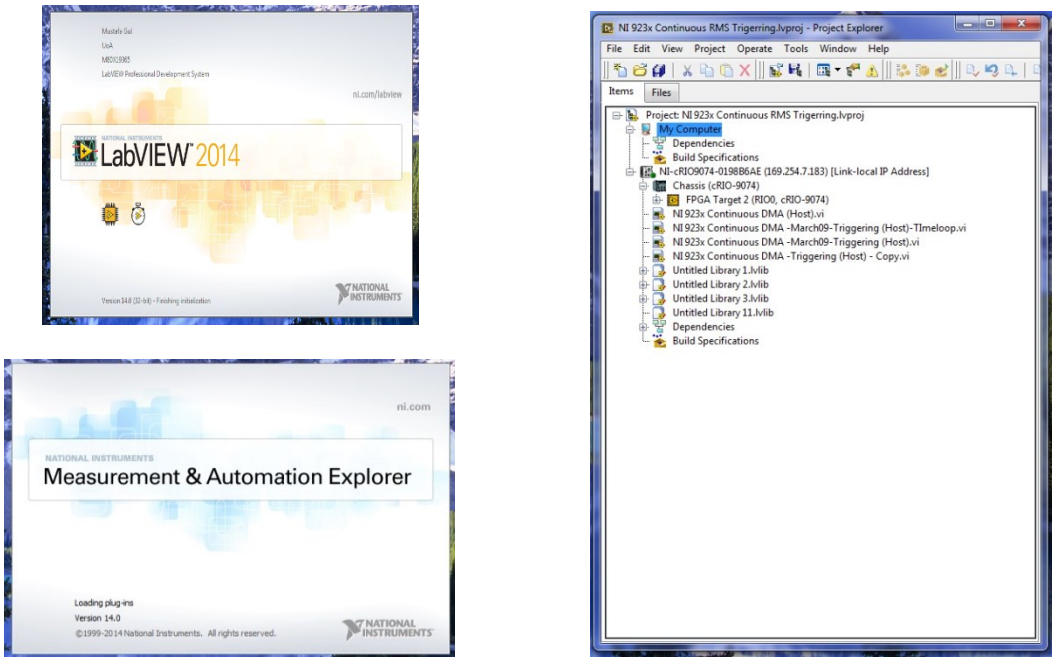

a) b)

Figure 5.11. LabVIEW software (a); and Monitoring Project (b)

Generally, LabVIEW provides us with two interfaces, namely the Block Diagram and the Front Panel. In block diagram mode, users can compile comments or code in order to program the requirements of the system. On the other hand, the front panel is the user interface tool where users can operate and control the monitoring system without much knowledge of LabVIEW programming. The system is programmed to continuously acquire acceleration at the sampling rate of 1652 Hz. The authors purposely program the project to save data of different time durations depending on the measurement time required. In this specific experiment, we decided that 1 minute of data is reasonable for the analysis. In addition, a triggering condition is generated in the monitoring program that begins saving a new set of data once the amplitude of a signal exceeds 0.01 m/s^2 RMS value in one second. Aside from automatic triggering, users can manually force the monitoring system to save data at any time.

The final user interface is shown in the front panel (Figure 5.12). The graph shows real-time data recorded from the five accelerometer sensors at the center; users can choose the sampling frequency at the top corner of the front panel. Also, users can visually see when the triggering condition is reached as the Boolean indicator begins flashing. In addition, the error indicators located at the right of the front panel can help users easily find errors occurring in the acquisition system.

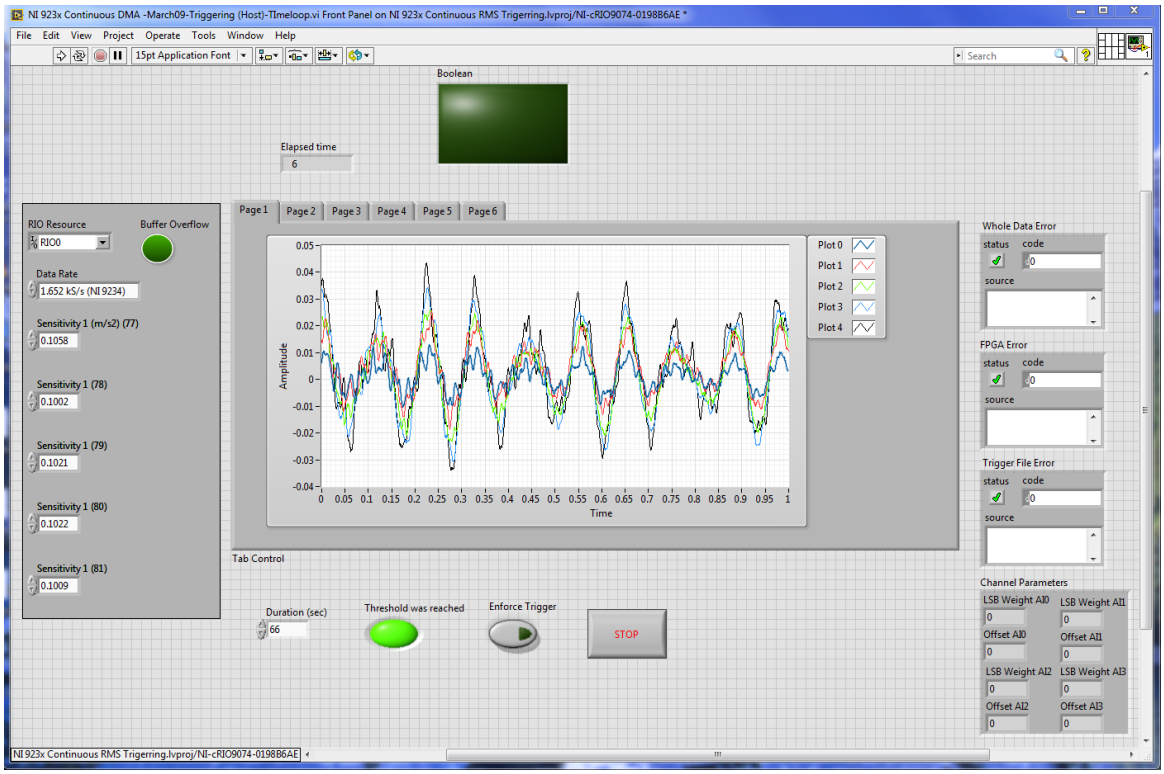

Figure 5.12. Front Panel (User Interface) of the Acquisition system

5.4.3 Communication

The cRIO-9074 communicates with the host computer via an Ethernet cable in the current configuration. However, it can wirelessly communicate with the host computer as well. File transfer with the FTP capabilities of WinSCP is used as the main tool to manage and transfer recorded data from the chassis to the host computer.

CHAPTER 6: DAMANGE SIMULATIONS AND RESUTLS

6.1 Baseline case (BC)

As discussed previously, the baseline case of the structure was configured as shown in Figure 5.7. The test structure can be simplified as a 4 DOF system where the stiffness k_1 to k_4 is the columns' stiffness at each floor and the mass is assumed to be lump mass along the stories. Ideally, we can write the stiffness and mass matrix of the structure as the following equations:

$$K = \begin{bmatrix} K_{11} & K_{12} & K_{13} & K_{14} \\ K_{21} & K_{22} & K_{23} & K_{24} \\ K_{31} & K_{32} & K_{33} & K_{34} \\ K_{41} & K_{42} & K_{43} & K_{44} \end{bmatrix} = \begin{bmatrix} k_1 + k_2 & -k_2 & 0 & 0 \\ -k_2 & k_2 + k_3 & -k_3 & 0 \\ 0 & -k_3 & k_3 + k_4 & -k_4 \\ 0 & 0 & -k_4 & k_4 \end{bmatrix} \tag{3.24}$$

$$M = \begin{bmatrix} m_{11} & 0 & 0 & 0 \\ 0 & m_{22} & 0 & 0 \\ 0 & 0 & m_{33} & 0 \\ 0 & 0 & 0 & m_{44} \end{bmatrix} \tag{3.25}$$

Overall, the test was conducted by two students who used either hammers or hands to excite the structure. The purpose of conducting the test with two students is that the authors want to show that using different experimenters does not have a large effect on the Damage Features calculated based on the methodology. For the baseline case and some damage cases, two students conducted independent tests on the structure and 1-minute data length was recorded. All data were compared to examine differences in results due to different experimenters. For each damage case, 10 one-minute trials were conducted and the Damage Features shown are the average of 10 tests. Also, in order to

show the variation of the results, standard deviation is provided in the parenthesis along with the average values.

The first student (Ngoan Do) conducted the baseline case and the typical vibration levels appear in Figure 6.1.

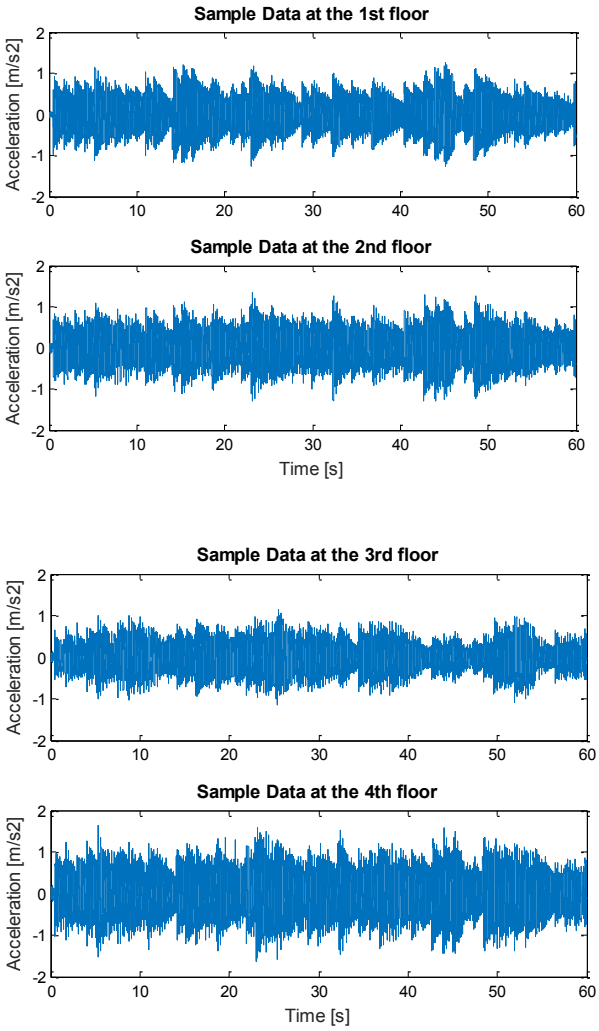

Figure 6.1: Typical acceleration at four floors

Frequency analysis was first conducted in order to confirm the agreement between the experimental structural and its numerical sap model. Table 6.1 shows the difference between frequencies defined from the sap model and the corresponding experimental one.

As can be seen, the sap model is able to simulate the natural frequencies of the experimental structure since the difference in the natural frequencies is reasonable.

Table 6.1. Comparison of Fundamental Frequencies

Frequency	Model	Experiment	Difference (%)
1st	12.61	12.91	2.36
2nd	41.44	41.95	1.21
3rd	63.33	68.97	8.18
4th	95.06	97.6	2.61

Table 6.2 and Table 6.3 contain the results of SDFs and MDFs. It is mentioned previously that SFDs at each entry represents the corresponding DOF of the structure. As can be seen, the DFs in both Tables show very small changes (approximately zero at all DOFs) which is as expected since the two data sets being compared come from the same state of the structure.

Table 6.2. SDFs for BC (Average and Standard Deviation of 10 Trials in Percent)

Ref Channel	1st	2nd	3rd	4th
1st	-0.08 (0.56)	-0.36 (1.49)	N/A	N/A
2nd	0.22 (1.89)	-0.24 (0.99)	0.65 (3.54)	N/A
3rd	N/A	-0.02 (2.76)	-0.01 (1.41)	0.27 (2.44)
4th	N/A	N/A	0.11 (2.93)	-0.14 (2.11)

Table 6.3. MDFs for BC (Average and Standard Deviation of 10 Trials in Percent)

Ref Channel	1st	2nd	3rd	4th
1st	0 (0)	-0.57 (1.08)	N/A	N/A
2nd	0.59 (1.11)	0 (0)	0.66 (1.46)	N/A
3rd	N/A	-0.64 (1.46)	0 (0)	0.18 (1.05)
4th	N/A	N/A	-0.17 (1.03)	0 (0)

It is worth noting that each column entry in the MDFs represents each DOF of the structure. Therefore, for convenience, the average of MDFs in Table 6.3 is calculated and added to the last row of Table 6.2 to create a new Table containing both SDFs and MDFs,

as shown in Table 6.4. Therefore, from this point onwards, the two damage features are summarized in only one table where the last row represents MDFs.

Table 6.4. DFs for BC using the first student data (Average and Standard Deviation of 10 Trials in Percent)

	Ref Channel	1st	2nd	3rd	4th
SDFs	1st	-0.08 (0.56)	-0.36 (1.49)	N/A	N/A
	2nd	0.22 (1.89)	-0.24 (0.99)	0.65 (3.54)	N/A
	3rd	N/A	-0.02 (2.76)	-0.01 (1.41)	0.27 (2.44)
	4th	N/A	N/A	0.11 (2.93)	-0.14 (2.11)
MDFs		0.59 (1.11)	0.61 (1.27)	0.25 (0.25)	0.18 (1.05)

The baseline case will continue to be checked using data from the other students who conducted the test independently. The damage features are shown in the following Table.

Table 6.5. DFs for BC using the second student data (Average and Standard Deviation of 10 Trials in Percent)

	Ref Channel	1st	2nd	3rd	4th
SDFs	1st	0.3 (0.43)	0.43 (0.48)	N/A	N/A
	2nd	0.3 (0.26)	0.92 (0.26)	1.86 (0.78)	N/A
	3rd	N/A	1.93 (0.47)	0.45 (0.4)	0.1 (0.27)
	4th	N/A	N/A	2.27 (0.78)	1.06 (0.79)
MDFs		-0.13 (0.62)	0.1 (0.47)	1.05 (0.5)	-2.15 (0.67)

As the Table 6.5 showed, all the DFs revealed quite small values near zero, except for SDF_{43} at 2.27%, which is not ideal. However, this error is acceptable since there are many factors affecting the transparency of the acceleration data including human factors, errors in SHM system, environmental effects due to the open area of the lab, and other experimental activities nearby.

Next, in order to completely confirm that the effects due to different experimenters are negligible, data from two students are cross checked in the baseline case. The results are shown inTable 6.6.

Table 6.6. DFs for BC using both students' data (Average and Standard Deviation of 10 Trials in Percent)

	Ref Channel	1st	2nd	3rd	4th
SDFs	1st	0.21 (1.01)	0.03 (1.18)	N/A	N/A
	2nd	0 (1.2)	-0.01 (0.96)	-1.13 (1.14)	N/A
	3rd	N/A	-0.49 (1.08)	0.47 (1.03)	-0.07 (1.44)
	4th	N/A	N/A	-0.49 (1.3)	0.26 (1.02)
MDFs		-0.03 (0.74)	0.35 (0.57)	-0.54 (0.53)	0.48 (0)

From the DFs in theTable 6.6, it can be concluded that different experimenters do not have a large effect on the DFs calculated based on the methodology. One aspect requiring mentioned here is that the results of the damage features deviate considerably from the mean values. For example, SDF_{23} in Table 6.5 was found to be 0.65%. However, the corresponding standard deviation was found to be 3.54%, which is quite large. Also, the same issue can be found in the following damage cases.

6.2 Stiffness Damage Cases (DC1)

6.2.1 Damage Case 1.1 (DC1.1): Replacement of One Aluminum Column between the Third and Fourth Floors

The first damage case was simulated by replacing one aluminum column (E=63GPa) between the third and fourth floors as shown in Figure 6.2. With this replacement, it is expected that an amount of $(63-200)/(4\times200)\% = -16.4\%$ will be revealed at K_{34}, K_{43}, K_{44} and $(63-200)/(8\times200)\% = -8.2\%$ K_{33} in the stiffness matrix of the structure which is equivalent to the SDFs. In addition, no mass changes would be found in the MDFs. As depicted in Table 6.7, SDF_{34}, SDF_{43}, SDF_{44} suffered a decrease of -11.49; -11.77; -11.41%, whereas a -7.16% decrement was found at SDF_{33}. In fact, the damage at the 4th floor linearly affects the structure's stiffness at K_{34}, K_{43}, K_{44}. The SDFs revealed exactly the position of damage and are almost the same as the expected value (-16.4%). The SDFs values were smaller than expected due to the overall stiffness of the structure, possibly due to other components, e.g. mass slab, etc., along with the columns stiffness. Also, there were no significant changes in the MDFs (the last row in the Table) which is reasonable since there was no damage in mass in this damage case.

Figure 6.2: DC 1.1

Table 6.7. DFs for DC1.1 (Average and Standard Deviation of 10 Trials in Percent)

	Ref Channel	1st	2nd	3rd	4th
SDFs	1st	1.29 (0.25)	-0.84 (0.49)	N/A	N/A
	2nd	1.14 (0.52)	0.14 (0.67)	-2.04 (1.15)	N/A
	3rd	N/A	-2.41 (1.41)	-7.16 (1.02)	-11.49 (0.97)
	4th	N/A	N/A	-11.77 (1.07)	-11.41 (1.02)
MDFs		1.00 (0.15)	-0.78 (0.52)	0.03 (0.75)	0.16 (0.48)

6.2.2 Damage Case 1.2 (DC1.2): Replacement of Two Aluminum Columns between the Third and Fourth Floors

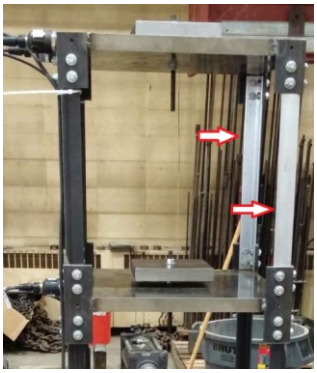

Figure 6.3: DC 1.2

Two aluminum columns were replaced in this damage case, which is two times more serious than it was in the first damage case. Table 6.8 shows the DFs in mass and stiffness of the structure where SFDs increased by 100% compared with the DC1.1 at the SFDs between the third and fourth floors. Those changes are consistent with the DC 1.1, which means that damage has happened between the third and fourth floor. However, the SDF_{23} and SDF_{32} showed small errors due to some unpreventable mistakes such as environment, noise, and human errors when conducting the test and the effects of the harsh environment of the opened lab. On the other hand, the MDFs continued to show very small values, indicating the mass at all floors has remained unchanged.

Table 6.8. DFs for DC1.2 (Average and Standard Deviation of 10 Trials in Percent)

	Ref Channel	1st	2nd	3rd	4th
SDFs	1st	0.1 (0.33)	-0.73 (0.55)	N/A	N/A
	2nd	-0.12 (0.52)	-0.33 (0.48)	-3.36 (0.85)	N/A
	3rd	N/A	-5.45 (0.99)	-15.87 (0.74)	-24.13 (0.89)
	4th	N/A	N/A	-21.58 (1.07)	-25.09 (1.07)
MDFs		0.31 (0.11)	-0.92 (0.33)	1.82 (0.55)	-1.58 (0.39)

6.2.3 Damage Case 1.3 (DC1.3): Replacement of One Aluminum Column between the First and Second Floors

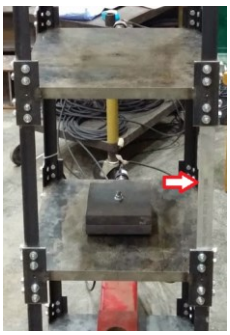

Figure 6.4. DC 1.3

The same damage scenario has been created in this case but instead the aluminum was replaced between the first and second floors. It can be seen in Table 6.9 that SDFs have decreased to -15.32% on average between the SDF_{12} and SDF_{21}. In addition, SDF_{11} and SDF_{22} showed an amount of -7.17% and -10.43%, respectively. Those changes revealed exactly the damage that occurred in the structure and it is similar to the DC1.1, although the damage location has moved to the first floor. Similarly, no changes were

found in the MDFs showing that no actual damage in mass has occurred in the structure.

Table 6.9. DFs for DC1.3 (Average and Standard Deviation of 10 Trials in Percent)

	Ref Channel	1st	2nd	3rd	4th
SDFs	1st	-7.17 (0.51)	-15.86 (0.8)	N/A	N/A
	2nd	-14.77 (0.69)	-10.43 (0.44)	-2.95 (2.67)	N/A
	3rd	N/A	0.07 (0.55)	0.39 (0.45)	0.72 (0.45)
	4th	N/A	N/A	-1.85 (1.38)	-2.89 (0.45)
MDFs		0.65 (0.44)	0.63 (1.15)	-1.86 (1.26)	1.32 (0.72)

6.2.4 Damage Case 1.4 (DC1.4): Replacement of Two Aluminum Columns between the First and Second Floors

A more serious damage scenario has been simulated in this case where two steel columns have been replaced by two aluminum ones between the first and second floors (Figure 6.5). It is expected that the DFs would show similar values as they were in DC1.2. Instead of significant changes around the third and fourth floor, however, the greatest changes would be seen between the first and second floor. In fact, an average of -23.5 was found at SDF_{12} and SDF_{21} and roughly -13% at SDF_{11} and SDF_{22}. It is clear that damage at the columns between the first and second floor has been uncovered and the severity of damage is twice as much as it was in the DC 1.3. This result demonstrates that two columns have suffered from a stiffness reduction.

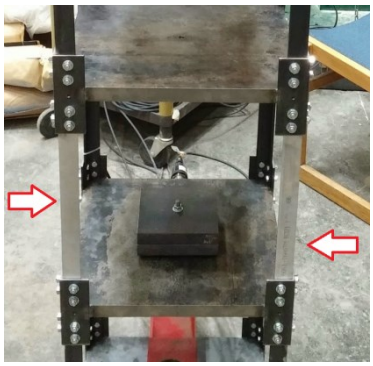

Figure 6.5. DC 1.4

Table 6.10. DFs for DC1.4 (Average and Standard Deviation of 10 Trials in Percent)

	Ref Channel	1st	2nd	3rd	4th
SDFs	1st	-13.11 (0.7)	-24.98 (1.22)	N/A	N/A
	2nd	-22.05 (1.2)	-13.28 (1.05)	1.23 (2.29)	N/A
	3rd	N/A	2.95 (0.69)	2.85 (0.5)	3.01 (0.64)
	4th	N/A	N/A	2.97 (1.87)	-0.94 (1.65)
MDFs		1.95 (0.4)	-0.67 (0.85)	-0.57 (1.1)	0.03 (0.79)

6.2.5 Damage Case 1.5 (DC1.5): Replacement of One Thinner Column at the Third and Fourth Floors

In this damage case, one thinner column with the cross sections of L $1\frac{1}{4} \times 1\frac{1}{4} \times \frac{1}{8}$" (I=1.827e-8m^4) was chosen to simulate minor damage between the third and the fourth floor (Figure 6.6). With this kind of damage, the researchers expected that a reduction from I=2.56e-8 m^4 to I=1.829e-8m^4 would result in a total stiffness reduction of $[(I_d - I_b)]/[4 \times I_b]\% = -7.14\%$at K_{34}, K_{43}, K_{44} and $[(I_d - I_b)]/[8 * \times I_b]\% = -3.57\%$ at K_{33} in the stiffness matrix of the structure. As can be seen in Table 6.11, the SDFs have successfully revealed the damage between the third and the fourth floor since there is a decrease of SDF_{34}, SDF_{43}, SDF_{44}. However, the SDFs may not define exactly the severity of the damage in this case, which is 3.2% on average of SDF_{34}, SDF_{43}, and SDF_{44}; and -2.89% at SDF_{33}. The reason would be the fact that components such as the slab components and lumped mass, as well as the stiffness of the columns have contributed to the overall stiffness of the structure. On the other hand, the MDFs in Table 6.11 showed that there are no changes in the mass of the structure. The results in this case are similar to the ones shown in DC1.1, thereby demonstrating strong agreement between the two damage cases.

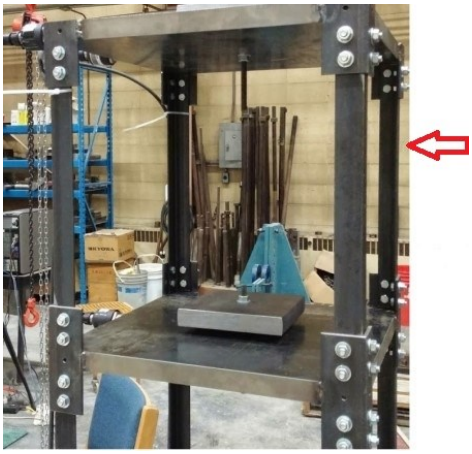

Figure 6.6. DC 1.5

Table 6.11. DFs for DC1.5 (Average and Standard Deviation of 10 Trials in Percent)

	Ref Channel	1st	2nd	3rd	4th
SDFs	1st	0.07 (0.67)	0.28 (1.42)	N/A	N/A
	2nd	-0.02 (0.78)	0.61 (0.16)	0.46 (2.94)	N/A
	3rd	N/A	0.35 (1.07)	-2.89 (0.69)	-4.4 (0.83)
	4th	N/A	N/A	-2.5 (1.67)	-2.7 (1.97)
MDFs		-0.14 (0.37)	0.08 (1)	0.7 (1.07)	-0.97 (0.47)

6.2.6 Damage Case 1.6 (DC1.6): Replacement of Two Thinner Columns at the Third and Fourth Floors

A Damage Case two times more dramatic than that in the DC1.5 is simulated in this section. Two thinner columns with the cross sections of L $1\frac{1}{4}\times 1\frac{1}{4}\times\frac{1}{8}$" (I=1.827e-8m^4) were chosen to simulate minor damage between the third and the fourth floor. As expected, the values of SDF_{34}, SDF_{43}, SDF_{44}, and SDF_{33} at Table 6.12 are almost two times as much as what it has been shown in Table 6.11 of DC1.5. In addition, the MDFs in the last row of the Table 6.12 are almost zeros at all entries, therefore indicating that the mass of the structure remained the same in this DC.

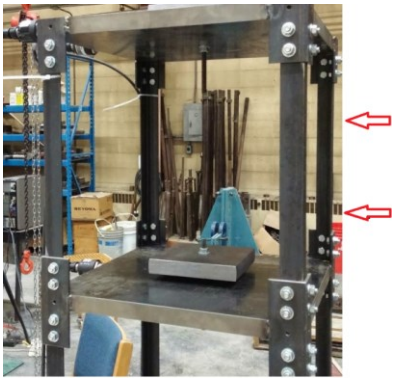

Figure 6.7. DC 1.6

Table 6.12. DFs for DC1.6 (Average and Standard Deviation of 10 Trials in Percent)

	Ref Channel	1st	2nd	3rd	4th
SDFs	1st	-0.14 (0.47)	-0.32 (0.94)	N/A	N/A
	2nd	-0.61 (1.34)	-0.43 (1.01)	-0.2 (1.92)	N/A
	3rd	N/A	-2.09 (1.38)	-5.39 (0.96)	-7.98 (1.13)
	4th	N/A	N/A	-6.56 (1.4)	-6.51 (1.25)
MDFs		-0.15 (0.26)	-0.53 (0.58)	1.16 (0.91)	-0.76 (0.73)

6.2.7 Damage Case 1.7 (DC1.7): Replacement of Three Thinner Columns at the Third and Fourth Floors

Three columns between the third and fourth floor were replaced with three thinner columns. The results of DFs are shown in Table 6.13. As explained previously, replacing three thinner columns would result in damage three times as serious as the DC 1.5 where damage happened at only one column. In fact, both MDFs and SDFs illustrated a similar trend as DC 1.5. The only difference is that the SDFs between the third and fourth floor are almost three times as much as those shown in Table 6.11. It is noted

Figure 6.8. DC 1.7

that no change in mass has occurred since the MDFs showed small values.

Table 6.13. DFs for DC1.7 (Average and Standard Deviation of 10 Trials in Percent)

	Ref Channel	1st	2nd	3rd	4th
SDFs	1st	0.46 (0.41)	0.43 (0.85)	N/A	N/A
	2nd	0.98 (1)	0.27 (0.62)	2.6 (1.51)	N/A
	3rd	N/A	-1.11 (1.18)	-7.59 (0.65)	-10.53 (1.17)
	4th	N/A	N/A	-8.14 (1.22)	-12.22 (1.07)
MDFs		0.27 (0.22)	-1.38 (0.37)	2.14 (0.51)	-1.3 (0.38)

6.2.8 Damage Case 1.8 (DC1.8): Replacement of Four Thinner Columns at the Third and Fourth Floors

In this case, one thinner column was added in order to simulate damage at both four columns on the same floor. As expected, the SDFs show in this case (Table 6.14), that the values between the third and fourth floor are exactly twice as much as in DC 1.6 where damage occurred at two columns. Similarly, MDFs showed insignificant changes, meaning that there is no damage in the mass of the structure.

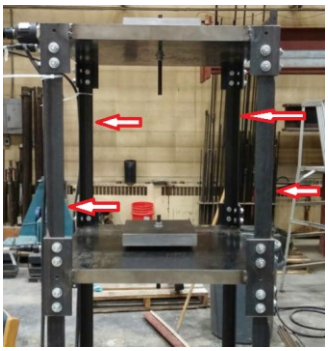

Figure 6.9. DC 1.8

It is worth noting that there are some errors up to 2% at some entries in both MDFs and SDFs in some damage cases. These errors are reasonable since they are not systematic errors and they appeared randomly within the entries. Also, the SDFs between the third and fourth floors increased linearly as the damage developed from DC1.5 to DC1.8. For this reason, it can be confirmed that the severity of damage is defined correctly and consistently by using the methodology.

Table 6.14. DFs for DC1.8 (Average and Standard Deviation of 10 Trials in Percent)

	Ref Channel	1st	2nd	3rd	4th
SDFs	1st	0.64 (0.6)	1.16 (0.92)	N/A	N/A
	2nd	1.51 (0.78)	1.47 (0.79)	2.48 (0.93)	N/A
	3rd	N/A	-0.55 (1.16)	-9.42 (0.86)	-14.64 (0.93)
	4th	N/A	N/A	-11.98 (0.83)	-14.88 (1.21)
MDFs		0.17 (0.15)	-1.1 (0.4)	2.06 (0.6)	-1.51 (0.39)

In the next four damage cases, the same damage scenarios created in DC1.5 to DC1.8 are replicated, but the damage location is moved to the columns between the first and the second floor.

6.2.9 Damage Case 1.9 (DC1.9): Replacement of One Thinner Column between the First and Second Floors

One thinner column was used to replace one column at the first floor similar to the DC 1.5. The damage now happened on the first floor instead of the third floor as in DC 1.5. In fact, the SDFs (Table 6.15) have clearly shown that damage has happened between the first and the second floor. The severity of the damage is relatively similar to what it was in the DC1.5, although the change has moved to the first floor. No mass has been changed and that is why the MDFs did not show any significant changes (Table 6.15).

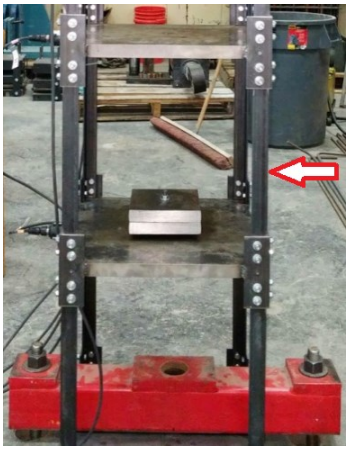

Figure 6.10. DC 1.9

Table 6.15. DFs for DC1.9 (Average and Standard Deviation of 10 Trials in Percent)

	Ref Channel	1^{st}	2^{nd}	3^{rd}	4^{th}
SDFs	1^{st}	-2.08 (0.42)	-4.95 (0.82)	N/A	N/A
	2^{nd}	-4.52 (0.81)	-2.00 (0.68)	-1.03 (1.89)	N/A
	3^{rd}	N/A	1.21 (1.07)	2.50 (0.69)	0.05 (0.98)
	4^{th}	N/A	N/A	0.70 (2.1)	2.09 (1.32)
MDFs		0.23 (0.11)	0.61 (0.49)	-0.53 (0.83)	-0.31 (0.64)

6.2.10 Damage Case 1.10 (DC1.10): Replacement of Two Thinner Columns between the First and Second Floors

Two thinner steel columns were used between the first and the second floor. It is unnecessary to explain in detail this case since it is similar to DC 1.6; however, note that the location of the damage is different. As observed in the DFs shown in the Table below, it is clear that the damage has occurred between the first and second floor since the SDFs in those DOFs are significant as opposed to the other entries in the SDFs matrix. As well, the severity of the SDFs between the 1st and 2nd floor are very similar to those in between the third and 4th floor in DC 1.6. In the MDFs, however, no significant values have been shown. Therefore, no changes in mass have happened.

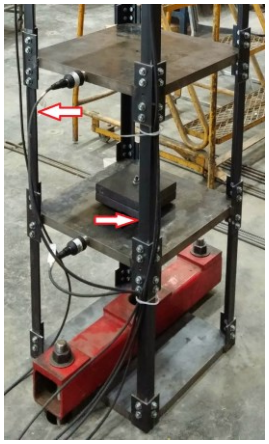

Figure 6.11. DC 1.10

Table 6.16. DFs for DC1.10 (Average and Standard Deviation of 10 Trials in Percent)

	Ref Channel	1st	2nd	3rd	4th
SDFs	1st	-4.35 (0.54)	-9.06 (0.93)	N/A	N/A
	2nd	-8.58 (1.23)	-5.01 (1.11)	-2.89 (2.28)	N/A
	3rd	N/A	0.35 (1.65)	1.85 (0.99)	-0.18 (1.24)
	4th	N/A	N/A	-0.38 (2.42)	1.15 (1.6)
MDFs		0.27 (0.27)	0.6 (0.6)	0.88 (0.88)	0.73 (0.73)

6.2.11 Damage Case 1.11 (DC1.11): Replacement of Three Thinner Columns between the First and Second Floors

The thinner columns between the first and the second floor have replaced three columns at the baseline case. Results of the computed SDFs and MDFs are shown in the Table 6.17. The results show that there is damage between the first and 2nd floor where the SDF_{12} and SDF_{21} are almost twice as much as SDF_{22} and SDF_{11}. This increment in SDFs is because the stiffness K_{11} and K_{22} in the stiffness matrix is

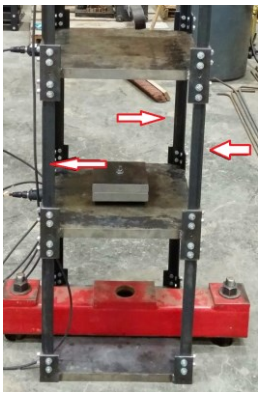

Figure 6.12. DC 1.11

made up of the stiffness of the columns at both the first and second floor, whereas the components K_{12} and K_{21} are comprised of only the stiffness of the columns at the first and second floor, respectively. There are no changes in mass in this case since the MDFs show no changes in the mass components.

Table 6.17. DFs for DC1.11 (Average and Standard Deviation of 10 Trials in Percent)

	Ref Channel	1st	2nd	3rd	4th
SDFs	1st	-6.75 (0.38)	-13.76 (0.72)	N/A	N/A
	2nd	-12.56 (0.71)	-7.09 (0.75)	-1.83 (1.58)	N/A
	3rd	N/A	1.34 (0.81)	2.7 (0.76)	0.57 (0.77)
	4th	N/A	N/A	1.57 (2.09)	2.21 (1.61)
MDFs		0.69 (0.24)	0.63 (0.57)	-0.71 (0.91)	-0.48 (0.76)

6.2.12 Damage Case 1.12 (DC1.12): Replacement of Four Thinner Columns between the First and Second Floors

All four columns have been replaced with thinner columns between the first and second floor in this case. The computed SDFs and MDFs are shown in Table 6.18 where strongly consistent results confirm the effectiveness of the method in evaluating the severity of damage as well as its locations. By comparison among the SDFs from the DC 1.9 to DC 1.12, the SDFs between the first and second floor increased linearly, which reflects exactly the severity of damage from DC 1.9 to DC 1.12. Detailed explanations can be found in the previous sections. In addition, the mass was found to be the same in this case as shown in the last row of Table 6.18.

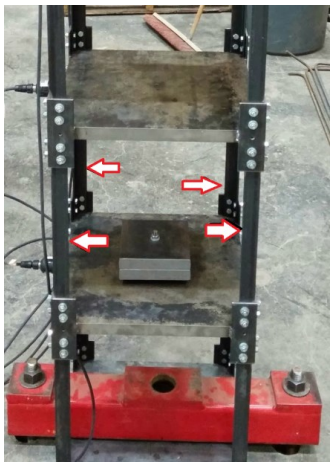

Figure 6.13. DC 1.12

Table 6.18. DFs for DC1.12 (Average and Standard Deviation of 10 Trials in Percent)

	Ref Channel	1st	2nd	3rd	4th
SDFs	1st	-8.15 (1.08)	-18 (0.79)	N/A	N/A
	2nd	-18 (1.44)	-10.38 (1.97)	-1.07 (3.39)	N/A
	3rd	N/A	-0.29 (1.67)	0.35 (1.63)	-1.54 (0.97)
	4th	N/A	N/A	-1.96 (2.04)	-0.57 (2.59)
MDFs		-0.01 (0.49)	0.29 (0.95)	-0.41 (1.13)	-1.18 (4.64)

6.3 Mass Change Simulations

In this section, damage in mass was simulated in order to validate the theoretical methodology and confirm its numerical applications. Mass at the third and fourth floor was removed accordingly. The results of these damage cases are shown in the following sub-sections.

6.3.1 DC 2.1: Removal of One Plate at the Third Floor

One plate (4.5 kg) at the third floor was removed in this damage case. As calculated approximately, the percentage of mass reduction over the total weight of the third floor (40 kg) would be 11.3%. In fact, the results in Table 6.19 showed good indications of mass removal at the third floor since there is a reduction of -13.73% at the MDF_3, which is reasonably close to the expected reduction calculated above. Moreover, it is reasonable to conclude that there is no damage in the stiffness since there is little change to the entries in the SDFs in Table 6.19.

Figure 6.14. DC 2.1

Table 6.19. DFs for DC2.1 (Average and Standard Deviation of 10 Trials in Percent)

	Ref Channel	1st	2nd	3rd	4th
SDFs	1st	1.31 (2.83)	-1.04 (2.9)	N/A	N/A
	2nd	0.55 (2.03)	0.69 (1.51)	-0.98 (2.85)	N/A
	3rd	N/A	-1.23 (2.85)	-2.55 (2.71)	-1.35 (2.68)
	4th	N/A	N/A	-0.42 (1.4)	-0.28 (0.55)
MDFs		1.64 (2.08)	-0.92 (1.23)	-13.73 (6.17)	-0.95 (0.93)

6.3.2 DC 2.2: Removal of One Plate at the Fourth Floor

The same kind of damage was simulated at the fourth floor of the structure with one plate removed (Figure 6.15). As tabulated in Table 6.20, the SDFs reveal no changes in the stiffness of the structure since there is no damage to the structure's stiffness. In contrast, it is clear that the mass at the fourth floor has reduced by -11.02%, as shown at the MDF_4. It is noted that there is a random error at the SDF_{23} in the Table 6.20 likely due to environmental effects in the lab or noise from other technical activity in the lab during the experiments.

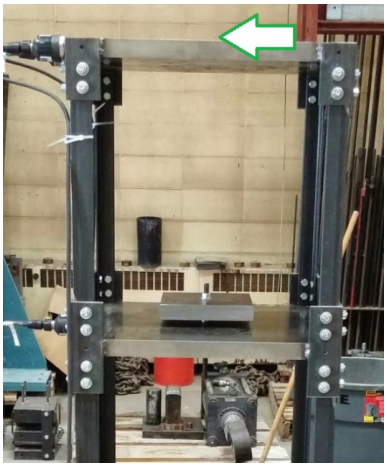

Figure 6.15. DC 2.2

Table 6.20. DFs for DC2.2 (Average and Standard Deviation of 10 Trials in Percent)

	Ref Channel	1st	2nd	3rd	4th
SDFs	1st	-0.08 (0.37)	0.01 (0.69)	N/A	N/A
	2nd	-1.01 (1.35)	-1.31 (1.02)	-3.55 (2.47)	N/A
	3rd	N/A	-1.21 (1.45)	0.1 (0.74)	-0.19 (1.04)
	4th	N/A	N/A	-0.19 (1.04)	1.51 (0.84)
MDFs		-1.02 (0.73)	1.75 (1.06)	-1.19 (0.65)	-11.02 (0.49)

6.4 Combined Damaged Simulations

In this section, multiple damage scenarios of mass and stiffness at different locations of the structure were simulated. The purpose of this section is to confirm the effectiveness of the proposed method in detecting multiple reductions in mass and stiffness of the system.

6.4.1 DC 3.1: Removal of One Plate at the Third and Fourth Floors

Firstly, two masses at the third and fourth floor were removed to create damage (Figure 6.16) in this case. The combined damage in mass at the two floors would result in considerable changes in MDFs at the third and fourth column of in the DFs Table. Table 6.21 shows a reduction of -11.39% at the MDF_3 that is the exact location and reduction of mass at the third floor. Similarly, a reduction of -14.16% appears in the mass of the fourth floor, although there is a small error in the severity of the damage. In contrast, no damage has been shown in the SDFs since there is only mass damage in the structure.

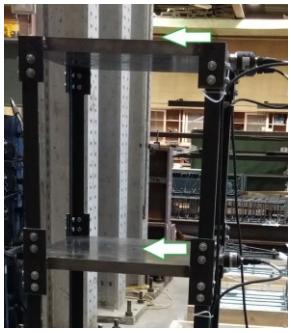

Figure 6.16. DC 3.1

Table 6.21. DFs for DC3.1 (Average and Standard Deviation of 10 Trials in Percent)

	Ref Channel	1st	2nd	3rd	4th
SDFs	1st	0.58 (0.47)	0.4 (0.94)	N/A	N/A
	2nd	-1.72 (2.32)	-0.85 (1.82)	-1.06 (3.66)	N/A
	3rd	N/A	-1.06 (3.66)	-2.09 (3.12)	-2.01 (3.4)
	4th	N/A	N/A	-2.01 (3.4)	-1.88 (2.29)
MDFs		-2.12 (1.66)	1.1 (0.87)	-11.39 (2.37)	-14.16 (2.09)

6.4.2 DC 3.2: Replacement of One Aluminum between the 1st and 2nd floor (DC1.3); the 3rd and 4th floor (DC1.1)

Multiple stiffness damages are induced in this case where one aluminum column is used to replace one column between the first and second floor and between the third and fourth floor. It is worth noting again that the magnitude of the SDFs and MDFs represent the percentage of the overall stiffness and mass changes in the system. Table 6.22 shows that the SDF_{12} and SDF_{21} are -16.11% and -13.90% respectively. Both values are close to -16.4% which is the expected actual damage based simply on the changes of modulus of elasticity. These reductions indicate damage at k_2,

Figure 6.17. DC 3.2

which is between the first and the second floor. Also, -8.65% and -6.85% at SDF_{11} and SDF_{22} demonstrate that the replacement of one aluminum column results in an 8.2% decrease in the total stiffness associated with the first DOF and second DOF. Similarly, the same damage pattern has been found between the third and fourth floor based on the SDF_{33}, SDF_{34}, SDF_{43}, SDF_{44} in Table 6.22. On the other hand, mass changes in all floors have remained the same since there are no big changes in the MDFs between the baseline case and this unknown case.

Table 6.22. DFs for DC3.2 (Average and Standard Deviation of 10 Trials in Percent)

	Ref Channel	1st	2nd	3rd	4th
SDFs	1st	-8.65 (0.45)	-16.11 (0.73)	N/A	N/A
	2nd	-13.9 (1.13)	-6.85 (1.61)	-0.14 (2.65)	N/A
	3rd	N/A	-0.45 (1.52)	-7.02 (0.87)	-11.84 (0.61)
	4th	N/A	N/A	-12.79 (1.72)	-11.36 (1.2)
MDFs		2.64 (0.7)	-1.42 (1.15)	-0.38 (1.68)	1.11 (1.76)

6.4.3 DC 3.3: One Plate Removal at the Fourth Floor + DC3.2

A combination of mass and stiffness damage is first introduced in this damage case. One mass at the fourth floor was removed and one aluminum column used between the first and second floor and between the third and the fourth floor, as in DC3.2. The DFs of mass and stiffness are computed and shown in Table 6.24. Similar to the DC 3.2, the SDF_{11}, SDF_{12}, SDF_{21}, SDF_{22}, SDF_{31}, SDF_{34}, SDF_{43}, and SDF_{44} in this case are almost similar to those in DC 3.2, which means the locations and severity of the stiffness damage have been defined correctly (stiffness reduction at the two locations shown in Figure 6.18). Moreover, a reduction of mass at the fourth floor is also recognized by the MDF_4 i.e. -10.73%, which is expected based on the hand calculation.

Figure 6.18. DC 3.3

Table 6.23. DFs for DC3.3 (Average and Standard Deviation of 10 Trials in Percent)

	Ref Channel	1st	2nd	3rd	4th
SDFs	1st	-8.19 (0.41)	-15.43 (0.72)	N/A	N/A
	2nd	-13.02 (2.21)	-6.88 (1.76)	-0.97 (4.16)	N/A
	3rd	N/A	1.04 (2.04)	-5.97 (1.14)	-10.68 (1.24)
	4th	N/A	N/A	-10.68 (1.24)	-10.26 (0.51)
MDFs		2.84 (2.08)	-0.31 (2.21)	-1.01 (1.16)	-10.73 (0.97)

6.4.4 DC 3.4: One Plate Removal at the Third and Fourth Floor + DC3.2

Two mass removals at the third and fourth floor in combination with DC 3.2 were simulated. As shown in Table 6.24, the stiffness damage between the first and second floor and between the third and fourth floor are revealed with the quantity of damage exactly same as the previous cases. In addition, two mass removals at the third and fourth floor defined by the MDFs are clearly seen with a reduction of -12.64% and -11.55%, respectively. Those quantities are nearly equal to the expected mass reduction at each floor, i.e. -11.30%.

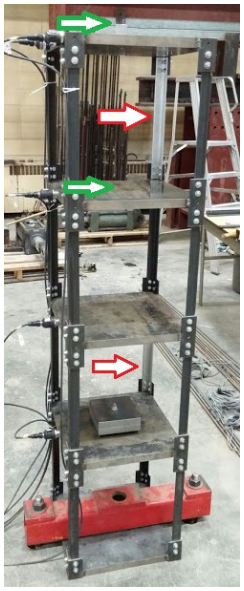

Figure 6.19. DC 3.4

Table 6.24. DFs for DC3.3 (Average and Standard Deviation of 10 Trials in Percent)

	Ref Channel	1st	2nd	3rd	4th
SDFs	1st	-8.45 (0.49)	-15.63 (0.71)	N/A	N/A
	2nd	-13.65 (1.06)	-7.22 (0.88)	-1.28 (1.63)	N/A
	3rd	N/A	-1.28 (1.63)	-8.42 (1.23)	-13.15 (1.21)
	4th	N/A	N/A	-13.15 (1.21)	-11.74 (0.76)
MDFs		2.35 (0.91)	-1.15 (0.43)	-12.64 (0.86)	-11.55 (0.61)

6.4.5 DC 3.5: Two Plates Removal at the First Floor + One Plate Removal at the Third and Fourth Floor + DC3.2

All additional masses at all floors are removed together with stiffness damage DC 3.2 to create a more complicated damage. It can be seen in the SDFs in Table 6.25, damage DC 3.2 is easily revealed since the changes in SDF_{11}, SDF_{12}, SDF_{21}, SDF_{22}, SDF_{31}, SDF_{34}, SDF_{43}, and SDF_{44} show a similar trend as they did in DC 3.2. In addition, the MDFs at the third and fourth floor are -11.04% and -11.11%, respectively, almost equal to the amount of mass reduction in those floors. Most importantly, a reduction of 23.32% is found at the MDF_{11} at the first floor. By estimation, the removal of two plates would cause a total mass reduction of 22.60% at that floor. Therefore, the indicator MDF_1 has been successful in not just defining the location of damage, but its severity as well.

Figure 6.20. DC 3.5

Table 6.25. DFs for DC3.5 (Average and Standard Deviation of 10 Trials in Percent)

	Ref Channel	1st	2nd	3rd	4th
SDFs	1st	-10.13 (1.23)	-15.47 (1.38)	N/A	N/A
	2nd	-15.47 (1.38)	-7.86 (0.96)	-0.63 (2.31)	N/A
	3rd	N/A	-0.63 (2.31)	-7.36 (1.75)	-12.67 (1.69)
	4th	N/A	N/A	-12.67 (1.69)	-12.24 (1.33)
MDFs		-23.32 (0.97)	0 (0)	-11.04 (1.53)	-11.11 (1.15)

6.4.6 DC 3.6: Replacement of Two Thinner Steel Columns between the 1st and 2nd Floors and between the 3rd and 4th Floors (DC 1.10+DC1.6)

This case is similar to DC 3.2 where stiffness damage occurred between the 1st and 2nd floor and between the 3rd and 4th floor. Instead of replacing one aluminum column, however, two thinner steel columns are used to replace two of the original columns at each position (Figure 6.21). This damage case is simply a combination of DC 1.6 and DC 1.10. Thus, it is expected that the DFs would yield the same agreement among those damage cases. As Table 6.26 shows, SDF_{12}; SDF_{21}; SDF_{11}; and SDF_{22} are -9.74% and -8.8%; -4.86% and -5.99%, respectively. Those SDFs are exactly as same as they were in the DC 1.6, which signals damage between the third and fourth floor. Similarly, the stiffness damage between the first and second floor has been successfully located since the SFDs between the first and fourth floor show similar values as they were in the DC 1.10. Overall, the stiffness damage at two locations has been revealed and there are no changes in the mass since the MDFs are almost entirely zero.

Figure 6.21. DC 3.6

Table 6.26. DFs for DC3.6 (Average and Standard Deviation of 10 Trials in Percent)

	Ref Channel	1st	2nd	3rd	4th
SDFs	1st	-4.86 (0.19)	-9.74 (0.33)	N/A	N/A
	2nd	-8.8 (1.71)	-5.99 (1.19)	-0.16 (3.36)	N/A
	3rd	N/A	-0.52 (0.96)	-3.68 (0.58)	-6 (0.77)
	4th	N/A	N/A	-7.48 (1.33)	-9.41 (0.82)
MDFs		1.04 (1.58)	-0.64 (2.06)	-0.61 (1.83)	1.61 (1.08)

6.4.7 DC 3.7: DC3.6 + One Plate Removal at the Fourth Floor

One mass removal has been added along with DC3.5 (Stiffness damage). From Table 6.27, it is clear that SDFs have successfully defined the damage and the quantity between the first and second floor and between the third and fourth floor. Further explanations of the computed SDFs can be found in the previous case. The mass removal at the fourth floor is revealed by the MDF_{44} decreasing to -11.06%.

Figure 6.22. DC 3.7

Table 6.27. DFs for DC3.7 (Average and Standard Deviation of 10 Trials in Percent)

	Ref Channel	1st	2nd	3rd	4th
SDFs	1st	-4.76 (0.13)	-9.36 (0.36)	N/A	N/A
	2nd	-8.79 (1.19)	-5.65 (0.78)	-2.73 (2.25)	N/A
	3rd	N/A	-0.08 (0.83)	-3.81 (0.66)	-6.76 (0.75)
	4th	N/A	N/A	-6.76 (0.75)	-6.75 (1.28)
MDFs		0.62 (0.99)	1.07 (1.4)	-2.66 (0.87)	-11.06 (1.18)

6.4.8 DC 3.8: DC3.7 + One Plate Removal at the Third and Fourth Floor

In this case, one more mass has been removed at the third floor, resulting in a more complicated damage in both mass and stiffness. As can be seen in Table 6.28, the MDF_3 and MDF_4 have the values of -13.63% and -11.30%, respectively, which is how the mass damage occurred in those floors. In addition to the mass reduction, the same damage in stiffness as the DC 3.5 has been clearly observed here since the SDFs in Table 6.28 between the first and second floor and the third and fourth floor revealed a similar pattern as in the DC3.5.

Figure 6.23. DC 3.8

Table 6.28. DFs for DC3.8 (Average and Standard Deviation of 10 Trials in Percent)

	Ref Channel	1st	2nd	3rd	4th
SDFs	1st	-4.17 (0.73)	-8.49 (1.16)	N/A	N/A
	2nd	-6.11 (1.80)	-3.63 (1.65)	-1.59 (2.86)	N/A
	3rd	N/A	-1.59 (2.86)	-5.53 (2.16)	-7.71 (2.05)
	4th	N/A	N/A	-6.62 (3.27)	-4.54 (6.72)
MDFs		2.60 (1.41)	-1.26 (0.67)	-13.63 (2.22)	-11.30 (4.04)

6.4.9 DC 3.9: DC3.8 + Two Plates Removal at the First Floor

The most serious damage case is simulated in this damage scenario where mass at all floors is removed and the stiffness damage DC 3.5 is used in addition. As expected, the total mass at the first floor has been reduced by 23.87% due to the fact that two plates have been removed on this floor. Moreover, the mass at the third and fourth floor has also reduced as demonstrated by the mass indicators MDF_3 and MDF_4 inTable 6.29. On the other hand, there is a reduction in stiffness at the two locations based on the same pattern of the SDFs that were observed in DC 3.5.

Figure 6.24. DC 3.9

Table 6.29. DFs for DC3.9 (Average and Standard Deviation of 10 Trials in Percent)

	Ref Channel	1st	2nd	3rd	4th
SDFs	1st	-6.49 (1.94)	-8.29 (2.48)	N/A	N/A
	2nd	-8.29 (2.48)	-5.12 (1.44)	-0.78 (2.64)	N/A
	3rd	N/A	-0.78 (2.64)	-4.38 (2.28)	-7.41 (2.38)
	4th	N/A	N/A	-7.41 (2.38)	-8.51 (1.01)
MDFs		-23.87 (1.08)	0 (0)	-13.38 (1.17)	-11.29 (1.32)

6.4.10 DC 3.10: Replacement of Four Thinner Steel Columns between the 1st and 2nd Floor and the 3rd and 4th Floor (DC 1.8 + DC 1.12)

A significant damage in stiffness has been chosen in this damage case, where all four columns at each floor are replaced. In this case, the four columns between the first and second floor and between the third and fourth floor have been replaced by four steel columns with thinner cross-section. In this damage, it is expected that the severity of the SDFs related to the damage locations would increase twice as much as they were in the DC 3.5 where only two columns have been replaced. As observed in Table 6.30, the SDFs between the first and second floors and the third and fourth floors reveal values, which are almost twice as they were in the corresponding entries in DC 3.5. This means that the damage's positions and severity have been defined very well. In terms of mass damage, there are no major changes in the MDFs thus showing that the mass in the structure remained the same before and after damage. However some small errors have been found in this DFs as shown in MDF_4 at 3.81%.

Figure 6.25. DC 3.10

Table 6.30. DFs for DC 3.10 (Average and Standard Deviation of 10 Trials in Percent)

	Ref Channel	1st	2nd	3rd	4th
SDFs	1st	-9.05 (0.31)	-17.42 (0.55)	N/A	N/A
	2nd	-13.13 (1.8)	-8.24 (2.04)	0.73 (1.87)	N/A
	3rd	N/A	1.66 (1.52)	-5.92 (0.95)	-11.48 (1.11)
	4th	N/A	N/A	-14.72 (1.74)	-16.46 (0.69)
MDFs		3.24 (1.04)	-1.6 (1.95)	-2.75 (0.76)	3.81 (0.55)

6.4.11 DC 3.11: DC3.10 +One Plate Removal at the Fourth Floor

Similar to the above damage cases, one mass has been removed at the fourth floor in addition to the damages in DC 3.10. The computed SDFs and MDFs results are shown in

Table 6.31 where the stiffness damage can be clearly found between the first and second floor and the third and the fourth floor. The stiffness reductions are almost twice as much as their corresponding counterparts in DC 3.10. Moreover, one mass reduction has been found at the fourth floor with a -10.51% decrease, which is exactly the same as the actual damage in the structure.

Figure 6.26. DC 3.11

Table 6.31. DFs for DC 3.10 (Average and Standard Deviation of 10 Trials in Percent)

	Ref Channel	1st	2nd	3rd	4th
SDFs	1st	-9.12 (1.93)	-17.52 (2.31)	N/A	N/A
	2nd	-14.97 (2.62)	-9.13 (2.64)	-1.16 (7.32)	N/A
	3rd	N/A	-0.11 (7.36)	-7.77 (4.1)	-13.3 (3.23)
	4th	N/A	N/A	-13.3 (3.23)	-14.07 (0)
MDFs		3.08 (5.55)	-0.9 (4.72)	-1.58 (4.79)	-10.51 (2.62)

6.4.12 DC 3.12: DC 3.11 +One Plate Removal at the Third Floor

In this case, one mass has been removed at the third floor together along with the stiffness damage of DC 3.11. As shown in Table 6.32, the only aspect different in this Table than the Table in the previous case is that the MDF_3 is -13.30%, which is almost equal to -11.3%, the actual mass reduction based on the estimation of mass reduction on the third floor. Also, the SDFs and the other MDFs entries demonstrated a similar trend as the previous case. Therefore, damage in the stiffness and mass of the structure have been successfully evaluated.

Figure 6.27. DC 3.12

Table 6.32. DFs for DC 3.12 (Average and Standard Deviation of 10 Trials in Percent)

	Ref Channel	1st	2nd	3rd	4th
SDFs	1st	-8.89 (2.7)	-17.25 (1.88)	N/A	N/A
	2nd	-13.91 (2.38)	-8.63 (3.52)	0.86 (8)	N/A
	3rd	N/A	0.86 (8)	-7.93 (4.03)	-13.14 (2.76)
	4th	N/A	N/A	-13.14 (2.76)	-15.39 (2.21)
MDFs		2.02 (6.3)	-2.3 (4.59)	-13.33 (2.41)	-11.49 (1.72)

6.4.13 DC 3.13: DC3.12 + Two Plates Removal at the 1st Floor

The previous case shows the mass and stiffness damage have been successfully identified. In order to further reinforce the ability of the method in qualifying the damage in mass and stiffness as well, all lumped masses on all floors are removed together with the stiffness damage created in the previous case. Table 6.32 shows the results of MDFs and SDFs, where the MDFs at the first, third, and fourth floor showed a decrease of 23.85%, 13.68%, and 11.98%, respectively, thereby closely confirmed the mass reduction amount. The stiffness damage has also been revealed in this case where the SDFs followed almost the same trend as they were in the DC 3.10.

Figure 6.28. DC 3.13

Table 6.33. DFs for DC 3.13 (Average and Standard Deviation of 10 Trials in Percent)

	Ref Channel	1st	2nd	3rd	4th
SDFs	1st	-10.7 (1.73)	-16.62 (1.94)	N/A	N/A
	2nd	-16.62 (1.94)	-9.85 (1.18)	-1.58 (3.68)	N/A
	3rd	N/A	-1.58 (3.68)	-9.15 (2.97)	-15 (3.08)
	4th	N/A	N/A	-15 (3.08)	-16.04 (1.33)
MDFs		-23.85 (1.3)	0 (0)	-13.68 (2.48)	-11.98 (1.76)

6.5 Discussion of Experimetal Results

Experimental results showed very good indicators about the locations, severity of mass, and stiffness damage. However, similar to the numerical case studies, some points require consideration.

- SDFs and MDFs in the baseline and the other cases showed very promising results when mass and stiffness change can be identified separately although there

are some minor errors with high standard deviation, especially in the baseline case where the maximum standard deviation was found to be 3.5%. Therefore, the method may not work very effectively with some damage that has changes smaller than this value.

- Obviously, the method has reached level 3 of damage detection, and this capability is advantageous. However, it is noted that the damage is located in a global manner rather than local manner. Strictly speaking, the methodology cannot locate exactly which structural members have suffered from damage, although the floors with damage can be identified.
- The severity of damage is defined as the relative change instead of absolute change, which is why the method has an assumption about mass change. Therefore, the proposed method may not work effectively for absolute bracing systems where stiffness is dependent throughout the whole systems.

CHAPTER 7: SUMMARY, CONCLUSIONS AND RECOMMENDATIONS

7.1 Summary and Conclusions

In this thesis, a new methodology for detecting, locating, and quantifying stiffness and mass changes using output only vibration data is presented. The method uses the/an Auto Regressive Moving Average model with eXogenous inputs (ARMAX) in conjunction with sensor clustering based on equation of motion. The thesis is divided into two main parts. In Part I – Theory and Numerical Applications, I present the theoretical basis for the development of the improved method based on time series models. Two numerical applications with various damage scenarios were employed to confirm the method's theory and assumptions. In Part II – Experimental Validation, I present the process of development of a lab-scale structure and instrumentation system along with the results and discussions.

In the first part, the ARMAX models are studied to create models for the dynamic response of structures when the sensor clustering concept is applied. By following some mathematical transformation and assuming that the mass is lumped at each DOF, I use the ARMAX models to represent the transformed equation of motion. I demonstrate that the ARMAX coefficients can be used to identify, locate, and quantify the changes in mass and stiffness of structures. By comparing the coefficients at the baseline case and damaged case and executing a loop calculation, I built two damage features, e.g. mass damage features (MDFs) and stiffness damage features (SDFs), to evaluate the damage. The first application of the proposed method is a 4-DOF spring mass system, and the second application employs the/a Phase-I IASC-ASCE benchmark numerical model. As presented, results from minor to complicated damage cases show that the method is successful in detecting, locating, and quantifying changes in mass and stiffness.

In the second part, a 4-storey shear structure is built in the lab for verification of the proposed method with experimental data. After the structure had been ready, I developed an SHM system for the test structure. For the SHM system, National Instruments devices,

e.g. NI 9074 Chassis; NI 2234 modules, were used for the hardware acquisition system, while PCB 393A03 accelerometers were used to measure vibration of the structure at different floors. LabVIEW by NI was utilized to develop a user-interface tool to control the SHM system. Once the framework of the automated SHM system was finished, the structure was tested under various damaged conditions with approximately 1200 tests conducted. The results from those damaged and baseline cases showed a very good agreement to those using numerical applications. Overall, it can be stated that the proposed method is a contribution to the damage detection process with some advantages, as listed below:

- It is almost the first time in the literature that changes in stiffness (damage) and changes in mass (operational effects) are detected, localized, and quantified separately by using two separate damage features.
- According to the levels defined by A Rytter (1993), the method has reached level 3 of damage identification for both stiffness and mass. Note that the damage location is defined in the global manner. Therefore, localized methods of damage detection could be needed to find exact damage locations.
- The ability to deal with a great amount of data shows potential for being implemented in a continuous SHM system.

7.2 Recommendations and Future Work

Although the method is very promising in damage detection as shown by different applications, there are still some limitations that require mention and recommendations for future work.

In the current form, vibration data from all important DOFs is required in order to fit the ARMAX models for building the damage features. For a simple shear type of buildings, it would not be a problem to anticipate the DOF of those structures. However, large structures like bridges contain various DOFs depending on the professional judgement of engineers, and it would not be feasible to capture all information from all DOFs. Therefore, a study on how to gather information about the structure's dynamic behaviour with data from the limit number of available DOFs should be conducted in the future to improve the economic and computational factors.

The proposed method works really well under the circumstance that the mass change does not change all the DOFS simultaneously and the occurring change should be either an increase or decrease. In other words, changes detected by using the proposed method are relative changes rather than absolute changes; and the vibration of one DOF is only related to its adjacent DOF. Therefore, the proposed method will not work with absolutely braced systems or systems with the stiffness of individual members inter-related. For these reasons, the method should be improved for such cases and a plan has been already drawn to improve the methodology before further applications.

The proposed method can apply for shear-type structures that are either typical or unique. However, it should be further developed to apply to more general structure types. Experiments with different structures such as a steel bridge with slabs and girders and adjustable boundary conditions should be conducted. Also, different sensor layouts, e.g. in-plane and spatial sensor placement, would be worth testing for more accurate results.

The method can exclude the effects of damping in the damage detection process: that is a beneficial feature because the process can be further simplified. However, changes in damping are worth studying, especially in some projects with efforts to reduce the excessive vibration by using damper systems. Therefore, the effects of damper installed in structures can be tested effectively.

Finally, and importantly, environmental effects such as temperature (Gu and Gul (2015); Kostic and Gul (2015)) should be taken into account since this factor can greatly contribute to changes in the dynamic response of structures and thus “true” damage can be mistaken. Studies on temperature effect elimination are recommended for future work and already being conducted by other members of the author`s research group.

REFERENCES

Ahmadian, H., Mottershead, J., & Friswell, M. (2000). Damage location indicators from substructure mode shapes. *Inverse Problems in Engineering, 8*(4), 309-323.

Allemang, R. J., & Brown, D. L. (1982). *A correlation coefficient for modal vector analysis.* Paper presented at the Proceedings of the 1st international modal analysis conference.

Andersen, P. (1997). *Identification of civil engineering structures using vector ARMA models.* unknown.

Attarian, V. A., Cegla, F. B., & Cawley, P. (2014). Long-term stability of guided wave structural health monitoring using distributed adhesively bonded piezoelectric transducers. *Structural health monitoring*, 1475921714522842.

A. Ikeda, Y. Minami, K. Fujita, and Takewaki. (2014). Smart system identification of super high-rise building using limited vibration data during the 2011 Tohoku earthquake. International Journal of High-Rise Buildings, Vol. 3, No. 4, 255-271.

Bao, C., Hao, H., & Li, Z.-X. (2013). Integrated ARMA model method for damage detection of subsea pipeline system. *Engineering Structures, 48*, 176-192.

Bernal, D., & Beck, J. (2004). Preface to the special issue on phase I of the IASC-ASCE structural health monitoring benchmark. *Journal of Engineering Mechanics-Asce, 130*, 1-2. doi: 10.1061/(asce)0733-9399(2004)130:1(1)

Bighamian, R., & Mirdamadi, H. R. (2013). Input/output system identification of simultaneous mass/stiffness damage assessment using discrete-time pulse responses, differential evolution algorithm, and equivalent virtual damped SDOF. *Structural Control and Health Monitoring, 20*(4), 576-592.

Bodeux, J.-B., & Golinval, J.-C. (2000). *ARMAV model technique for system identification and damage detection.* Paper presented at the European COST F3 Conference on System Identification & Structural Health Monitoring.

Box, G. E. P., Jenkins, G. M., & Reinsel, G. C. (1994). *Time Series Analysis: Forecasting and Control*: Prentice Hall.

Caicedo, J. M., Dyke, S. J., & Johnson, E. A. (2004). Natural excitation technique and eigensystem realization algorithm for phase I of the IASC-ASCE benchmark problem: Simulated data. *Journal of Engineering Mechanics-Asce, 130*, 49-60. doi: 10.1061/(asce)0733-9399(2004)130:1(49)

Carpinteri, A., & Lacidogna, G. (2006). Damage monitoring of an historical masonry building by the acoustic emission technique. *Materials and Structures, 39*(2), 161-167.

Catbas, F. N., Brown, D. L., & Aktan, A. E. (2006). Use of modal flexibility for damage detection and condition assessment: case studies and demonstrations on large structures. *Journal of Structural Engineering*.

Chae, M., Yoo, H., Kim, J., & Cho, M. (2012). Development of a wireless sensor network system for suspension bridge health monitoring. *Automation in Construction, 21*, 237-252.

Ching, J. Y., Muto, M., & Beck, J. L. (2006). Structural model updating and health monitoring with incomplete modal data using Gibbs sampler. *Computer-Aided Civil and Infrastructure Engineering, 21*(4), 242-257. doi: 10.1111/j.1467-8667.2006.00432.x

De Boe, P., & Golinval, J.-C. (2003). Principal component analysis of a piezosensor array for damage localization. *Structural health monitoring, 2*(2), 137-144.

de Lautour, O. R., & Omenzetter, P. (2010). Damage classification and estimation in experimental structures using time series analysis and pattern recognition. *Mechanical Systems and Signal Processing, 24*(5), 1556-1569.

De Roeck, G., Maeck, J., Michielsen, T., & Seynaeve, E. (2002). *Traffic-induced shifts in modal properties of bridges.* Paper presented at the SPIE proceedings series.

Dharap, P., Koh, B. H., & Nagarajaiah, S. (2006). Structural health monitoring using ARMarkov observers. *Journal of Intelligent Material Systems and Structures, 17*, 469-481. doi: 10.1177/1045389x06058793

Do, T. N. and Gül, M (2015). "Detection of Stiffness and Mass Changes Separately using Time Series Analysis with Output-only Vibration Data," *10th International Workshop on Structural Health Monitoring (IWSHM),* Stanford, CA, US. (Accepted).

Doebling, S. W., Farrar, C. R., & Prime, M. B. (1998). A summary review of vibration-based damage identification methods. *Shock and Vibration Digest, 30*(2), 91-105.

Fan, W., & Qiao, P. Z. (2011). Vibration-based Damage Identification Methods: A Review and Comparative Study. *Structural Health Monitoring-an International Journal, 10*, 83-111. doi: 10.1177/1475921710365419

Figueiredo, E., Figueiras, J., Park, G., Farrar, C. R., & Worden, K. (2011). Influence of the autoregressive model order on damage detection. *Computer-Aided Civil and Infrastructure Engineering, 26*(3), 225-238.

Figueiredo, E., & Park, G. (2011). Machine learning algorithms for damage detection under operational and environmental variability. *Structural health monitoring, 10*(6), 559-572.

Giurgiutiu, V. (2005). Tuned Lamb wave excitation and detection with piezoelectric wafer active sensors for structural health monitoring. *Journal of Intelligent Material Systems and Structures, 16*(4), 291-305.

Gu, J. and Gül, M (2015). "Structural Damage Detection with Modal Frequencies under Temperature Variability using Modified Auto-Associative Neural Network Technique," *10th International Workshop on Structural Health Monitoring (IWSHM),* Stanford, CA, US. (Accepted).

Gul, M., & Catbas, F. N. (2009). Statistical pattern recognition for Structural Health Monitoring using time series modeling: Theory and experimental verifications. *Mechanical Systems and Signal Processing, 23*(7), 2192-2204.

Gul, M., & Catbas, F. N. (2009). Statistical pattern recognition for Structural Health Monitoring using time series modeling: Theory and experimental verifications. *Mechanical Systems and Signal Processing, 23*, 2192-2204. doi: 10.1016/j.ymssp.2009.02.013

Gul, M., & Catbas, F. N. (2011). Structural health monitoring and damage assessment using a novel time series analysis methodology with sensor clustering. *Journal of Sound and Vibration, 330*(6), 1196-1210.

Gul, M., & Catbas, F. N. (2011). Structural health monitoring and damage assessment using a novel time series analysis methodology with sensor clustering. *Journal of Sound and Vibration, 330*, 1196-1210. doi: 10.1016/j.jsv.2010.09.024

Hearn, G., & Testa, R. B. (1991). MODAL-ANALYSIS FOR DAMAGE DETECTION IN STRUCTURES. *Journal of Structural Engineering-Asce, 117*, 3042-3063. doi: 10.1061/(asce)0733-9445(1991)117:10(3042)

Hong, Y. H., Kim, H.-K., & Lee, H. S. (2010). Reconstruction of dynamic displacement and velocity from measured accelerations using the variational statement of an inverse problem. *Journal of Sound and Vibration, 329*(23), 4980-5003.

Huang, Z., Liu, G., Todd, M., & Mao, Z. (2013). *Damage detection using vector auto-regressive models.* Paper presented at the SPIE Smart Structures and Materials+ Nondestructive Evaluation and Health Monitoring.

Im, S. B., Hurlebaus, S., & Kang, Y. J. (2013). Summary Review of GPS Technology for Structural Health Monitoring. *Journal of Structural Engineering, 139*, 1653-1664. doi: 10.1061/(asce)st.1943-541x.0000475

Johnson, E. A., Lam, H. F., Katafygiotis, L. S., & Beck, J. L. (2004). Phase I IASC-ASCE structural health monitoring benchmark problem using simulated data. *Journal of Engineering Mechanics-Asce, 130*, 3-15. doi: 10.1061/(asce)0733-9399(2004)130:1(3)

Ju, F. D., & Mimovich, M. E. (1988). Experimental Diagnosis of Fracture Damage in Structures by the Modal Frequency Method. *Journal of Vibration, Acoustics, Stress, and Reliability in Design, 110*(4), 456-463. doi: 10.1115/1.3269550

Kessler, S. S., Spearing, S. M., & Soutis, C. (2002). Damage detection in composite materials using Lamb wave methods. *Smart Materials and Structures, 11*(2), 269.

Kim, Kim, N., Yoon, J., & Jung, D. (1999). *Effect of vehicle mass on the measured dynamic characteristics of bridges from traffic-induced vibration test.* Paper presented at the PROCEEDINGS-SPIE THE INTERNATIONAL SOCIETY FOR OPTICAL ENGINEERING.

Kim, H., & Melhem, H. (2004). Damage detection of structures by wavelet analysis. *Engineering Structures, 26*(3), 347-362.

Kim, J.-T., Ryu, Y.-S., Cho, H.-M., & Stubbs, N. (2003). Damage identification in beam-type structures: frequency-based method vs mode-shape-based method. *Engineering Structures, 25*(1), 57-67.

Ko, J., & Ni, Y. (2005). Technology developments in structural health monitoring of large-scale bridges. *Engineering Structures, 27*(12), 1715-1725.

Koo, K., Brownjohn, J., List, D., & Cole, R. (2013). Structural health monitoring of the Tamar suspension bridge. *Structural Control and Health Monitoring, 20*(4), 609-625.

Kostic, B. and Gül, M (2015). "Damage Detection under Varying Temperature Influence using Artificial Neural Networks and Time Series Analysis Methods," *10th International Workshop on Structural Health Monitoring (IWSHM),* Stanford, CA, US. (Accepted).

Kullaa, J. (2003). Damage detection of the Z24 bridge using control charts. *Mechanical Systems and Signal Processing, 17*(1), 163-170.

Kurata, M., Kim, J., Zhang, Y., Lynch, J. P., Van der Linden, G., Jacob, V., . . . Sheng, L.-H. (2011). *Long-term assessment of an autonomous wireless structural health monitoring system at the new Carquinez Suspension Bridge.* Paper presented at the SPIE Smart Structures and Materials+ Nondestructive Evaluation and Health Monitoring.

Kuwabara, M., Yoshitomi, S., & Takewaki, I. (2013). A new approach to system identification and damage detection of high-rise buildings. Structural Control and Health Monitoring, 20(5), 703-727.

Lakshmi, K., & Rama Mohan Rao, A. (2014). A robust damage-detection technique with environmental variability combining time-series models with principal components. *Nondestructive Testing and Evaluation, 29*(4), 357-376.

Lee, U., & Shin, J. (2002). A frequency response function-based structural damage identification method. *Computers & Structures, 80*(2), 117-132.

Lei, Y., Jiang, Y., & Xu, Z. (2012). Structural damage detection with limited input and output measurement signals. *Mechanical Systems and Signal Processing, 28*, 229-243.

Lei, Y., Kiremidjian, A., Nair, K., Lynch, J., Law, K., Kenny, T., . . . Kottapalli, A. (2003). *Statistical damage detection using time series analysis on a structural health monitoring benchmark problem.* Paper presented at the Proceedings of the 9th international conference on applications of statistics and probability in civil engineering.

Levy, H., & Lessman, F. (1961). *Finite difference equations*: New York, Macmillan [1961] [1st American ed.].

Link, M., & Weiland, M. (2012). Computational model updating based on stochastic test data and modelling parameters - a tool for structural health monitoring. *Proceedings of International Conference on Noise and Vibration Engineering*

(Isma2012) / International Conference on Uncertainty in Structural Dynamics (Usd2012), 4733-4744.

Liu, K., Law, S., Xia, Y., & Zhu, X. (2014). Singular spectrum analysis for enhancing the sensitivity in structural damage detection. *Journal of Sound and Vibration, 333*(2), 392-417.

Lu, Y., & Gao, F. (2005). A novel time-domain auto-regressive model for structural damage diagnosis. *Journal of Sound and Vibration, 283*(3), 1031-1049.

Lynch, J. (2005). *Damage characterization of the IASC-ASCE structural health monitoring benchmark structure by transfer function pole migration.* Paper presented at the Proceedings of the ASCE Structures Congress and the Forensic Engineering Symposium.

Lynch, J. P., & Loh, K. J. (2006). A summary review of wireless sensors and sensor networks for structural health monitoring. *Shock and Vibration Digest, 38*(2), 91-130.

Maity, D., & Tripathy, R. R. (2005). Damage assessment of structures from changes in natural frequencies using genetic algorithm. *Structural Engineering and Mechanics, 19*(1), 21-42.

Mei, L., Mita, A., & Zhou, J. (2015). A Substructural Damage Identification Approach for Shear Structure Based on Changes in the First AR Model Coefficient Matrix. *Journal of Structures, 2015*.

Mei, Q. (2014). *Investigation of Time Series Analysis Based Damage Detection Methodologies for Structural Health Monitoring.* University of Alberta.

Mei, Q., & Gül, M. (2014). Novel Sensor Clustering–Based Approach for Simultaneous Detection of Stiffness and Mass Changes Using Output-Only Data. *Journal of Structural Engineering*.

Minami, Y., Yoshitomi, S., & Takewaki, I. (2013). System identification of super high-rise buildings using limited vibration data during the 2011 Tohoku (Japan) earthquake. Structural Control and Health Monitoring, 20(11), 1317-1338.

Moaveni, B., Hurlebaus, S., & Moon, F. (2013). Special Issue on Real-World Applications of Structural Identification and Health Monitoring Methodologies Introduction. *Journal of Structural Engineering, 139*, 1637-1638. doi: 10.1061/(asce)st.1943-541x.0000779

Monroig, E., & Fujino, Y. (2006). Damage identification based on a local physical model for small clusters of wireless sensors.

Mosavi, A. A., Dickey, D., Seracino, R., & Rizkalla, S. (2012). Identifying damage locations under ambient vibrations utilizing vector autoregressive models and Mahalanobis distances. *Mechanical Systems and Signal Processing, 26*, 254-267.

Mujica, L. E., Ruiz, M., Pozo, F., Rodellar, J., & Gueemes, A. (2014). A structural damage detection indicator based on principal component analysis and statistical hypothesis testing. *Smart Materials and Structures, 23*(2). doi: 10.1088/0964-1726/23/2/025014

Nair, K. K., & Kiremidjian, A. S. (2007). Time series based structural damage detection algorithm using Gaussian mixtures modeling. *Journal of dynamic systems, measurement, and control, 129*(3), 285-293.

Nair, K. K., Kiremidjian, A. S., & Law, K. H. (2006). Time series-based damage detection and localization algorithm with application to the ASCE benchmark structure. *Journal of Sound and Vibration, 291*(1), 349-368.

Noman, A. S., Deeba, F., & Bagchi, A. (2012). Health monitoring of structures using statistical pattern recognition techniques. *Journal of Performance of Constructed Facilities*.

Omenzetter, P., & Brownjohn, J. M. W. (2006). Application of time series analysis for bridge monitoring. *Smart Materials and Structures, 15*(1), 129.

Pandey, A., & Biswas, M. (1994). Damage detection in structures using changes in flexibility. *Journal of Sound and Vibration, 169*(1), 3-17.

Pandey, A. K., Biswas, M., & Samman, M. M. (1991). DAMAGE DETECTION FROM CHANGES IN CURVATURE MODE SHAPES. *Journal of Sound and Vibration, 145*, 321-332. doi: 10.1016/0022-460x(91)90595-b

Park, N.-G., & Park, Y.-S. (2003). Damage detection using spatially incomplete frequency response functions. *Mechanical Systems and Signal Processing, 17*(3), 519-532.

Reda Taha, M. M. (2010). A neural-wavelet technique for damage identification in the ASCE benchmark structure using phase II experimental data. *Advances in Civil Engineering, 2010*.

Roy, K., Bhattacharya, B., & Ray-Chaudhuri, S. (2015). ARX model-based damage sensitive features for structural damage localization using output-only measurements. *Journal of Sound and Vibration*.

Rytter, A. (1993). *Vibration Based Inspection of Civil Engineering Structures, 1993.* Ph. D. dissertation.

Rytter, A. (1993). *Vibrational based inspection of civil engineering structures.* unknown.

Salawu, O. (1997). Detection of structural damage through changes in frequency: a review. *Engineering Structures, 19*(9), 718-723.

Sampaio, R., Maia, N., & Silva, J. (1999). Damage detection using the frequency-response-function curvature method. *Journal of Sound and Vibration, 226*(5), 1029-1042.

Shih, C., Tsuei, Y., Allemang, R., & Brown, D. (1988). Complex mode indication function and its applications to spatial domain parameter estimation. *Mechanical Systems and Signal Processing, 2*(4), 367-377.

Shiradhonkar, S., & Shrikhande, M. (2011). Seismic damage detection in a building frame via finite element model updating. *Computers & Structures, 89*(23), 2425-2438.

Siebel, T., Friedmann, A., Koch, M., & Mayer, D. (2012). *Assessment of Mode Shape-Based Damage Detection Methods under Real Operational Conditions*. Paper presented at the Proceedings of the 6th European Workshop on Structural Health Monitoring.

Sohn, H. (2007). Effects of environmental and operational variability on structural health monitoring. *Philosophical Transactions of the Royal Society of London A: Mathematical, Physical and Engineering Sciences, 365*(1851), 539-560.

Sohn, H., Czarnecki, J. A., & Farrar, C. R. (2000). Structural health monitoring using statistical process control. *Journal of Structural Engineering, 126*(11), 1356-1363.

Sohn, H., & Farrar, C. R. (2001). Damage diagnosis using time series analysis of vibration signals. *Smart Materials and Structures, 10*(3), 446.

Sohn, H., Farrar, C. R., Hunter, N. F., & Worden, K. (2001). Structural health monitoring using statistical pattern recognition techniques. *Journal of dynamic systems, measurement, and control, 123*(4), 706-711.

Sohn, H., Thompson, G., Robertson, A., Park, G., & Farrar, C. (2004). Online damage detection for theme park rides. *The 22nd International Modal Analysis Conference*.

Sohn, H., Worden, K., & Farrar, C. R. (2002). Statistical damage classification under changing environmental and operational conditions. *Journal of Intelligent Material Systems and Structures, 13*(9), 561-574.

Trendafilova, I., & Manoach, E. (2008). Vibration-based damage detection in plates by using time series analysis. *Mechanical Systems and Signal Processing, 22*(5), 1092-1106.

VanZwol, T. R., Cheng, J. R., & Tadros, G. (2008). Long-term structural health monitoring of the Crowchild Trail Bridge. *Canadian Journal of Civil Engineering, 35*(2), 179-189.

West, W. M. (1984). Illustration of the use of modal assurance criterion to detect structural changes in an Orbiter test specimen. *Air Force Conference on Aircraft Structural Integrity*, 1–6.

Wong, K. Y. (2004). Instrumentation and health monitoring of cable-supported bridges. *Structural Control and Health Monitoring, 11*(2), 91-124.

Xing, Z., & Mita, A. (2012). A substructure approach to local damage detection of shear structure. *Structural Control and Health Monitoring, 19*(2), 309-318.

Yao, R., & Pakzad, S. N. (2014). Damage and noise sensitivity evaluation of autoregressive features extracted from structure vibration. *Smart Materials and Structures, 23*(2), 025007.

Zhan, C., Li, D., & Li, H. (2014). A local damage detection approach based on restoring force method. *Journal of Sound and Vibration, 333*(20), 4942-4959.

Zhang, Fan, L., & Yuan, W. (2002). Traffic-induced variability in dynamic properties of cable-stayed bridge. *Earthquake engineering & structural dynamics, 31*(11), 2015-2021.

Zhang, J., Xu, J., Guo, S., & Wu, Z. (2013). Flexibility-based structural damage detection with unknown mass for IASC-ASCE benchmark studies. *Engineering Structures, 48*, 486-496.

Zhang, D., & Johnson, E. A. (2013). Substructure identification for shear structures I: Substructure identification method. Structural Control and Health Monitoring, 20(5), 804-820.

Zhao, J., Ivan, J. N., & DeWolf, J. T. (1998). Structural damage detection using artificial neural networks. *Journal of Infrastructure Systems, 4*(3), 93-101.

Zhong, S., Oyadiji, S. O., & Ding, K. (2008). Response-only method for damage detection of beam-like structures using high accuracy frequencies with auxiliary mass spatial probing. *Journal of Sound and Vibration, 311*(3), 1075-1099.